INFORMATION TO USERS

The most advanced technology has been used to photograph and reproduce this manuscript from the microfilm master. UMI films the text directly from the original or copy submitted. Thus, some thesis and dissertation copies are in typewriter face, while others may be from any type of computer printer.

The quality of this reproduction is dependent upon the quality of the copy submitted. Broken or indistinct print, colored or poor quality illustrations and photographs, print bleedthrough, substandard margins, and improper alignment can adversely affect reproduction.

In the unlikely event that the author did not send UMI a complete manuscript and there are missing pages, these will be noted. Also, if unauthorized copyright material had to be removed, a note will indicate the deletion.

Oversize materials (e.g., maps, drawings, charts) are reproduced by sectioning the original, beginning at the upper left-hand corner and continuing from left to right in equal sections with small overlaps. Each original is also photographed in one exposure and is included in reduced form at the back of the book. These are also available as one exposure on a standard 35mm slide or as a 17" x 23" black and white photographic print for an additional charge.

Photographs included in the original manuscript have been reproduced xerographically in this copy. Higher quality 6" x 9" black and white photographic prints are available for any photographs or illustrations appearing in this copy for an additional charge. Contact UMI directly to order.

U·M·I

University Microfilms International
A Bell & Howell Information Company
300 North Zeeb Road, Ann Arbor, MI 48106-1346 USA
313/761-4700 800/521-0600

Order Number 9009716

Self- and cross-phase modulation effects on the nonlinear propagation of ultrashort pulses in optical fibers

Baldeck, Patrice L., Ph.D.

City University of New York, 1989

U·M·I
300 N. Zeeb Rd.
Ann Arbor, MI 48106

SELF- AND CROSS- PHASE MODULATION EFFECTS ON THE NONLINEAR PROPAGATION OF ULTRASHORT PULSES IN OPTICAL FIBERS

by

P. L. BALDECK

A dissertation submitted to the Graduate Faculty in Engineering in partial fulfillment of the requirements for the degree of Doctor of Philosophy, The City University of New York.

1989

This manuscript has been read and accepted for the Graduate Faculty in Engineering in satisfaction of the dissertation requirement for the degree of Doctor of Philosophy.

8/1/89
Date

Robert R Alfano
Chair of Examining Committee

8/2/89
Date

Jacques E. Bouvenisti
Executive Officer

Professor Dorsinville

Professor Ho

Professor Yao Li

Professor Ahmed

Professor Agrawal

Supervisory Committee

THE CITY UNIVERSITY OF NEW YORK

ABSTRACT

SELF- AND CROSS- PHASE MODULATION EFFECTS ON THE NONLINEAR PROPAGATION OF ULTRASHORT PULSES IN OPTICAL FIBERS

by

P. L. BALDECK

Adviser: R.R. Alfano, Distinguished Professor of Science and Engineering.

The thesis describes the effects of self- and cross- phase modulation on the propagation of ultrashort pulses in optical fibers.

In the first part of the thesis, we review the theory of self-phase modulation and studies the generation and compression of femtosecond supercontinua using single-mode optical fibers and high-refractive index prisms.

In the second part of the thesis, we investigate theoretically and experimentally spectral and temporal effects of cross-phase modulation on the propagation of interacting ultrashort pulses in optical fibers. In addition, we study XPM and SPM effects on the generation processes of picosecond stimulated Raman pulses and stimulated four photon mixing pulses. All

these effects are important for their potential applications for the generation and control of terahertz pulses.

In the third part of the thesis, we report on the generation of ultrashort pulses with terahertz repetition rates. In an experiment using short lengths of a single-mode optical fibers, we have for the first time generated modulation instability pulses in the normal dispersion regime of optical fibers. In an other experiment we have generated up to 15 terahertz repetition rate pulses by modulation instability oscillations in a femtosecond dye laser.

In the fourth part of the thesis, we study spatial effects on the nonlinear propagation of picosecond pulses in multimode optical fibers. We demonstrate the self-focusing and single-mode propagation of Raman pulses in a fiber able to sustain more than 100,000 modes. In addition, we have developed a new theory for the nonlinear propagation of ultrashort pulses in graded-index waveguides. Our theory predicts new results such as a reverse of the frequency-chirp sign, i.e. sign of the self-phase modulation, due to diffraction effects inside the waveguide. A major consequence of this theoretical prediction is the possibility to propagate solitons and to compress pulses in the normal dispersion regime of optical fibers.

In the fifth part of the thesis, we give some insights to future works that could investigate applications of XPM for the generation and control of ultrashort pulses with teraherz repetition rates.

The final section highlights the problems that needs to be addressed which are the outgrowth of my research.

To My Wife Marianne Baldeck

ACKNOWLEDGEMENTS

I would like to take this opportunity to express my sincere thanks to my parents Laurent and Gisele Baldeck, whose many sacrifices lead me to pursue higher education. For this, I will be always grateful.

It is a great pleasure to acknowledge my deep appreciation to my thesis advisor R.R. Alfano, Distinguished Professor of Science and Engineering of The City College of New York, for his patient guidance, rigorous training, continued encouragement, numerous invaluable suggestions and discussions during the course of this research, critical reading and proofreading the thesis, and most of all for his help selecting and changing my thesis subject. I am particularly grateful to Professors Roger Dorsinville, P.P. Ho, and Jamal T. Manassah of The City College of New York, Doctor N. Ockman of The Institute of Ultrafast Spectroscopy and Lasers, Doctor Peter Delfyett of Bellcore, and most of all to Professor Govind P. Agrawal now of the University of Rochester for their valuable theoretical or experimental assistances. I wish to express my sincere thanks to the faculty of the Electrical Engineering Department for their instruction and help, especially to Professors Yao Li, and Samir Ahmed. I would also like to thank all my fellow colleagues of The Institute of Ultrafast Spectroscopy and Lasers, and Photonics Application Laboratory for providing sunshine during my stay in New York city.

This research was made possible from the financial and educational support provided by Hamamatsu Photonics K.K of Japan under the leadership of President T. Hiruma which is most deeply appreciated.

Finally, special thanks goes to my wife, Marianne, for her unbounded love, encouragement, patience, and understanding.

Table of Contents

List of Figures

Chapter 2:

Chapter 6:

CHAPTER 1

INTRODUCTION

1.1 Self- and Cross-Phase Modulation

Two most important nonlinear phenomena in the propagation of ultrashort pulses are self- and cross- phase modulations.

Self-phase modulation (SPM) is the principal mechanism responsible for the generation of picosecond[1-4] and femtosecond[5] white-light supercontinua. When an intense ultrashort pulse propagates through a medium, it distorts the atomic configuration of the material, and time modulates the refractive index. Hence, the phase of the pulse becomes time-modulated, which causes the generation of new frequencies. SPM generation of ultrashort supercontinuum pulses is the backbone of white light and tunable femtosecond spectroscopy which is increasingly used in physics, chemistry and biology.[6-9] In addition, self-phase modulation is used for pulse compression and dispersionless propagation (i.e. soliton) which occur when SPM effects compensate temporal broadenings from group-velocity dispersion.[10]

Cross-phase modulation (XPM) is a newly-identified phenomenon with important potential for applications based on the picosecond and femtosecond pulse technology.[11] XPM is similar to SPM, but corresponds to

the phase modulation caused by the nonlinear refractive index induced by a copropagating pulse. The XPM generated by pump pulses can be used in

terahertz devices to generate and control, with femtosecond time response, the spectral, temporal, and spatial properties of ultrashort probe pulses. In addition, XPM is intrinsic to, and therefore alters, the generation processes of stimulated Raman scattering (SRS) pulses, second harmonic generation (SHG) pulses , and stimulated four photon mixing (SFPM) pulses.

1.2 Thesis Statement and Organization

The goal of the thesis research is to study the temporal and spectral effects of self- and cross- phase modulations on the propagation of ultrashort pulses in optical fibers.

The thesis objective is to teach and study the physics and potential engineering applications of novel nonlinear phase modulation processes in optical fibers. These effects are studied for short optical fiber lengths and in the case of normal dispersion regime to best fit the propagation conditions of femtosecond pulses from CPM lasers, and picosecond pulses from mode-locked Nd:YAG lasers.

During the course of this thesis, five related topics are investigated: 1) the SPM generation of supercontinuum femtosecond pulses using optical fibers, 2) XPM effects on copropagating pulses in optical fibers, 3) the terahertz pulse generation arising from modulation instability, 4) spatial effects on the

nonlinear propagation of pulses in large-core optical fibers, and 5) future applications of our work.

The first part of the thesis reviews the theory of self-phase modulation and studies the generation of femtosecond supercontinua using single-mode optical fibers. In the supercontinuum process, pre-amplified pulses from the master oscillator are transformed by self-phase modulation in burst of "white" light which can be used either as probe pulses in time-resolved differential absorption experiments, or after spectral selection, amplification, and temporal compression as a source of tunable femtosecond pulses. We present spectral measurements of supercontinuum generation in optical fibers. These measurements allow us to study the nonlinear propagation of femtosecond pulses in single-mode optical fibers.

In the second part of the thesis, we investigate spectral and temporal effects of cross-phase modulation on the propagation of interacting ultrashort pulses in optical fibers. These effects are important for their potential applications for the generation and control of terahertz pulses. We study experimentally and theoretically the spectral and temporal effects generated by pump pulses on copropagating probe pulses. We also investigate the SPM and XPM effects on the generation processes of picosecond stimulated Raman pulses and stimulated four photon mixing pulses, processes which are widely considered for the design of broadband and tunable all-optical amplifiers.

In the third part of the thesis, we report on the generation ultrashort pulses with terahertz repetition rates. In an experiment using short lengths of a single-mode optical fibers, we have for the first time generated modulation instability pulses in the normal dispersion regime of optical fibers. In an other experiment we have generated up to 15 terahertz repetition rate pulses by modulation instability oscillations in a femtosecond dye laser.

In the fourth part of the thesis, we study spatial effects on the nonlinear propagation of picosecond pulses in multimode optical fibers. In large core optical fibers, the nonlinear refractive index induced by the propagation of intense ultrashort pulses not only has a temporal dependence which gives rise to the SPM and XPM effects (parts 1 and 2 of this thesis) but also has a spatial dependence which can alter the guiding properties of the waveguide. Indeed, we demonstrate the self-focusing and single-mode propagation of Raman pulses in a fiber able to sustain more than 100,000 modes. Such spatial effect of the waveguide nonlinearity is interesting to investigate as it involves the physics of nonlinear mode-coupling and could lead to new applications. In the process to explain our experimental results, we have developed a new theory for the nonlinear propagation of ultrashort pulses in graded-index waveguides. Our theory predicts new results such as a reverse of the frequency-chirp sign, i.e. sign of the self-phase modulation, due to diffraction effects inside the waveguide. A major consequence of this theoretical prediction is the possibility to propagate solitons and to compress pulses in the normal dispersion regime of optical fibers.

In the fifth part of the thesis research we give some insights to future works that could investigate applications of XPM for the generation and control of ultrashort pulses with terahertz repetition rates.

Finally, I present the highlights of unanswered questions my research left for future students.

1.3 References

1. R.R. Alfano, Editor, *The Supercontinuum Laser Source,* (Springer-Verlag, Berlin, Heilderberg, 1989).
2. R.R. Alfano and S.L. Shapiro. Phys. Rev. Lett. **24**, 584-587, 592-594, and 1219-12222 (1970).
3. R.R. Alfano, L. Hope, and S. Shapiro. Phys. Rev. **A6**, 433-438 (1972).
4. R.R. Alfano, *Interactions of picosecond pulses with matter* , Ph. D. Thesis at New York University and GTE, GTE Technical report TR72-330.1 (1972).
5. R. Fork, C. Shank, C. Hirliman, and R. Yen. Opt. Lett. 8, 1-3 (1983).
6. S. Shapiro, Editor, *Ultrashort Light Pulses* , 2nd ed., (Springer-Verlag, Berlin, Heilderberg, 1984).
7. R.R. Alfano, Editor, *Biological Events Probed by Ultrafast spectroscopy* , (Academic Press, London, 1982); *Ultrafast Semiconductor Processes* , Vol. 1 and 2 (Academic Press, London, 1984).
8. W. Kaiser, Editor, *Ultrashort Laser Pulses and Applications* , (Springer-Verlag, Berlin, Heilderberg, 1988).
9. *Proceedings of the International Conferences on Ultrafast Phenomena* , Volumes 4, 14, 23, 38, 46, and 48 of the Springer Series in Chemical Physics.
10. Govind P. Agrawal, *Nonlinear Fiber Optics,* (Academic Press, London, 1989).

11. P.L. Baldeck, P.P. Ho, and R.R. Alfano. Chapter 4 in *The Supercontinuum Laser Source* , edited by R.R. Alfano (Springer-Verlag, Berlin, Heilderberg, 1989), pages 117-183.

CHAPTER 2

SELF-PHASE MODULATION EFFECTS ON THE NONLINEAR PROPAGATION OF ULTRASHORT PULSES IN SINGLE-MODE OPTICAL FIBERS

The first part of my research was to characterize the generation of femtosecond supercontinua using single-mode optical fibers. The generation of supercontinua is one of the most important step in the development of a femtosecond laser system. In the supercontinuum process, pre-amplified pulses from the master oscillator are transformed by self-phase modulation in burst of "white" light which can be used either as probe pulses in time-resolved differential absorption experiments, or after spectral selection and amplification as a source of tunable femtosecond pulses. Early measurements on supercontinua involved the nonlinear interaction of picosecond pulses with liquids or bulk glasses, and femtosecond pulses with flowing jets. The generation of femtosecond supercontinuua in optical fibers has been only occasionally investigated, and is still the subject of intense theoretical and experimental research.

In this chapter we review the self-phase modulation theory,[1-6] and present spectral and temporal measurements of supercontinuum generation in optical fibers. We discuss the importance of self-focusing, group velocity dispersion, self-steepening, and initial pulse chirping on the supercontinuum

generation. Finally, we show how these supercontinuum pulses can be compressed in time by using a sequence of four high-refractive index prisms.

2.1 Self-Phase Modulation Theory

2.1.1 Nonlinear and Dispersive Wave Equation

The optical electromagnetic field of supercontinuum pulses must ultimately satisfy Maxwell's wave vector equation:

$$\nabla X (\nabla X E) + \frac{1}{c^2}\frac{\partial^2 E}{\partial t^2} = -\mu_0 \frac{\partial^2 P}{\partial t^2} \tag{2.1}$$

which can be reduced to:[6]

$$\frac{\partial A}{\partial z} + k^{(1)}\frac{\partial A}{\partial t} + \frac{i}{2}k^{(2)}\frac{\partial^2 A}{\partial t^2} - \frac{k^{(3)}}{6}\frac{\partial^3 A}{\partial t^3} + \frac{\alpha}{2}A = i\gamma|A|^2 A - a_1\frac{\partial(|A|^2 A)}{\partial t} - a_2 A\frac{\partial|A|^2}{\partial t} \tag{2.2.a}$$

$$\gamma = \frac{\omega_0}{c} n_2 \frac{1}{A_{eff}} \tag{2.2.b}$$

$$a_1 = 2\gamma/\omega_0 \tag{2.2.c}$$

$$a_2 = i\gamma T_r \tag{2.2.d}$$

where A(z,t) is the complex envelope of the electric field, $k^{(n)}=\partial^n k/\partial\omega^n$ are evaluated at ω_0, the total refractive index n is defined by $n^2=\chi^{(1)} + 3/4$, $\chi^{(3)}=n^2_0 n_2 IA(t)I^2$, α is for the medium losses, n_2 is the effective nonlinear refractive index, A_{eff} is the effective core area, and T_r is the time response of the nonlinearity $\chi^{(3)}$.

Equation 2.2 is the third-order nonlinear and dispersive equation which has been found to describe the characteristics of femtosecond pulses propagating in optical fibers. Equation 2.2 has been derived using the following approximations: 1) linearly-polarized electric fields, 2) homogeneous radial fields, 3) slowly-varying envelope, 4) isotropic and non magnetic medium, 5) negligible Raman effect, and 6) wavelength-independent nonlinear susceptibility $\chi^{(3)}$.

In equation 2.2, from the left side the first two terms describe the envelope propagation at the group velocity $v_g=[k^{(1)}]^{-1}$. The 3rd and 4th terms determine the temporal pulse broadening due to the group velocity dispersion. The 5th term is for the medium losses while the 6th term characterizes the first order of the nonlinear polarization, which is responsible for the self-phase modulation effect and spectral broadening. The 7th term describes the pulse steepening which occurs because the pulse peak propagates slower due to the nonlinear refractive index n_2A^2. The 8th term takes into account the time response of the electronic nonlinearity which leads to the self-frequency shift. In supercontinuum generation, the temporal and spectral shapes (extent, asymmetry, and modulation structure) are affected by the above terms which occur simultaneously and interactively.

However, equation 2.2 is not complete. It does not take into account phenomena such as self-focusing, four-photon parametric generation, and stimulated Raman scattering.

2.1.2 Self-Phase Modulation (SPM) Mechanism

The basic mechanism and properties of SPM can be explored using the simplified nonlinear wave equation:[2]

$$\frac{\partial A}{\partial z}+\frac{1}{v_g}\frac{\partial A}{\partial t}=i\frac{\omega_0}{c}\frac{n_2}{A_{eff}}|A|^2A \tag{2.3}$$

which is obtained from equation 2.2 after neglecting group-velocity dispersion, absorption, self-steepening, and self-frequency shift.

Denoting a and α the amplitude and phase of the electric field envelope

$A=a\exp(i\alpha)$, equation 2.3 reduces to:

$$\frac{\partial a}{\partial z}+\frac{1}{v_g}\frac{\partial a}{\partial t}=0 \tag{2.4a}$$

$$\frac{\partial \alpha}{\partial z}+\frac{1}{v_g}\frac{\partial \alpha}{\partial t}=\frac{\omega_0}{c}n_2\frac{a^2}{A_{eff}} \tag{2.4b}$$

The analytical solutions are:

$$a(\tau) = a_0 F(\tau) \tag{2.5a}$$

and

$$\alpha(z,t) = \frac{\omega_0}{c} n_2 \frac{1}{A_{eff}} \int_0^z a^2 dz' = \frac{\omega_0}{c} n_2 \frac{a_0^2}{A_{eff}} F^2(\tau) z \tag{2.5b}$$

where $F(\tau)$ is the pulse shape envelope and τ is the local time $\tau=\tau-z/v_g$.

The electric field envelope solution of equation 2.3 is given by:

$$A(z,t) = a(\tau) \exp\left(i \frac{\omega_0}{c} n_2 \frac{a_0^2}{A_{eff}} F^2(\tau) z \right) \tag{2.6a}$$

and

$$E(z,t) = A(z,t) \exp i(k_0 z - \omega_0 t) \tag{2.6.b}$$

The main physics of the supercontinuum generation is contained in equation 2.6a. As shown in figure 2.1.1a, the phase of a pulse propagating in a distorted medium becomes time-dependent. There is self-phase modulation, and the electric field frequency is shifted (Fig. 2.1.1b).

Since the pulse duration is much larger than the optical period $2\pi/\omega_0$ (slowly-varying approximation), the electric field at each position τ within the pulse shape has a specific local and instantaneous frequency which is given by

$$\omega(\tau) = \omega_0 + \delta\omega(\tau) \tag{2.7a}$$

where

$$\delta\omega(\tau) = -\frac{\partial\omega}{\partial t} = -\frac{\omega_0}{c} n_2 \frac{a_0^2}{A_{eff}} z \frac{\partial F^2}{\partial\tau} \tag{2.7b}$$

The $\delta\omega(\tau)$ is frequency shift generated at the time location τ of the pulse shape. The frequency shift is proportional to the derivative of the pulse envelope. Thus, the frequency shift varies at each point of the pulse shape. It

corresponds to the generation of new frequencies which result in wider spectra, and shorter pulses at given frequencies. Figure 2.1.1b shows the frequency distribution of the electric field within the pulse shape. the leading edge, the pulse peak, and the trailing edge have red-shifted, non-shifted, and blue-shifted frequencies, respectively. The maximum frequency broadening on Stokes and anti-Stokes sides occurs at the inflexion points τ_1 and τ_2. Moreover, identical frequency shifts appear at different time locations. For example, in figure 2.1.1b the point τ' and τ'' have the same frequency shift $\delta\omega$ and the same absolute frequency $\omega = \omega_0 + \delta\omega$. The electric field amplitude spectrum is obtained by taking the Fourier transform of the complex temporal envelope $A(z,\tau)$:

$$A(\Omega,z) = \frac{1}{2\pi}\int_{-\infty}^{+\infty} A(\tau,z)\, e^{i\Omega\tau} d\tau \qquad (2.8)$$

where $\Omega = \omega - \omega_0$.

The intensity spectrum is given by;

$$S(\Omega,z) = \frac{c}{4\pi}\left| A(\Omega,z) \right|^2 \tag{2.9}$$

In practical cases, the phase of $A(z,\tau)$ is large compared with π, and the method of stationary phase leads to:[2]

$$\Delta\omega(z)_{max} = \frac{\omega_0}{c} n_2 \frac{a_0^2}{A_{eff}} z \left[\frac{\partial F^2}{\partial t}(\tau_1) - \frac{\partial F^2}{\partial t}(\tau_2) \right] \tag{2.10}$$

and,

$$S(\Omega,z) = \frac{c}{4\pi}\frac{2\pi c}{\omega_0 z} \left\{ \frac{A_{eff}}{n_2} \frac{F(\tau')}{\partial^2 F^2/\partial\tau^2(\tau')} + \frac{F(\tau'')}{\partial^2 F^2/\partial\tau^2(\tau'')} \right.$$

$$\left. + 2\frac{F(\tau')F(\tau'')}{\sqrt{\partial^2 F^2/\partial\tau^2(\tau')\,\partial^2 F^2/\partial\tau^2(\tau'')}} \cos\left[\Omega(\tau'-\tau'') + \frac{w_0}{2c\frac{n_2}{A_{eff}} a_0^2 z \left(F(\tau')^2 - F(\tau'')^2 \right)} \right] \right\} \tag{2.11}$$

where $\Delta\omega_{max}$ is the maximum frequency spread, τ_1 and τ_2 are the pulse envelope inflexion points, and τ' and τ'' are the points of the pulse shape which have the same frequency $\omega = \omega_0 + \delta\omega$.

The last term of equation 2.11 produces the periodic structure in the SPM spectrum via interferences of the frequency phases generated at the points τ' and τ''. Notice that the spectral structures cannot be explained by theories based on the linear chirp approximation for which a specific frequency shift corresponds to a unique time τ.

An estimate of the modulation frequency $\Delta\omega_M$ can be made by calculating the maximum number of interference minima, and dividing this number into the maximum broadening. A straightforward calculation leads to:

$$\delta\omega_M \approx 2\pi \frac{\partial F^2/\partial\tau(\tau_1)}{F(\tau_1)^2} \approx 2\pi \frac{\partial F^2/\partial\tau(\tau_2)}{F(\tau_2)^2} \qquad (2.12)$$

Assuming Gaussian shaped pulses $F(\tau) = \exp(-\tau^2/2\tau^2_0)$, we have:

$$\frac{\partial F^2/\partial\tau(\tau_1)}{F(\tau_1)^2} = \frac{\partial F^2/\partial\tau(\tau_2)}{F(\tau_2)^2} = \frac{\sqrt{2}\, e^{-0.5}}{\tau_0} = \frac{0.86}{\tau_0} \qquad (2.13a)$$

Therefore, the maximum frequency broadening (full width) $\Delta\omega(z)_{max}$ is given by:

$$\Delta\omega(z)_{max} = 1.7 \frac{\omega_0}{c} n_2 \frac{a_0^2}{A_{eff}} \frac{z}{\tau_0} \qquad (2.13b)$$

The total spectral width $\Delta\omega(z)$ is given by:

$$\Delta\omega(z)^2 = \Delta\omega_0^2 + \Delta\omega(z)_{max}^2 \qquad (2.13c)$$

The modulation period $\Delta\omega_M$ is given by:

$$\Delta\omega_M = \frac{1.7\,\pi}{\tau_0} \qquad (2.13d)$$

where $\Delta\omega_0$ is the initial spectral width (FWHM), and τ_0 is the initial 1/e temporal pulse width. From equation 2.13b the spectral broadening is proportional to the pulse peak power, the interaction length, and inversely

proportional to the pulse duration. However, the average modulation period depends only on the inverse of the pulse duration.

The chirping -- the temporal distribution of frequencies in the pulse shape or frequency sweep -- is an important characteristic of SPM broadened pulses. In the linear chirp approximation, the chirp coefficient c is usually defined by the phase relation:

$$\alpha = c\tau^2 \tag{2.14}$$

For a Gaussian electric field envelope and linear approximation, the envelope reduces to

$$F^2(\tau) = e^{-\tau^2/\tau_0^2} \approx 1 - \tau^2/\tau_0^2 \tag{2.15}$$

The linear chirp coefficient derived from equations 2.6 and 2.15 becomes:

$$c = \frac{\omega_0}{c} n_2 \frac{a_0^2}{A_{eff}} \frac{z}{\tau_0^2} \tag{2.16}$$

The above analytical expressions for the spectral broadening, spectral modulation period, and linear chirp coefficients have been derived from the simplest form of the nonlinear wave equation which does not include the effects of group-velocity dispersion, self-steepening, self-frequency shift, and self-focusing.

2.1.3 A Numerical Example for Femtosecond Pulses:

Typical parameters and numbers for femtosecond pulses generated by a CPM laser and amplified by a copper vapor laser are:

Central wavelength: $\lambda = 620$ nm

Time duration before amplification: $\Delta\tau = 80$ fsec (FWHM) $= 1.76\ \tau$ (for $sech^2$ pulses) $\Rightarrow \tau = 45$ fsec.

Time duration after amplification: $\Delta\tau = 100$ fsec (FWHM) $\Rightarrow \tau_0 = 57$ fsec.

Maximum energy coupled into the fiber: E = 10 nJ

Maximum peak power: $P = E/\Delta\tau_0 = 100$ kW

Nonlinear refractive index: $n_2 = 3.2\ 10^{-16}\ cm^2/W$

Single-mode optical fiber radius: $r = 1.25\ \mu m$

Normalized frequency: $V = 1.8 \Rightarrow w = 1.37\ r$ (effective core radius)

Effective area: $A_{eff} = \pi w^2 = 9.2\ 10^{-8}\ cm^2$

Maximum peak intensity: $I = P/A_{eff} = 1.1\ TW/cm^2$

Nonlinear phase shift:

$$\alpha\ (z = 7\ mm) = \frac{\omega_0}{c} n_2 \frac{a_0^2}{A_{eff}} z = 25\ rd$$

Modulation frequency:

$$\Delta\omega_M = \frac{1.7\pi}{\tau_0} = 9.4\ 10^{13}\ rd/sec \Rightarrow \Delta\lambda_M = 19\ n\ m$$

Maximum frequency broadening:

$$\Delta\omega(z)_{max} = 1.7 \frac{\omega_0}{c} n_2 \frac{a_0^2}{A_{eff}} \frac{z}{\tau_0} = 7.3\ 10^{14}\ rd/sec \Rightarrow \Delta\lambda_{max} = 150\ n\ m$$

Linear chirp coefficient:

$$c = \frac{\omega_0}{c} n_2 \frac{a_0^2}{A_{eff}} \frac{z}{2\tau_0^2} = 7.7\ 10^{-3}\ rd/fsec^2$$

2.2 Self-Phase Modulation Measurements with 500-fsec Pulses

2.2.1 Experimental Arrangement

Spectral measurements have been performed using the output from a CPM ring dye laser combined with a four-stage YAG-pumped dye amplifier system.[9] Pulses of 500 femtosecond duration at 625 nm were amplified to an energy of about 1 mJ at a repetition rate of 20 Hz. Pulses were weakly focused into the sample. Output pulses were imaged on the slit of a 1/2m Jarell-ash spectrometer and spectra were recorded using an optical multichannel analyzer OMA2.

Femtosecond supercontinua were generated in various solids and liquids such as calcite, quartz, water, benzene, ethanol, lead glass, pyrex, PrF3, $KNiF_3$, and silica optical fibers. Sample lengths ranged from 2 to 10 mm. The single-mode optical fiber at visible wavelengths was custom-made by Corning Glass. The cut-off wavelength was 462 nm, the core diameter 2.5 μm, and the refractive index difference 0.24%.

2.2.2 General Experimental Observations

Typical supercontinuum spectra generated by 500 fs pulses are displayed in figure 2.2.1. For reference, the laser spectrum is shown in figure 2.2.1a. All continuum spectra were similar despite the different materials. the spectra

were wide and modulated. Spectral shapes, extents and modulation periods changed significantly from shot to shot using the same material. Spectra seemed to depend more on pulse fluctuations (time duration and peak power) than on the state of the material: solids (dielectric, semiconductor, magnetic) of liquids. Spectral widths extended up to 5 000 cm^{-1}. Most of the laser energy was frequency broadened and there was no well defined intense spike at the laser frequency. Spectral modulation periods ranged from 100 to 350 cm^{-1} with an average of about 160 cm^{-1}.

2.23 Maximum Spectral Extent

The simplified SPM theory predicts a SPM spectral extent varying as in equation 2.13b. The maximum SPM spectral width has been investigated as functions of the input peak power a_0^2, and sample length z. the experiment was performed using a single-mode optical fiber for which the peak power and interaction length could be better controlled than for bulk materials. In bulk materials, intense laser beams self-focus and break into unstable filaments. Figure 2.2.2 shows a typical sequence of spectral broadening versus increasing input peak powers using 500 fs pulses. As for the other samples, the spectra were modulated. The spectral extent is plotted against pulse energy in figure 2.2.3. the relative energy of each pulse was calculated by integrating its total broadened spectral distribution. As predicted, the supercontinuum extent increased linearly with the input pulse intensity. The spectral broadening was independent of the optical length (Fig. 2.2.4). Due to the

group velocity dispersion temporal broadening the SPM spectral broadening occurred in the first few centimeters of the fiber for femtosecond pulses.

2.2.4 Spectral Modulation

As shown in figures 2.2.1 and 2.2.2 the spectral modulation is a definite characteristic of supercontinuum spectra. The spectral modulation period can be estimated by equation 2.13d. Using this relation, the average modulation period of 160 cm^{-1} corresponds to an initial pulse duration of 400 fs which is in good agreement with the pulse duration of the amplified CPM pulses.

2.2.5 Chirp-Frequency Sweep

The chirp (frequency sweep) of supercontinuum pulses is one of the major signature of SPM broadened pulses. It has become an important characteristic of SPM broadened pulses used for pulse compression. The frequency sweep of supercontinuum pulses propagating in CCl_4 is shown in figure 2.2.5. The chirp has been measured in our laboratory with a 2 ps-resolution streak camera.[7] The results are in agreement with the above theory (Fig. 2.2.6). Recently, Dorsinville et al. generated supercontinuum pulses by focusing 25 ps-pulses into a 5 cm-long cell filled with D_2O.[8] Using 10 nm-bandwidth narrow band filters, they were able to generate tunable pulses of less than 3-ps in the range 480-590 nm (Fig. 2.2.7) showing that for each narrow spectral band of a SPM pulse there corresponds a narrow pulse in time.

2.3 Higher Order Effects on Self-Phase Modulation

A complete description of SPM-generated spectral broadening should take into account higher-order effects such as self-focusing, group-velocity dispersion, self-steepening, and initial pulse chirping and asymmetry. Theses effects change the observed spectral and temporal profiles.

2.3.1 Self-Focusing

In the earliest experiments using ps-pulses, supercontinuum pulses were often generated in small-scale filaments which resulted from the self-focusing of intense laser beams.[2] Self-focusing arises from the radial dependence of the nonlinear refractive index $n(r) = n_0 + n_2E^2(r)$. It has been observed in many liquids, bulk material, and most recently in optical fibers (part 5 of thesis). Its effects on the the supercontinuum pulse generation can be viewed as good and bad. On the one hand, it facilitates the supercontinuum generation by concentrating the laser beam energy. On the other hand, self-focusing is a random and unstable process which is not as controllable as one would prefer for the design of a "white laser source". However, femtosecond supercontinua are generated with thinner samples than picosecond supercontinua which reduces, but does not totally eliminate self-focusing effects. This is an area for future investigation.

2.3.2 Group-Velocity Dispersion

Group-velocity dispersion (GVD) arises from the wavelength dependence of the group-velocity. The first order GVD term $k^{(2)}$ leads to a symmetrical temporal broadening. A typical value for the broadening rate arising from $k^{(2)}$ is 500 fs/m.nm (in silica at 532 nm). In the case of supercontinuum generation, spectral widths are generally large (several hundred of nm), but interaction lengths are usually small (< 1cm). therefore, the temporal broadening arising from GVD is often small for picosecond pulses but is important for femtosecond pulses. Limitations on spectral extents of supercontinuum generation are also related to GVD. Although the spectral broadening should increase linearly with the medium length, it quickly reaches a maximum as shown in figure 2.2.4. This is because GVD, which is large for pulses having SPM-broadened spectra, reduces the pulse peak power and broadens the pulse duration.

The third order dispersion $\beta^{(3)}$ is responsible for asymmetrical distortion and modulation of temporal shapes. Since the spectra of supercontinuum pulses are exceptionally broad, this term should also lead to asymmetrical distortions of temporal and spectral shapes of supercontinuum pulses generated in thick samples.

2.3.3 Self-Steepening

Pulse shapes and spectra of intense supercontinuum pulses have been found to be asymmetric. There are two potential sources for asymmetrical broadening in supercontinuum generation. The first one arises from the second order GVD term $k^{(3)}$ as discussed previously.

The second one is self-steepening, which is intrinsic to the SPM process and occurs even in non dispersive media. Due to the intensity and time dependence of the refractive index, the supercontinuum pulse peak sees a higher refractive index than its edges. Because of $v_g = c/n_g$, the pulse peak travels slower than the leading and trailing edges. This results in a sharpened trailing edge. Self-steepening occurs and more blue-shifted frequencies (sharp trailing edge) are generated than red-shifted frequencies.

2.3.4 Initial Pulse Chirping

Most femtosecond and picosecond pulses are generated with initial chirps. these chirps arises from GVD and SPM which occurs in the laser cavity. Recently, Agrawal has computed the nonlinear and dispersive equation for initially chirped picosecond pulses.[2] As shown in figure 2.3.1, the spectral broadening is reduced for positive chirps and enhanced for negative chirps in the normal dispersion regime. Moreover, the spectral distribution of SPM is also affected by the initial chirp.

2.4 Supercontinuum Generation by Propagating 100-fsec Pulses in Single-Mode Optical Fibers

In the process to build a 30-fsec laser system, we have studied the nonlinear propagation and pulse compression of 100-fsec pulses. This section discusses the supercontinuum generation of 100-fsec pulses propagating in single-mode optical fibers. Pulse compression measurements are presented in the next section.

The experimental set-up is shown in figure 2.4.1. Femtosecond pulses where generated from a newly-designed CPM dye laser with a quasi-linear ring cavity. 80-fsec time duration pulses at 82 MHz were routinely obtained using an intracavity 4-prism sequence.[10] These pulses were subsequently amplified at 6.5 kHz using a copper-vapor-laser pumped amplifier. After amplification the time duration and energy of pulses were about 100 fsec and 0.5 μJ, respectively. The amplified pulses were coupled into the 2.5 μm-core diameter fiber described in section 2.2.1. In the following measurements the fiber length was 7 mm.

A high intensities nonlinear phenomena occuring inside the optical fiber modify the spectral and temporal distributions of the 100-fsec input optical pulses. Figure 2.4.2 shows how the pulse spectrum changes for increasing input intensities. Self-phase modulation broadens the spectrum for peak intensities larger than 0.1 TW/cm^2 (about 10 kW peak power and 1 nJ energy). A frequency continuum of about 150 nm is obtained for an input peak intensity of about 1 TW/cm^2.

Figures 2.4.3 and 2.4.4 show the functional relationship between the supercontinuum spectral width (FWHM) and the energy of pulses coupled inside the fiber. The solid line is the theory from the following equations (Section 2, equations 2.13b-c):

$$\Delta\omega(z)^2 = \Delta\omega_0^2 + \Delta\omega(z)_{max}^2 \tag{2.17a}$$

$$\Delta\omega(z)_{max} = 1.7\frac{\omega_0}{c} n_2 \frac{a_0^2}{A_{eff}} \frac{z}{\tau_0} \tag{2.17b}$$

The following parameter values have been used to plot equations 2.17a-b in figures 2.4.3 and 2.4.4: $\Delta\lambda_0$ = 5 nm, n_2=3.2 10^{-16} cm^2/W, A_{eff}=9.2 10^{-8} cm^2, z=7 mm, and $\Delta\tau_0$=1.76τ_0 (assuming a $sech^2(t)$ pulse shape).

If one uses the input pulse width as a fitting parameter one obtains a good agreement between experiment and theory with a $\Delta\tau_0$=126-fsec input pulse duration (FWHM) (Fig. 2.4.4) rather than with the expected 100-fsec pulse duration (Fig. 4.4.3). This correction seems realistic as the theory leading to equations 2.17a-b is a first order theory which does not take into account group-velocity dispersion effects and, therefore, temporal broadening inside the fiber. In addition, the factor 1.7 in equation 2.17b as been obtained for Gaussian pulses and would be slightly different for the assumed secant-hyperbolic pulses. The good agreement of the simple theory of SPM described by equation 2.17a-b and our measurements clearly demonstrates that SPM is responsible for the spectral broadening of femtosecond pulses. This result is important as the spectral widths of picosecond supercontinuua have been measured to be 1 to 2 orders of magnitude than expected by the SPM theory.[2,5]

Spectral changes are very similar to those measured by Boyer and al. (dashed lines in Fig. 2.4.5).[11] In particular our measurements show the same asymmetrical broadening which has been theoretically fitted by varying the input pulse asymmetry (solid lines in Fig. 2.4.5).[11] This is the only argument which can reasonably explain spectral asymmetry that we measured for small broadenings at low intensities (Fig. 2.4.2).[11-14] The temporal asymmetry of our input pulse could originate from temporal reshaping by the intra-cavity saturable absorber or the one placed after the amplifier to eliminate the amplified stimulated emission background.

Figure 2.4.6 shows the functional relationship between the supercontinuum temporal width (FWHM) and the energy of pulses coupled inside the fiber. Data points are deconvoluted assuming a $sech^2(t)$ pulse shape which is a rough approximation. The pulse width broadens from 250 fsec to about 800 fsec. This temporal broadening is due to the combined effect of group-velocity dispersion and self-phase modulation.

2.5 Femtosecond Pulse Compression using a Four-Prism Sequence

In this section, we present our measurements on the temporal compression of the supercontinuum pulses described above.

The ultimate shortness of a pulse is limited by the extent of its spectral distribution. The incertitude principle indicates that for secant-hyperbolic pulses:

$$\Delta\tau_0.\Delta\nu_0 \geq 0.315 \qquad (2.17)$$

where $\Delta\tau_0$ and $\Delta\nu_0$ are the temporal and spectral widths of the pulse, respectively.

Dye lasers have very wide spectral gains which produce short pulses. It is possible to generate pulses as short as 27 fsec using dye jets and the colliding ring cavity geometry.[15] To produce shorter pulses there is a need to broaden more the spectral content of pulses. This is generally obtainable through the supercontinuum generation process.[5] As discussed in section 2.1, supercontinuum pulses are chirped. Red-shifted frequencies are generated at the pulse front, while blue-shifted frequencies are generated at the trailing edge. Diffraction gratings or/and prism sequences have been used to remove the SPM chirp and consequently to compress pulses.[16-21]

In this experiment we compressed spectral broadened pulses to time duration as short as 28 fsec by using a sequence of 4-prisms (figure 2.5.1). The prisms where cut at Brewster angle in a SF-11 glass, which is a high-refractive index glass.

A 4-prism sequence introduces a (negative or positive) time dispersion which can be controlled by varying the prism separation and the amount of glass in the pulse path. In the linear chirp approximation, the time duration of a pulse passing through a 4-prism sequence is given by:[20-21]

$$\Delta\tau_{out} = \Delta\tau_0 \left[1 + \left(\frac{\phi''}{\Delta\tau_0^2}.4.\ln 2\right)^2\right]^{1/2} \qquad (2.18)$$

where $\Delta\tau_0$ is the minimal pulse width obtainable, and ϕ'' is the total linear chirp accumulated by the pulse in the fiber and while passing through the prism sequence.

It is obvious from equation 2.18 that the pulse is minimum when the prism sequence is adjusted such as $\phi'' = 0$, i.e. when the linear part of the supercontinuum chirp has been compensated by the linear part of the chirp introduced by the prism sequence.

Figures 2.5.2 and 2.5.3 show how the time duration of the supercontinuum pulse is reduced by varying the amount of glass in the path of the supercontinuum pulse passing through the 4-prism compressor. The amount of glass in the optical path of the pulse is controlled by translating one of the prism with a micrometer. Figures 2.5.2 and 2.5.3 correspond to the compression of supercontinuum pulses generated in optical fiber lengths of 7-mm and 20-mm, respectively. These figures show that the minimum pulse widths (FWHM) are 170 fsec and 28 fsec pulses for the short and long fiber, respectively. The solid lines are the theoretical fits using equations 2.18. The theoretical equations are given by $\Delta\tau_0=170(1+1.3(x-1.85))^{1/2}$ and $\Delta\tau_0=28(1+8(x-1.85))^{1/2}$ for figures 2.5.2 and 2.5.3, respectively. x characterizes the amount of chirp generated by the prisms in the optical path.[20-21]

The better compression result with the 20 mm fiber is explained by the effect of GVD on the linearization of the supercontinuum chirp. We have seen in section 2.2 that the chirp generated by SPM in a non-dispersive medium is highly nonlinear., i.e. it is the derivative of the pulse shape. Such a nonlinear chirp cannot be fully compensated by a grating pair or a 4-prism

sequence. The supercontinuum process in optical fibers occurs simultaneously with the temporal broadening due to group-velocity dispersion. It has been shown that in this case GVD tends to linearize the supercontinuum chirp. As a consequence, the compression efficient is improved and shorter pulses are obtained. When used separately, the grating pair or 4-prism sequence cannot compensate for 3rd and higher orders of GVD. Therefore, the optical fiber length has to be optimized.[19] It has to be long enough to linearize the supercontinuum chirp enough, but not too long to limit the adverse effects of high order GVD terms. Figures 2.5.1 and 2.5.2 show that better results are obtained with a 20-mm long optical fiber than with a 7-mm long. Our best repeatable and stable result for the compression of a supercontinuum pulse with a 4-prism sequence is shown in Figure 2.5.3. The autocorrelation pulse width is about 47 fsec which corresponds to a 27-fsec pulse width if a $\mathrm{sech}(t)^2$ pulse shape is assumed. This result is not fully optimized. A more systematic study using different optical fibers lengths might allow us to get shorter pulses.

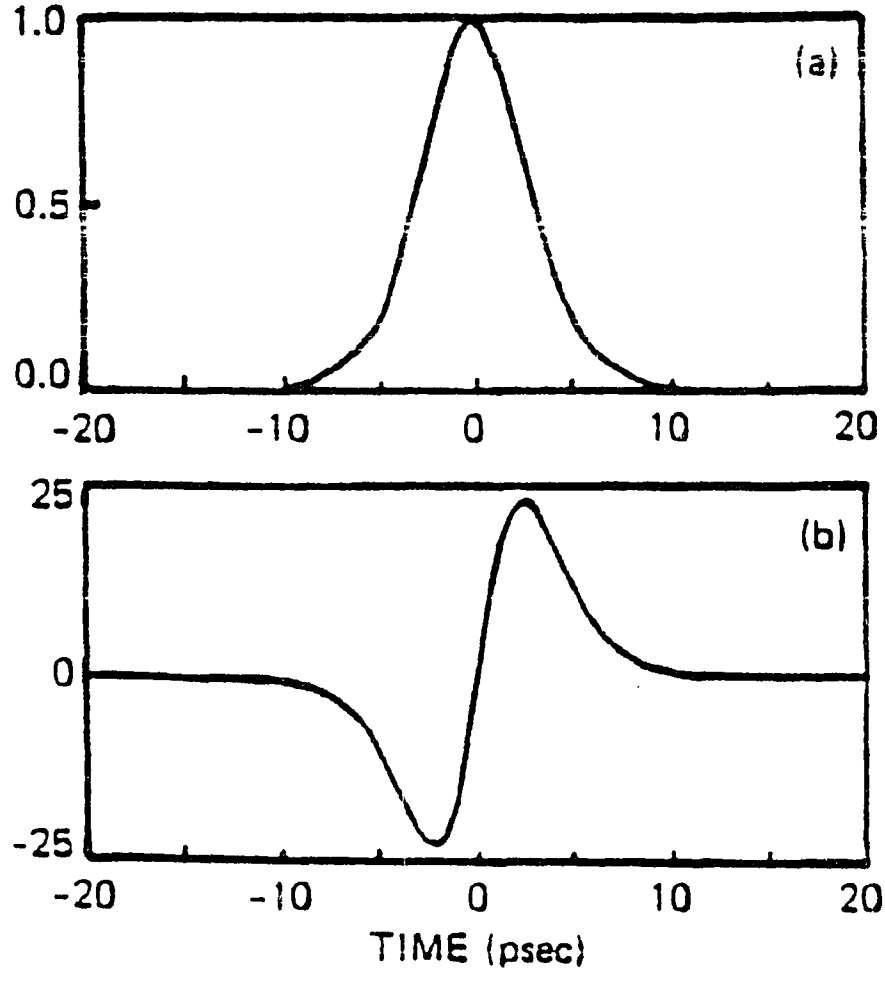

Fig. 2.1.1 (a) Time dependent phase $\alpha(z,t)$ generated by self-phase modulation (SPM). (b) Time distribution of SPM-shifted frequencies $\partial\omega/\partial\tau = -\partial\alpha/\partial\tau$.

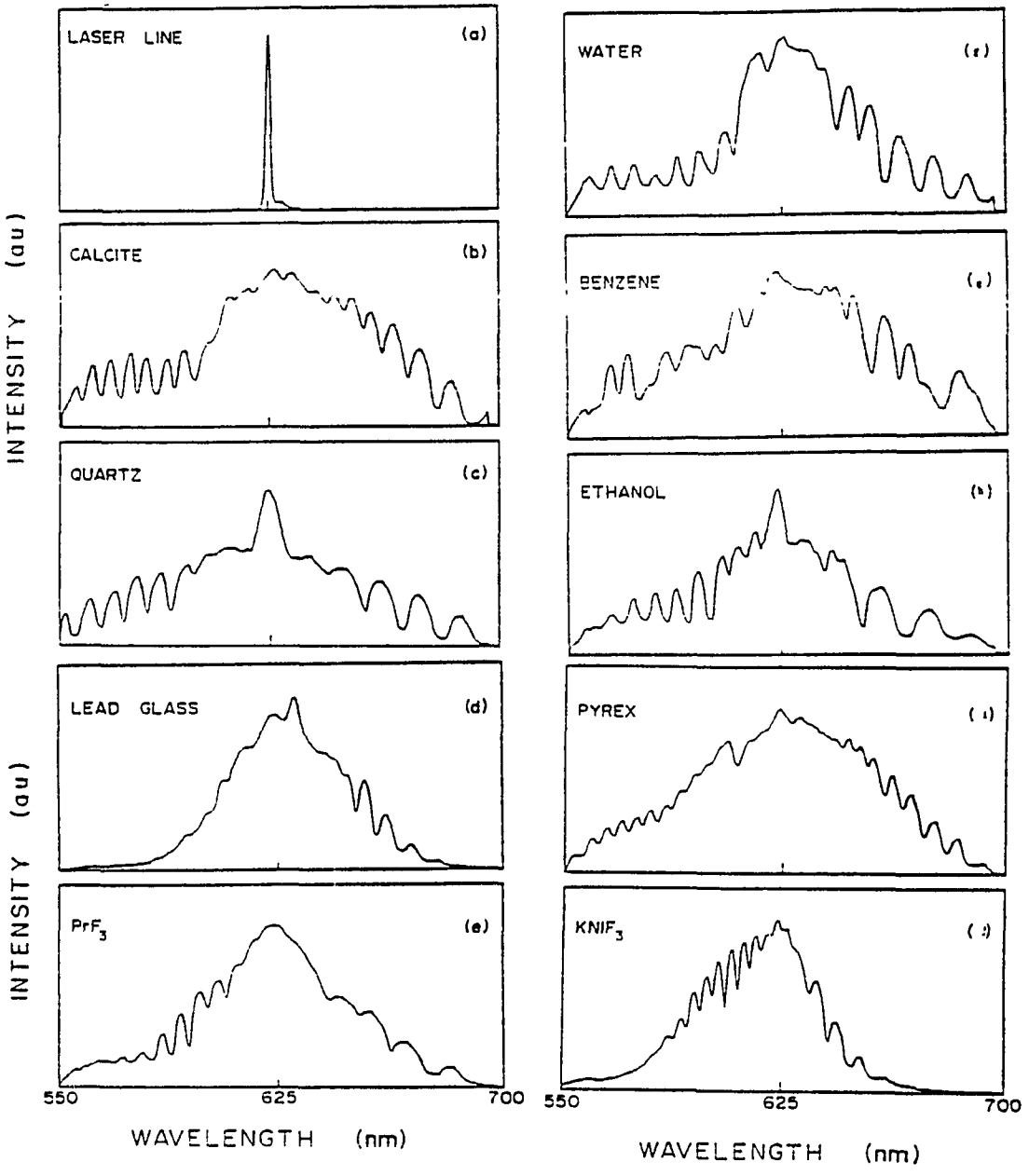

Fig. 2.2.1 Spectra of femtosecond supercontinuum pulses in various media.

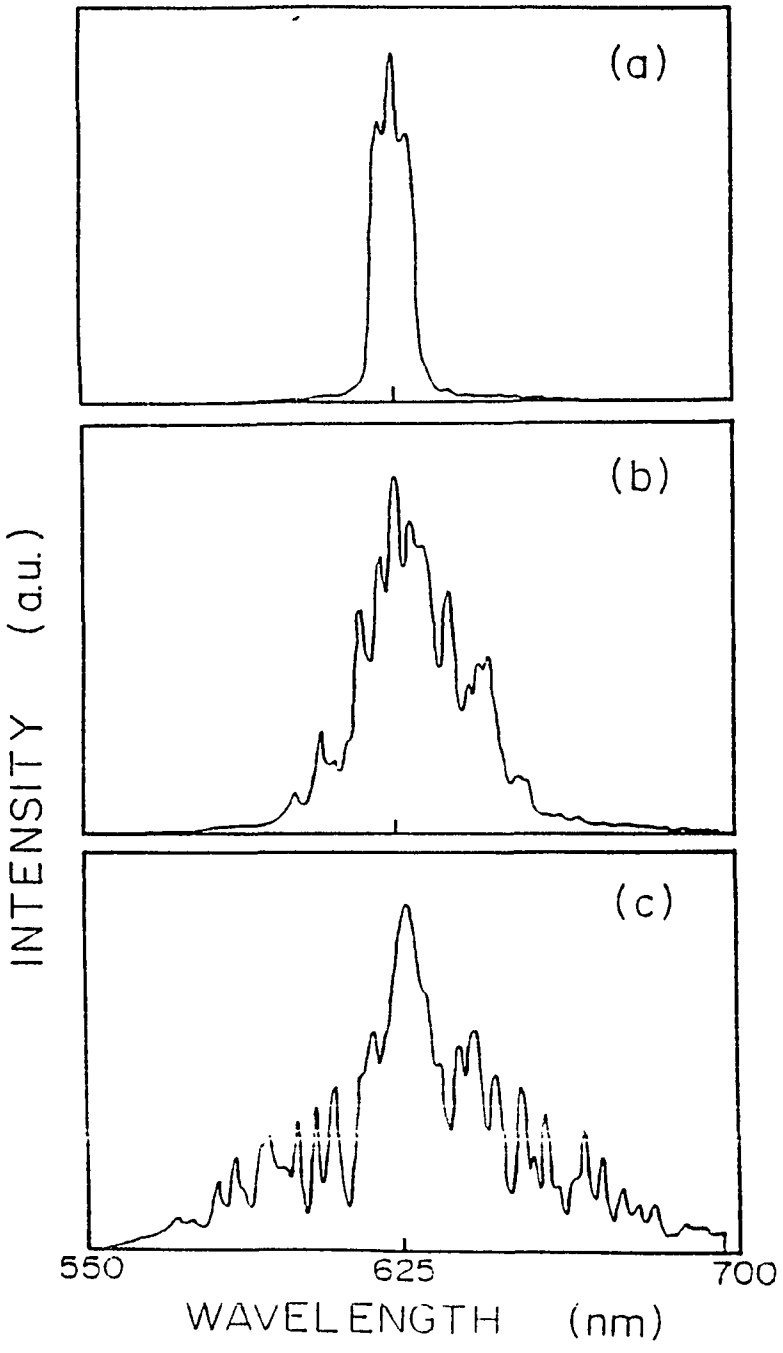

Fig. 2.2.2 Sequence of spectral broadening *versus* increasing input energy in a single-mode optical fiber (length=30 cm). the pump intensity was increased from a) to c).

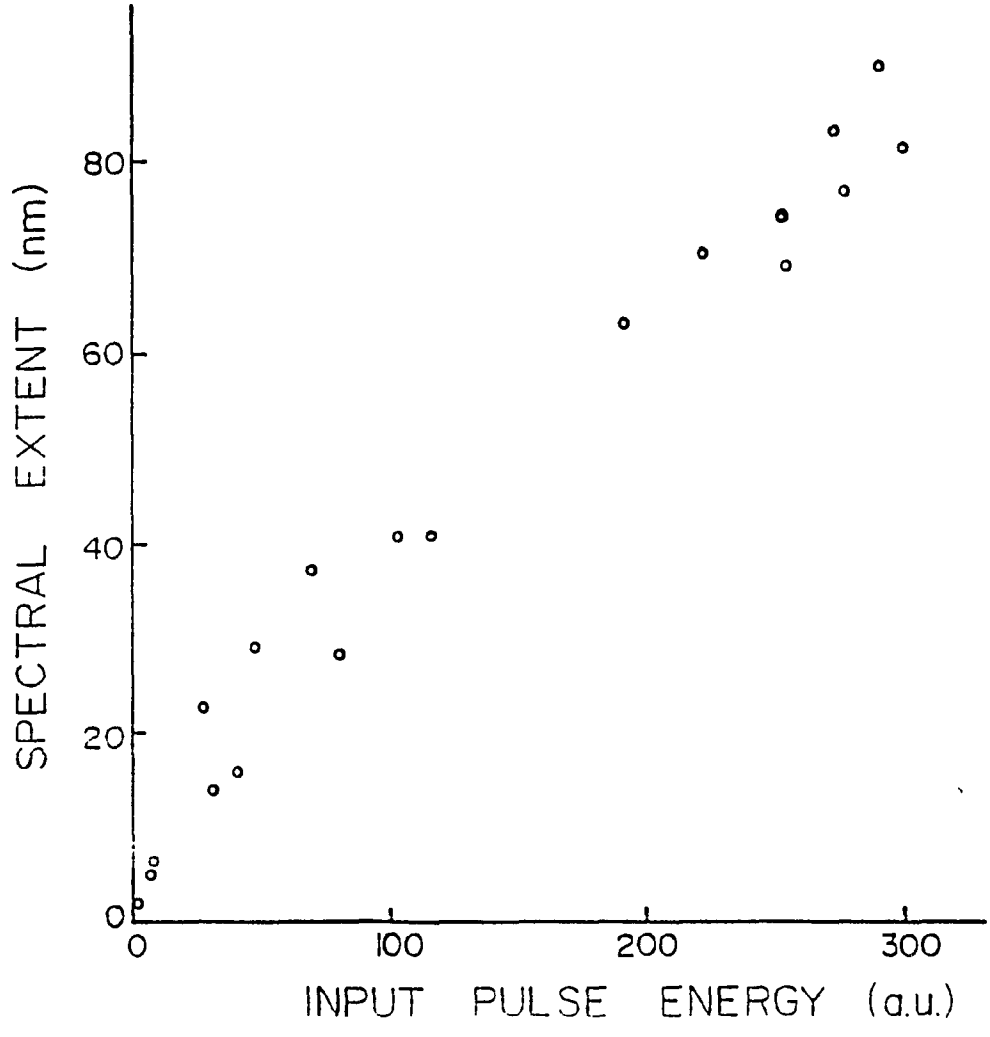

Fig. 2.2.3 SPM spectral broadening *versus* input pulse energy in a single-mode optical fiber (length = 30 cm).

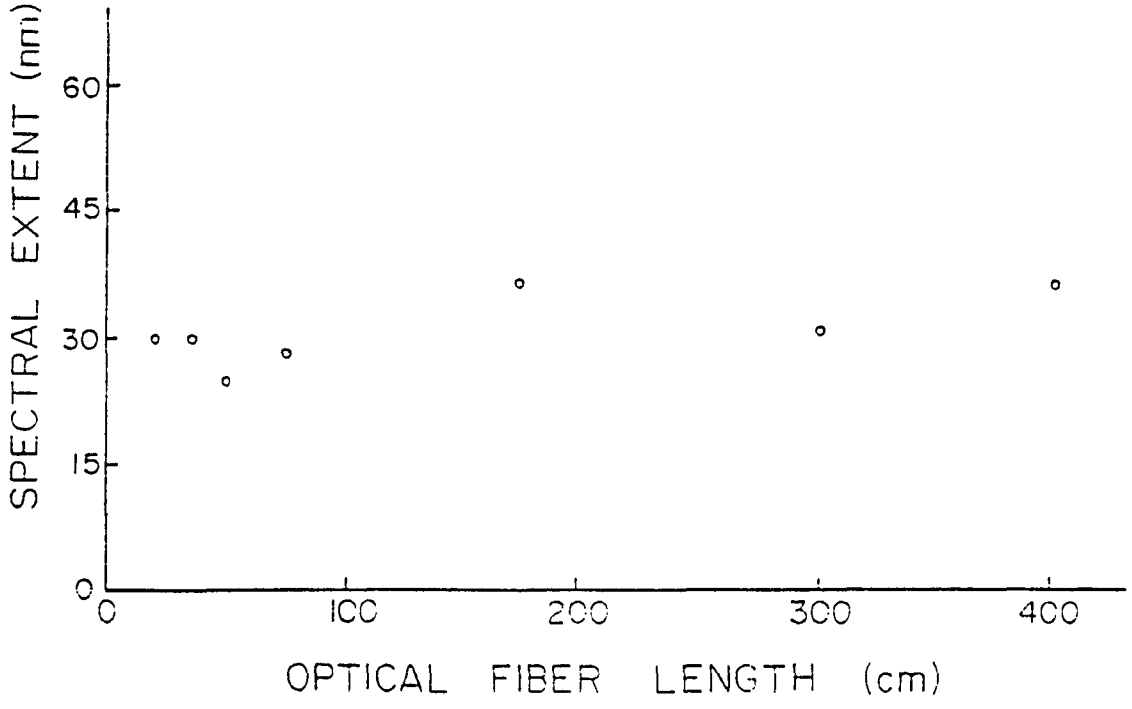

Fig. 2.2.4 SPM spectral broadening *versus* optical fiber length.

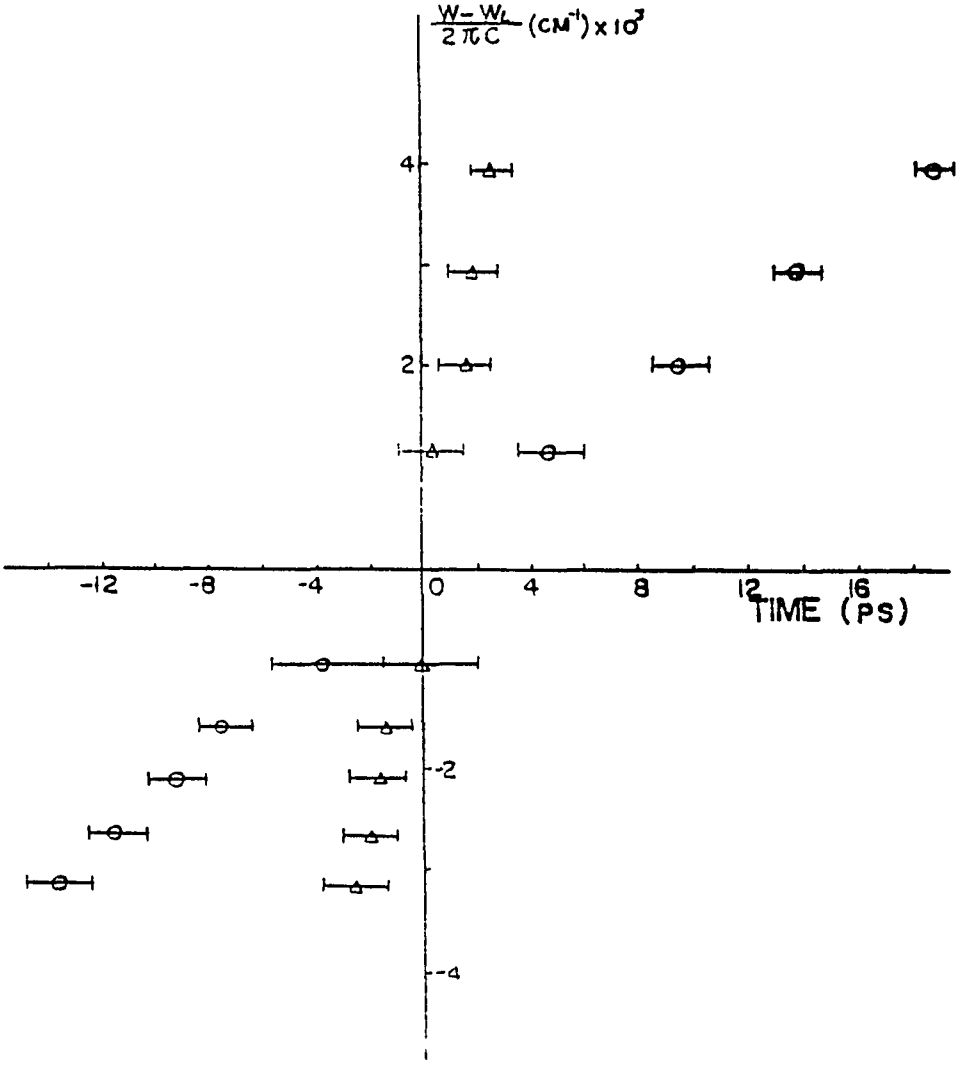

Fig. 2.2.5 Measured supercontinuum distribution at different wavelengths: 0, data points with correction of the optical path in filters; Δ, data points with the correction of both the optical path in filters and group-velocity dispersion in liquid.[7]

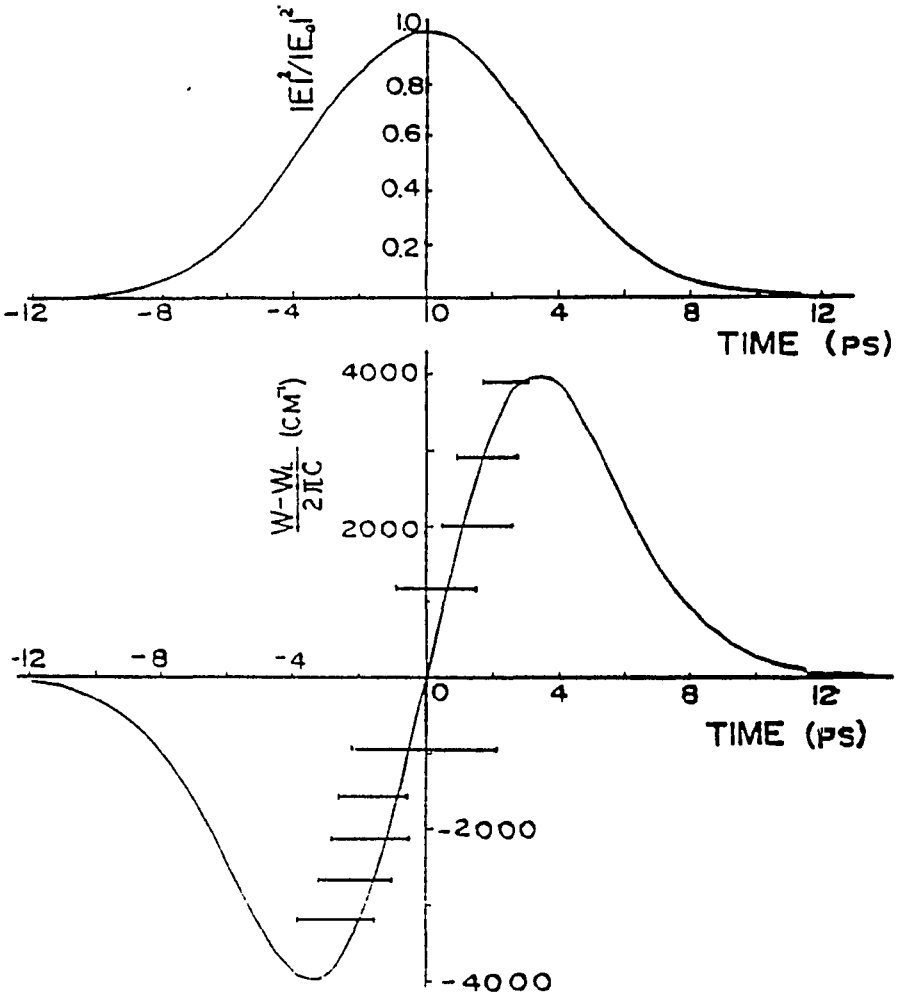

Fig. 2.2.6 Comparison of the measured temporal distribution of supercontinuum with the SPM model.[7]

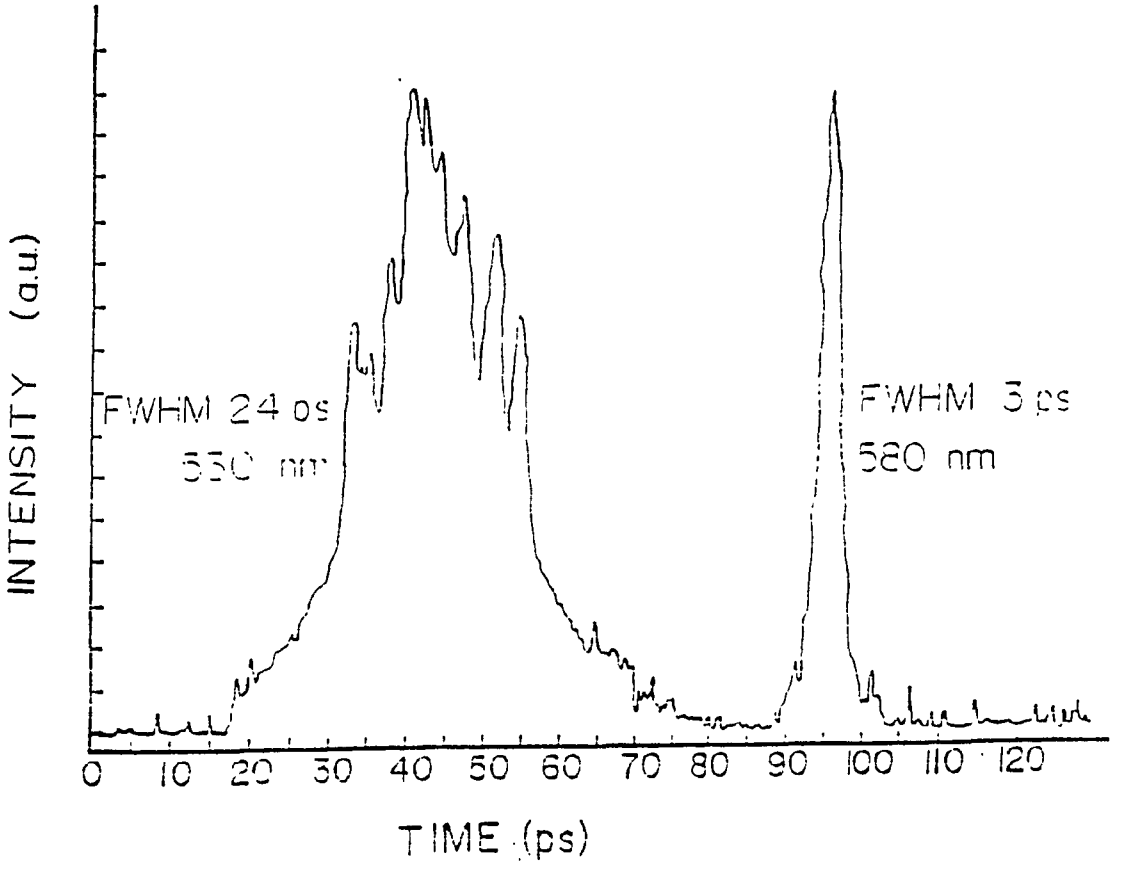

Fig. 2.2.7 Streak camera temporal profile of the 530 nm incident pulse and 10 nm bandwidth pulse at 580 nm. The 3-ps pulse was obtained by spectral filtering a SPM frequency continuum generated in D_2O.[8]

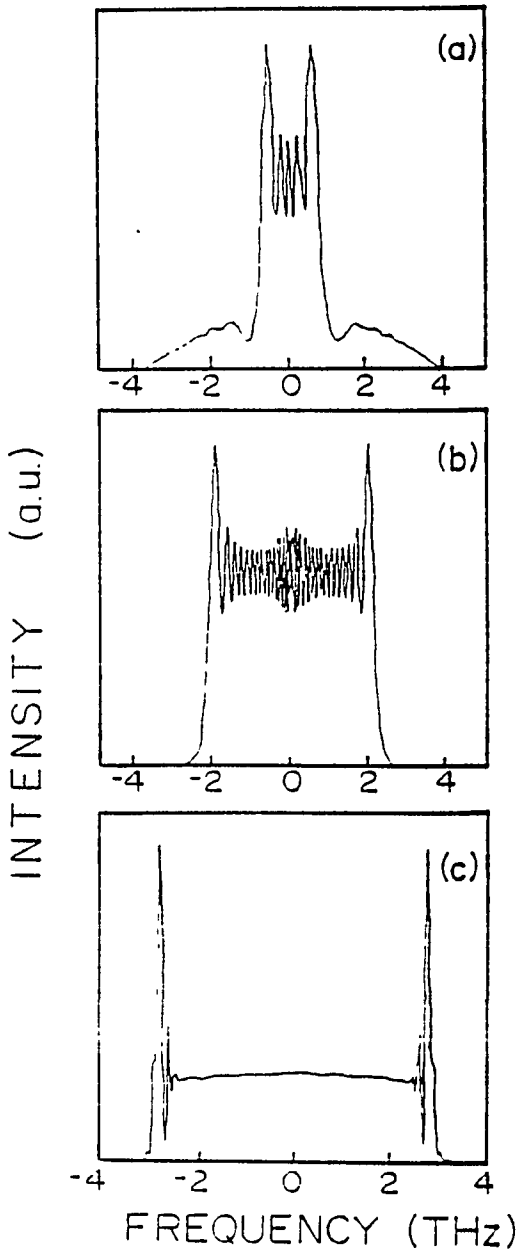

Fig. 2.3.1 Influence of initial chirping on SPM-broadened spectra in optical fibers. Peak power = 1 kW. (a) c=50, (b) c=0, (c) c=-50.[6]

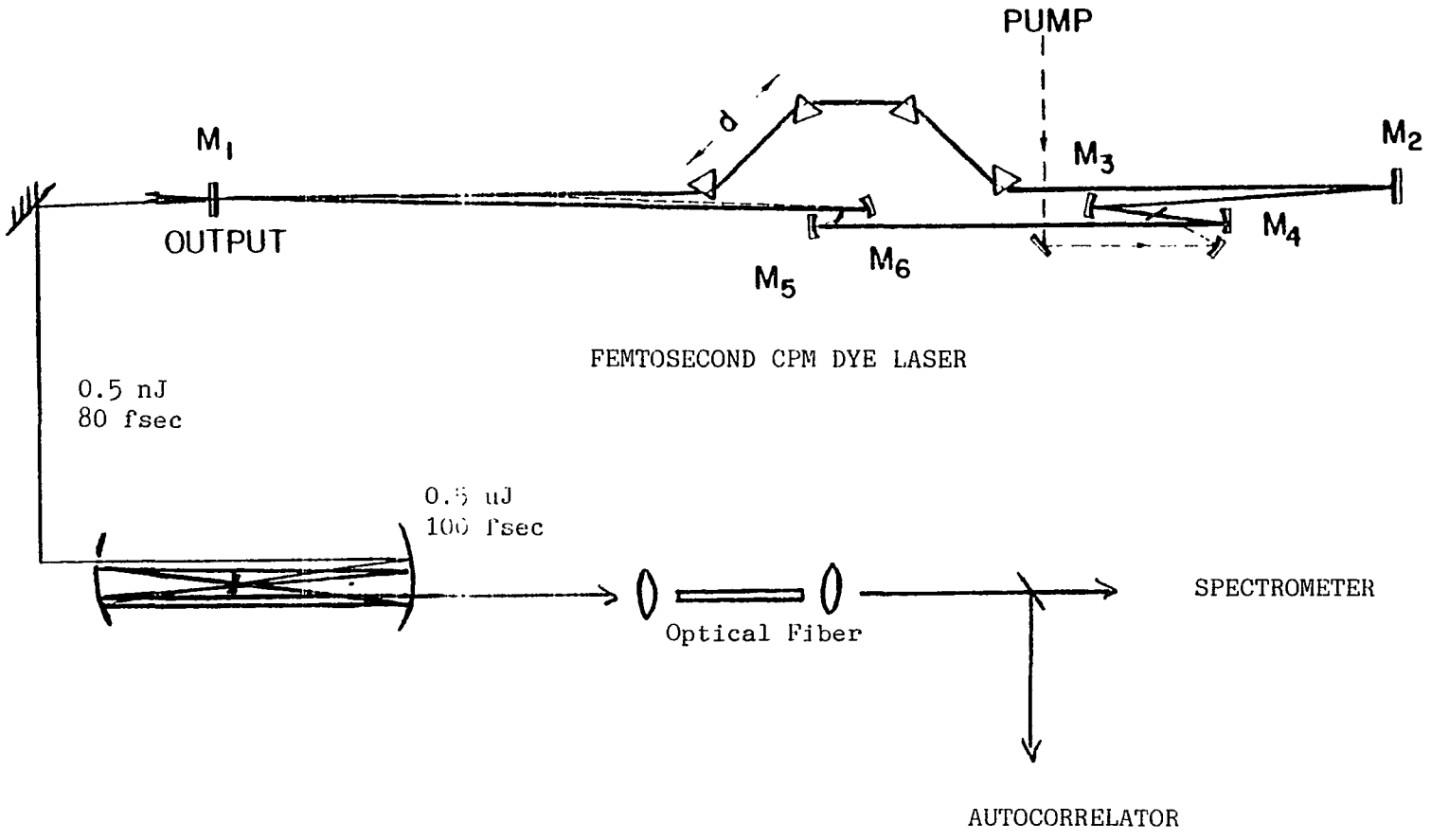

Fig. 2.4.1 Femtosecond laser and amplifier.

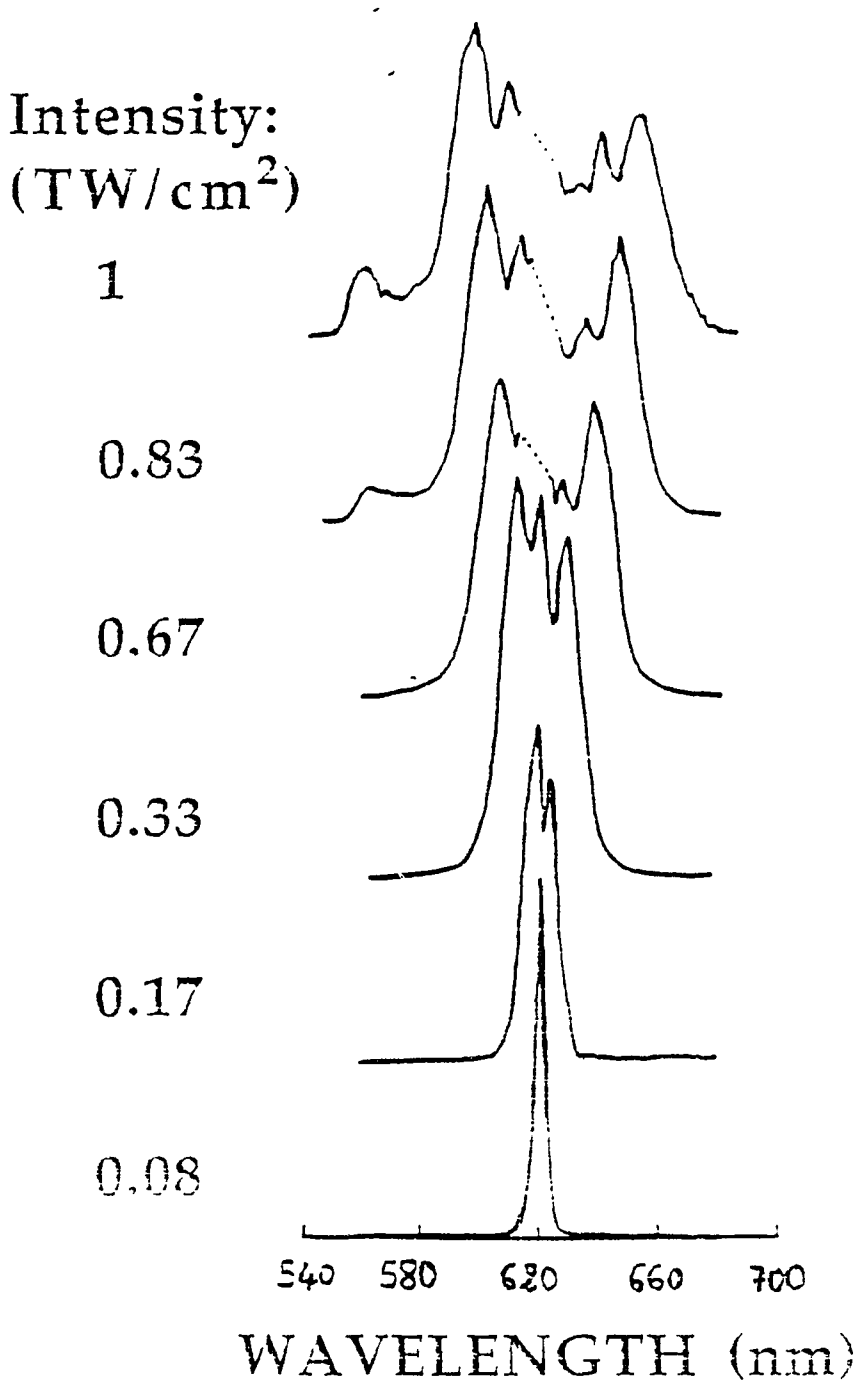

Fig. 2.4.2 Femtosecond supercontinuum generation in a 7-mm long optical fiber.

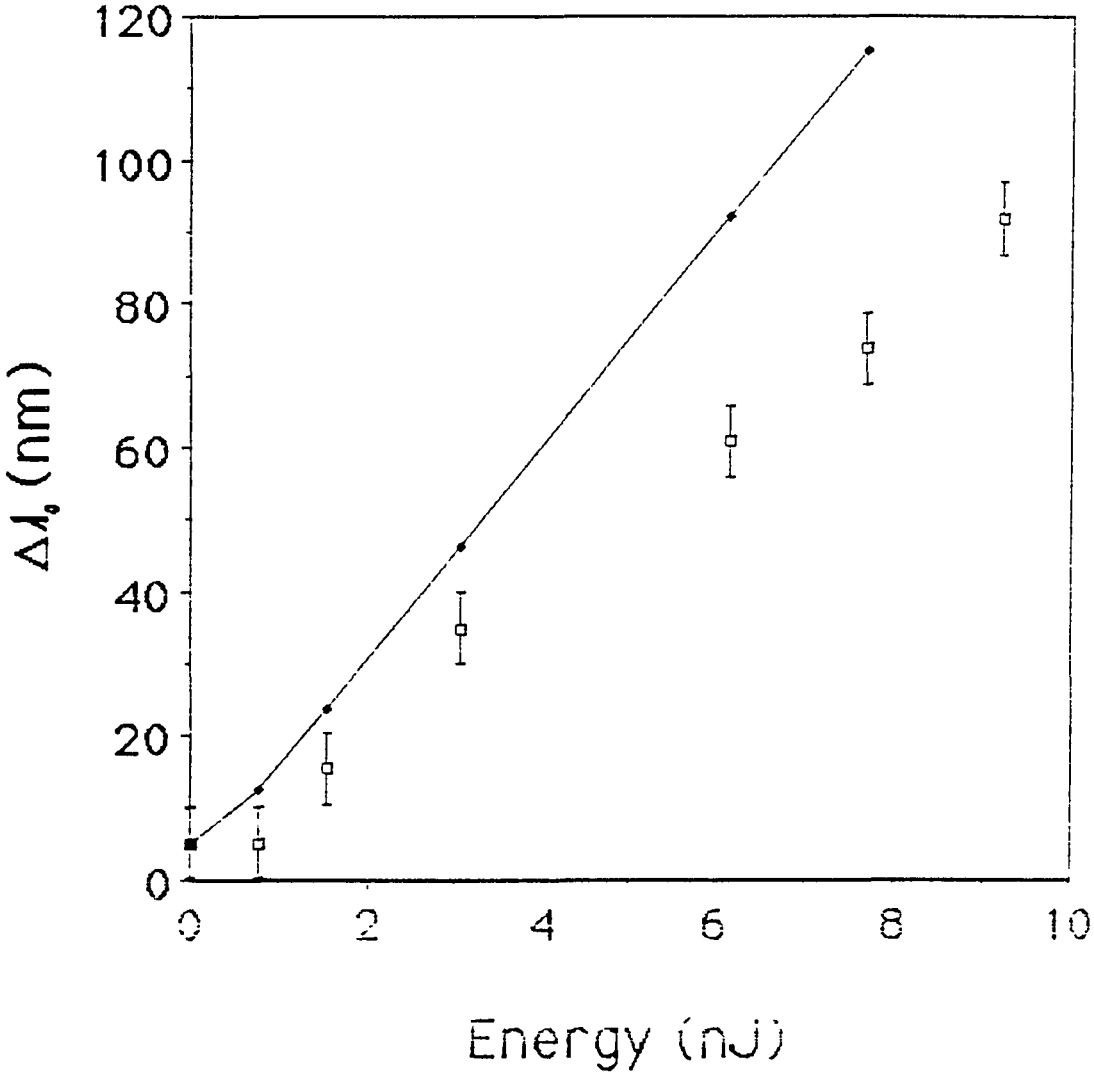

Fig. 2.4.3 Supercontinuum spectral width versus the input pulse energy coupled into the fiber. The solid line is the theoretical fit using equations 2.17a-b for a 100-fsec pulse duration.

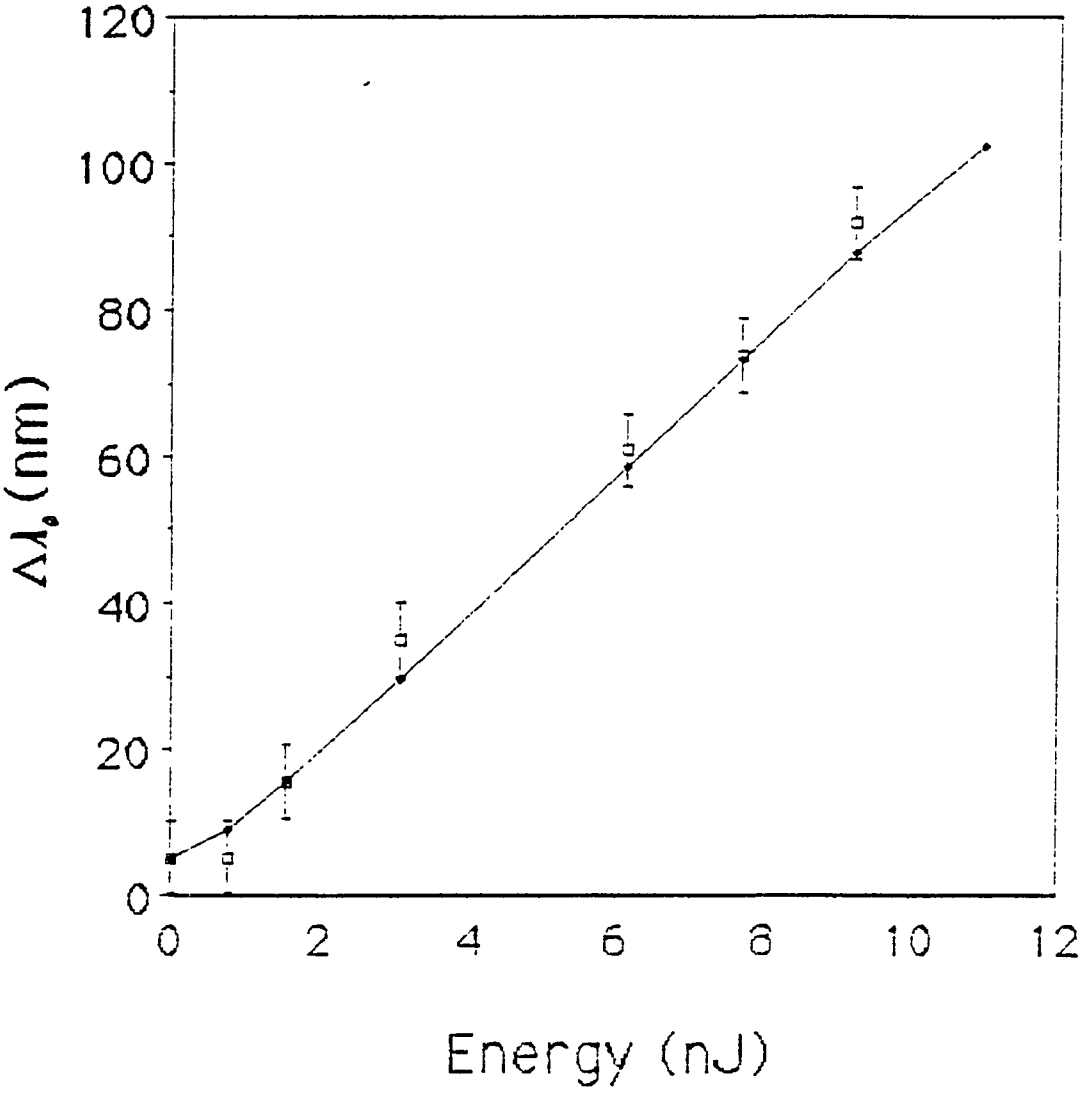

Fig. 2.4.4 Same as figure 2.4.3 with the theoretical fit for a 126-fsec pulse duration.

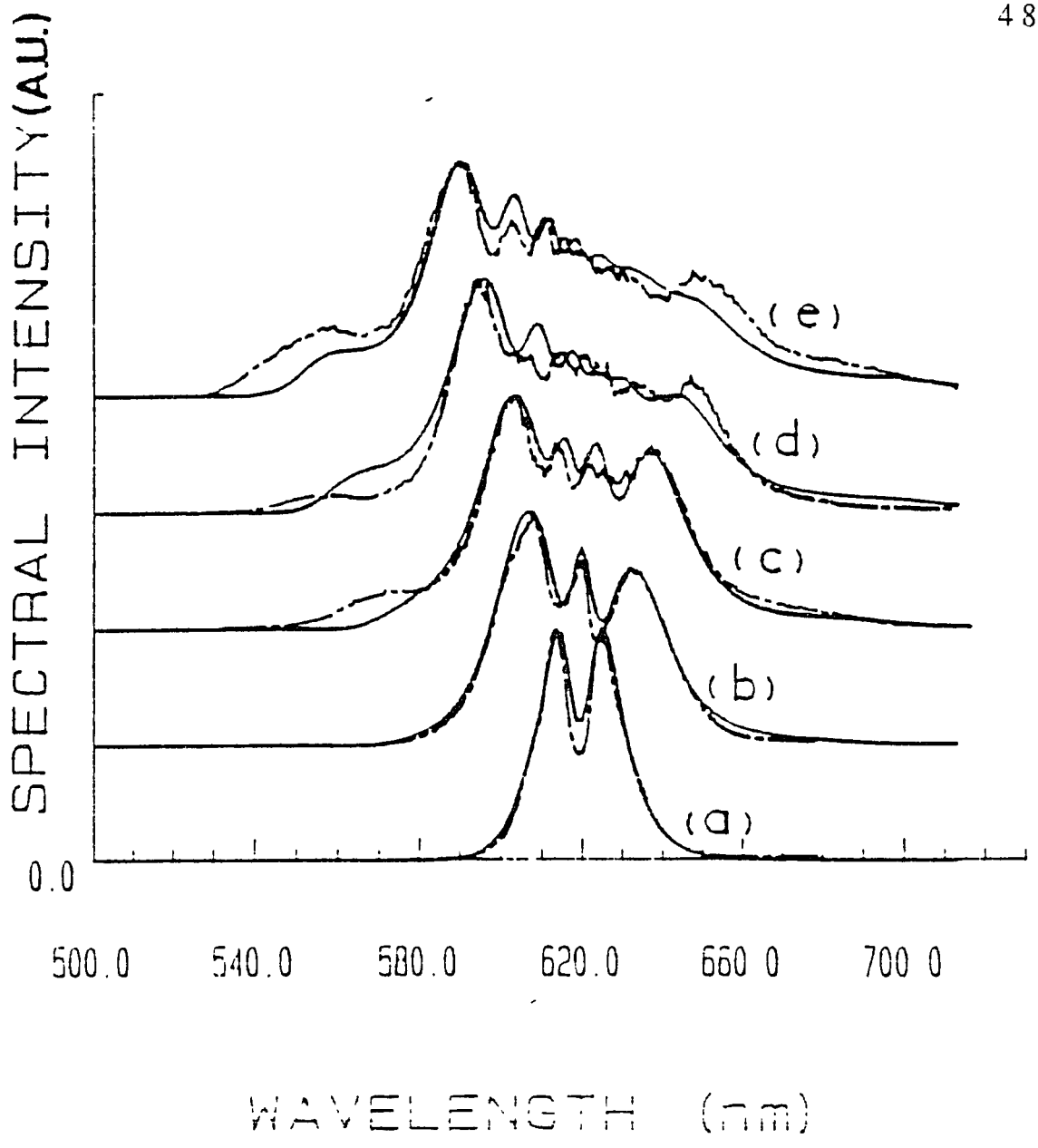

Fig. 2.4.5 Femtosecond supercontinuum generation in optical fibers by Boyer and Franco (solid curves).[11] The theoretical fits (dashed curves) correspond to 55-fsec pulses with intensities of 0.25, 0.7, 1.3, 2.0 and 3.0 TW/cm^2 for curves (a) to (e), respectively.

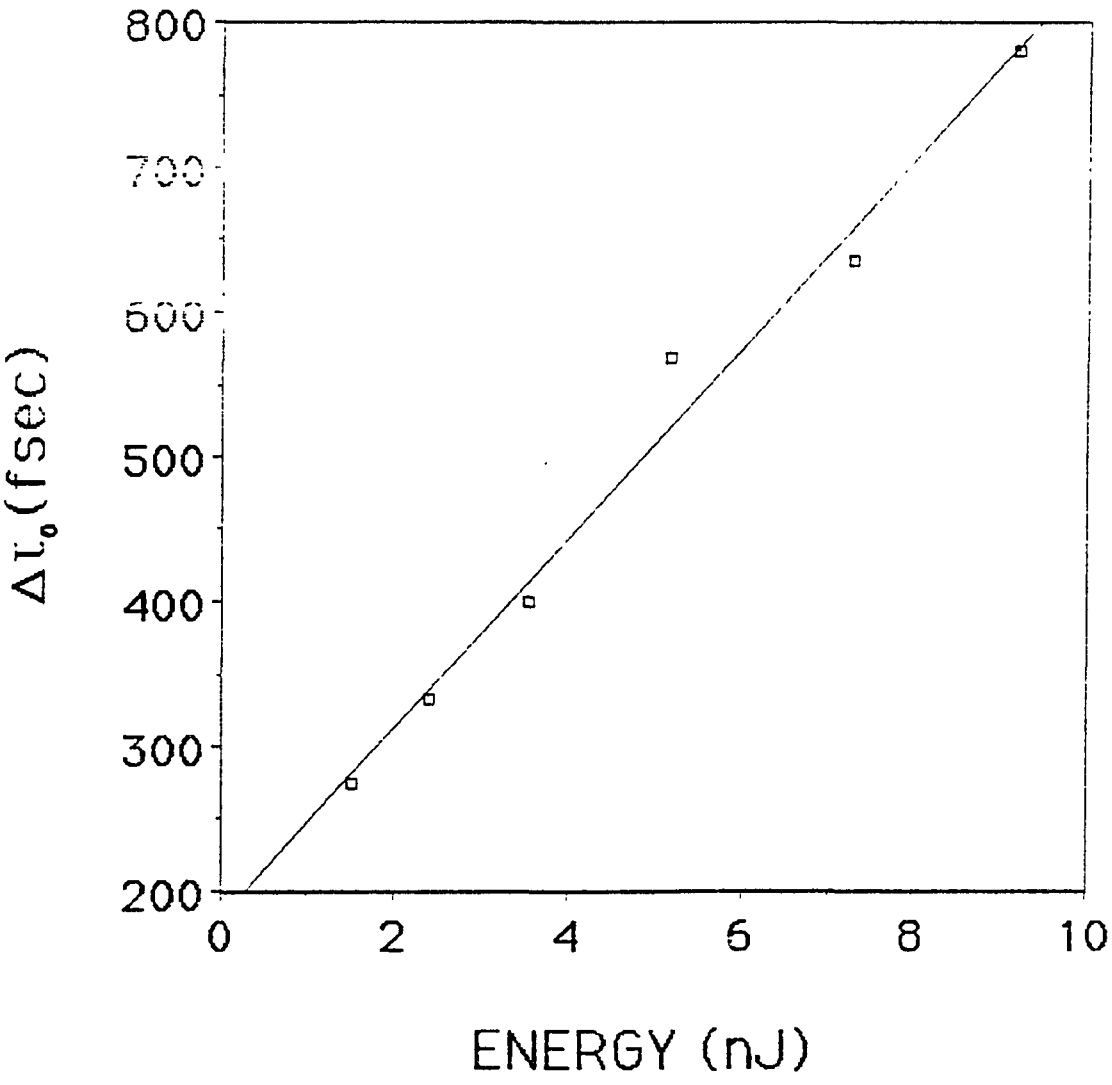

Fig. 2.4.6 Supercontinuum temporal width versus the input pulse energy coupled into the fiber.

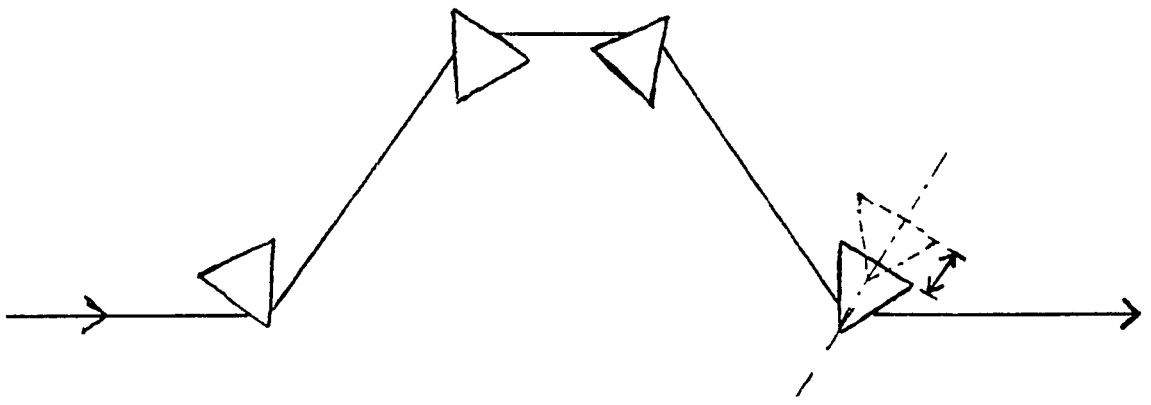

Fig. 2.5.1 Schematic of a 4-prism femtosecond pulse compressor.

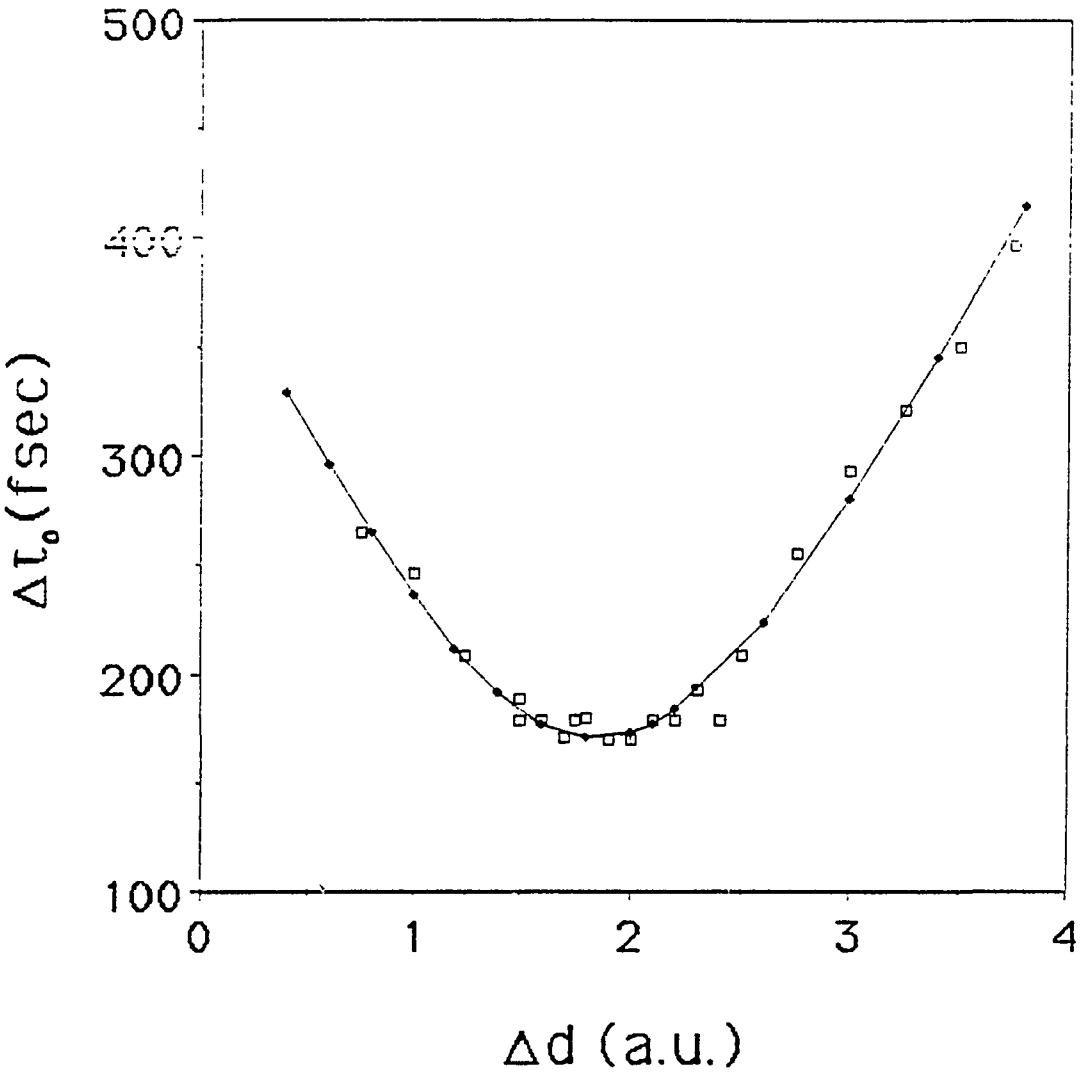

Fig. 2.5.2 Temporal width of a compressed supercontinuum pulse versus the amount of glass in the 4-prism pulse compressor. The supercontinuum pulse wás obtained with a 7-mm fiber length.

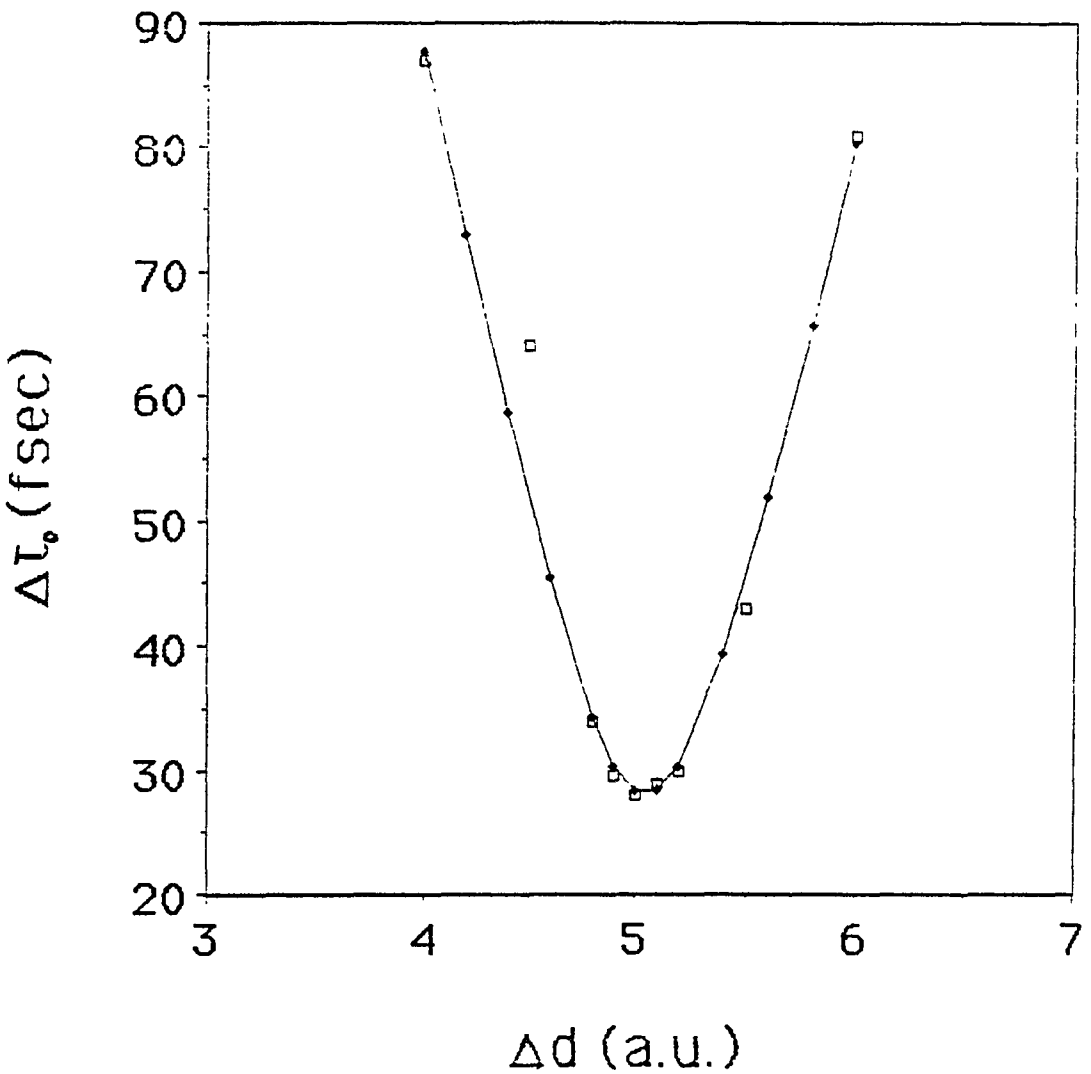

Fig. 2.5.3 Same as 2.5.1 for supercontinuum pulses obtained with a 20-mm fiber length.

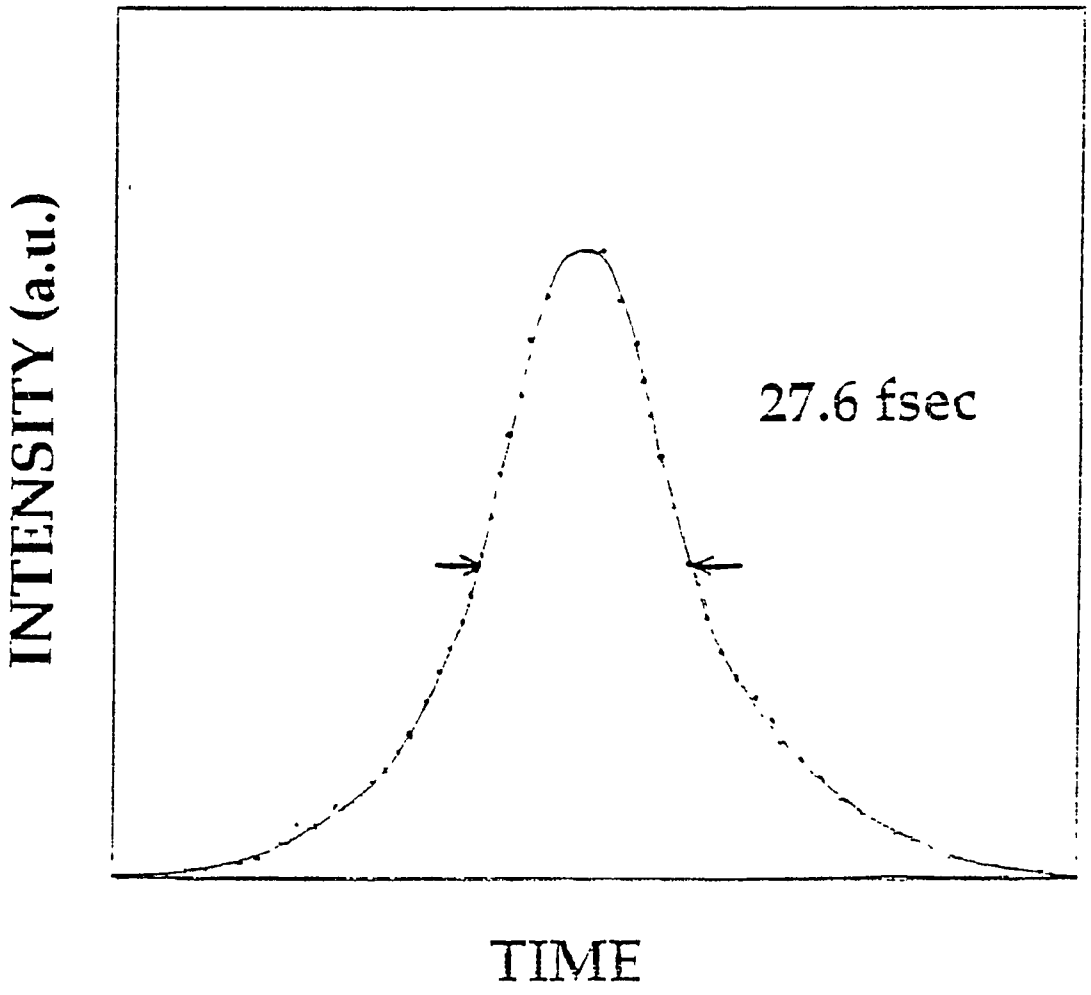

Fig. 2.5.4 Autocorrelation of a supercontinuum pulse compressed with a 4-prism sequence.

2.6 References

1. N. Bloembergen. *Nonlinear Optics* (Benjamin, Reading, Mass., 1977).

2. R.R. Alfano, *Interactions of picosecond pulses with matter* , Ph. D. Thesis, GTE Technical report TR72-330.1 (1972).

3. Y.R. Shen. *Principles of Nonlinear Optics* (Wiley, New York, 1984).

4. M. Schubert and B. Wilhelmi. *Nonlinear Optics and Quantum Electronics* (John Wiley, New York, 1986).

5. R.R. Alfano, Editor, *The Supercontinuum Laser Source,* (Springer-Verlag, Berlin, Heilderberg, 1989).

6. Govind P. Agrawal, *Nonlinear Fiber Optics* (Academic Press, London, 1989), and references therein.

7. Q. X. Li, T. Jimbo, P.P. Ho, and R.R. Alfano. Appl. Opt. **25,** 1869-1871 (1986).

8. R. Dorsinville, P. Delfyett, and R.R. Alfano. Appl. Opt. **26** (1987).

9. P.L. Baldeck, P.P. Ho, and R.R. Alfano. Rev. Phys. Appl. **22,** 1677-1694 (1987).

10. M. Mihailidi, Y. Budanski, X. M. Zhao, Y Takiguchi, and R.R. Alfano. Opt. Lett. **13,** 987 (1988).

11. G.R. Boyer and M.A. Franco. Opt. Lett. **14,** 465-467 (1989).

12. E. Bourkoff, W. Zhao, R.I. Joseph, and D.N. Christodoulides. Opt. Lett. **12,** 272-274 (1987).

13. E. Bourkoff, W. Zhao, R.I. Joseph, and D.N. Christodoulides. Opt. Comm. **62,** 284-288 (1987).

14. Weimin Zhao and E. Bourkoff. IEEE J. Quantum Electron. **QE-24,** 365-372 (1988).

15. E.P. Treacy. IEEE J. Quantum Electron. **QE-9,** 454 (1969).

16. J.G. Fujimoto, A.M. Weiner, and E.P. Ippen. Appl. Phys. Lett. **44**, 832 (1984).

17. J.M. Halbout and D. Grischkovsky. Appl. Phys. Lett. **45**, 1281 (1984).

18. W.H. Knox, R.L. Fork, M.C. Downer, R.H. Stolen, A. Valdmanis, and C.V. Shank. Appl. Phys. Lett. **46**, 1120 (1985).

19. W.J. Tomlinson and W.H. Knox. J. Opt. Soc. Am. **B4**, 1404 (1987).

20. F. Salin and A. Brun. J. Appl. Phys. **61**, 4736-4739 (1987).

21. R.L. Fork, O.E. Martinez, and J.P. Gordon. Opt. Lett. **9**, 150 (1984).

CHAPTER 3

CROSS-PHASE MODULATION: A NEW TECHNIQUE FOR CONTROLLING THE PROPERTIES OF ULTRASHORT PULSES

3.1 Introduction.

Self-phase modulation (SPM) is the principal mechanism responsible for the generation of picosecond and femtosecond white-light supercontinua.[1] When an intense ultrashort pulse propagates through a medium, it distorts the atomic configuration of the material, which changes the refractive index. The pulse phase is time-modulated, which causes the generation of new frequencies. This phase modulation originates from the pulse itself (*self*-phase modulation). It can also be generated by a copropagating pulse (*cross*-phase modulation).

Several schemes of nonlinear interaction between optical pulses can lead to cross-phase modulation (XPM). For example, XPM is intrinsic to the generation processes of stimulated Raman scattering (SRS) pulses, second harmonic generation (SHG) pulses, and stimulated four photon mixing (SFPM) pulses. More important, the XPM generated by pump pulses can be

used to control, with femtosecond time response, the spectral, temporal, and spatial properties of ultrashort probe pulses.

Early studies on XPM characterized induced polarization effects (optical Kerr effect) and induced phase changes, but did not investigate spectral, temporal and spatial effects on the properties of ultrashort pulses. In 1980, Gersten, Alfano, and Belic predicted that Raman spectra of ultrashort pulses would be broadened by XPM.[2] The first experimental observation of XPM spectral effects dates to the early 1986, when it was reported that intense picosecond pulses could be used to enhance the spectral broadening of weaker pulses copropagating in bulk glasses.[3-4] Since then, several groups have been studying XPM effects generated by ultrashort pump pulses on copropagating Raman pulses,[5-13] second harmonic pulses,[14-18] stimulated four-photon mixing pulses,[19] and probe pulses. [4,20,30,31]

Recently, it has been shown that XPM leads also to the generation of modulation instability,[21-26] solitary waves,[8,27] and pulse compression[28-30]. Finally, XPM effects on ultrashort pulses have been proposed to tune the frequency of probe pulses,[31] to eliminate the soliton self-frequency shift effect,[32] and to control the spatial distribution of light.[33]

This chapter presents our key theoretical and experimental research that has predicted and described spectral, and temporal effects attributed to XPM. In Section 3.2, the basis of the XPM theory is outlined. The nonlinear polarizations, XPM phases, and spectral distributions of copropagating pulses are computed. The effects of pulse walk-off, input time delay, and group velocity dispersion time broadening are particularly discussed. In Section 3.3,

measurements of spectral broadening enhancement, induced-frequency shift, and XPM-induced optical amplification are presented. Sections 3.4, and 3.5 consider the effects of XPM on Raman pulses, and stimulated four-photon mixing pulses, respectively. Finally, section 3.6 presents the theory and measurements of modulation instability induced by cross-phase modulation in the normal dispersion region of optical fibers.

3.2 Cross-Phase Modulation Theory.

3.2.1 Coupled Nonlinear Equations of Copropagating Pulses.

The methods of multiple scales and slowly varying amplitude (SVA) are the two independent approximations used to derive the coupled nonlinear equations of copropagating pulses. The multiple scale method which have been used for the first theoretical study on induced-phase modulation is described in Ref. 4. The following derivation is based on the SVA approximation. [34]

The optical electromagnetic field of two copropagating pulses must ultimately satisfy Maxwell's vector equation:

$$\nabla x \nabla x \mathbf{E} = -\mu_0 \frac{\partial \mathbf{D}}{\partial t} \qquad (3.1\text{-a})$$

and

$$\mathbf{D} = \varepsilon \mathbf{E} + \mathbf{P}^{NL} \qquad (2.1\text{-b})$$

where ϵ is the medium permitivity at low intensity, and $\mathbf{P}^{NL}$ is the nonlinear polarization vector.

Assuming: a pulse duration much longer than the response time of the medium, an isotropic medium, the same linear polarization for the copropagating fields, and no frequency dependence for the nonlinear susceptibility $\chi^{(3)}$, the nonlinear polarization reduces to:

$$P^{NL}(r, z,t) = \chi^{(3)} E^3(r, z, t) \tag{3.2}$$

where the transverse component of the total electric field can be approximated by:

$$E(r, z, t) = \frac{1}{2}\left\{ A_1(r, z, t)\, e^{i\left(\omega_1 t - \beta_1 z\right)} + A_2(r, z, t)\, e^{i\left(\omega_2 t - \beta_2 z\right)} + c.c. \right\} \tag{3.3}$$

A_1 and A_2 refer to the envelopes of copropagating pulses of carrier frequency ω_1 and ω_2, β_1 and β_2 are the corresponding propagation constants, respectively.

Substituting Eq. 3.3 into Eq. 3.2 and keeping only the terms synchronized with ω_1 and ω_2, one obtains:

$$P^{NL}(r, z, t) = P_1^{NL}(r, z, t) + P_2^{NL}(r, z, t) \tag{3.4-a}$$

$$P_1^{NL}(r, z, t) = \frac{3}{8}\chi^{(3)}\left(|A_1|^2 + 2|A_2|^2\right)A_1 e^{i(\omega_1 t - \beta_1 z)} \tag{3.4-b}$$

$$P_2^{NL}(r, z, t) = \frac{3}{8}\chi^{(3)}\left(|A_2|^2 + 2|A_1|^2\right)A_2 e^{i(\omega_2 t - \beta_2 z)} \tag{3.4-c}$$

Equivalently, using $n_2 = 3\chi^{(3)}/8n$, one obtains:

$$n(\omega_1) = n_{01} + n_2(|A_1|^2 + 2|A_2|^2) \tag{3.4-d}$$

$$n(\omega_2) = n_{02} + n_2(2|A_1|^2 + |A_2|^2) \tag{3.4-e}$$

P_1^{NL} and P_2^{NL}, and $n(\omega_1)$ and $n(\omega_2)$ are the nonlinear polarizations and intensity-dependent refractive indexes at frequencies ω_1 and ω_2, respectively. The second terms in the right sides of Eqs. 3.4-b-e are cross-phase modulations terms. Note, the factor of two. For optical fibers $n_2 = 3.2X\ 10^{-16}\ cm^2/W$.

Combining Eqs. 3.1-3.4 and using the slowly-varying envelope approximation (at the first order for the nonlinearity), one obtains the coupled nonlinear wave equations:

$$\frac{\partial A_1}{\partial z}+\frac{1}{v_{g1}}\frac{\partial A_1}{\partial t}+\frac{i}{2}\beta_1^{(2)}\frac{\partial^2 A_1}{\partial t^2}=i\frac{\omega_1}{c}n_2\left[\left|A_1\right|^2+2\left|A_2\right|^2\right]A_1 \qquad (3.5\text{-a})$$

$$\frac{\partial A_2}{\partial z}+\frac{1}{v_{g2}}\frac{\partial A_2}{\partial t}+\frac{i}{2}\beta_2^{(2)}\frac{\partial^2 A_2}{\partial t^2}=i\frac{\omega_2}{c}n_2\left[\left|A_2\right|^2+2\left|A_1\right|^2\right]A_2 \qquad (3.5\text{-b})$$

where v_{gi} is the group velocity for the wave i, and $\beta_i^{(2)}$ is the group velocity dispersion for the wave i.

In the most general case, numerical methods are used to solve Eqs. 3.5. However, they have analytical solutions when the group-velocity dispersion temporal broadening can be neglected.

Denoting, the amplitude and phase of the pulse envelope by a and α, that is:

$$A_1(\tau, z)= a_1(\tau, z)\, e^{i\alpha_1(\tau, z)} \quad \text{and} \quad A_2(\tau, z)= a_2(\tau, z)\, e^{i\alpha_2(\tau, z)} \qquad (3.6)$$

Assuming $\beta_1^{(2)} \approx \beta_2^{(2)} \approx 0$, Eqs. 3.5-a and 3.5-b reduce to:

$$\frac{\partial a_1}{\partial z} = 0 \tag{3.7-a}$$

$$\frac{\partial \alpha_1}{\partial z} = i \frac{\omega_1}{c} n_2 \left[a_1^2 + 2a_2^2 \right] \tag{3.7-b}$$

$$\frac{\partial a_2}{\partial z} + \left(\frac{1}{v_{g2}} - \frac{1}{v_{g1}} \right) \frac{\partial a_2}{\partial \tau} = 0 \tag{3.7-c}$$

$$\frac{\partial \alpha_2}{\partial z} = i \frac{\omega_2}{c} n_2 \left[a_2^2 + 2a_1^2 \right] \tag{3.7-d}$$

where $\tau = (t - z/v_{g1})/T_0$ and T_0 is the 1/e pulse duration.

In addition, Gaussian pulses are chosen at z=0:

$$A_1(\tau, z=0) = \sqrt{\frac{P_1}{A_{eff}}}\, e^{-\tau^2/2} \tag{3.8-a}$$

$$A_2(\tau, z=0) = \sqrt{\frac{P_2}{A_{eff}}}\, e^{-(\tau - \tau_d)^2/2} \tag{3.8-b}$$

where P is the pulse peak power, A_{eff} is the effective cross-section area, and $\tau_d = T_d/T_0$ is the normalized time delay between pulses at z=0.

With the initial conditions defined by Eqs. 3.8, Eqs. 3.5 have analytical solutions when temporal broadenings are neglected:

$$A_1(\tau, z) = \sqrt{\frac{P_1}{A_{eff}}}\, e^{-\tau^2/2}\, e^{i\,\alpha_1(t, z)} \tag{3.9-a}$$

$$A_2(\tau, z) = \sqrt{\frac{P_2}{A_{eff}}}\, e^{-\left(\tau - \tau_d - \frac{z}{L_w}\right)^2/2}\, e^{i\alpha_2(\tau, z))} \tag{3.9-b}$$

$$\alpha_1(\tau, z) = \frac{\omega_1}{c} n_2 \frac{P_1}{A_{eff}} z\, e^{-\tau^2} + \sqrt{\pi}\, \frac{\omega_1}{c} n_2 \frac{P_2}{A_{eff}} L_w \left[\mathrm{erf}(\tau - \tau_d) - \mathrm{erf}\left(\tau - \tau_d - \frac{z}{L_w}\right) \right] \tag{3.9-c}$$

$$\alpha_2(\tau,z)=\frac{\omega_2}{c}n_2\frac{P_2}{A_{eff}}z\,e^{-\left(\tau-\tau_d-\frac{z}{L_w}\right)^2}+\sqrt{\pi}\frac{\omega_2}{c}n_2\frac{P_1}{A_{eff}}L_w\left[\mathrm{erf}(\tau)-\mathrm{erf}\left(\tau-\frac{z}{L_w}\right)\right] \tag{3.9-d}$$

where $L_W=T_o/(1/v_{g1}-1/v_{g2})$ is defined as the walk-off length. T_0 is the 1/e pulse duration.

Equations 3.9-c and 3.9-d show that the phases $\alpha_i(\tau,z)$ of copropagating pulses which overlap in a nonlinear Kerr medium are modified by a cross-phase modulation via the peak power $P_{j\neq i}$. In the case of ultrashort pulses this cross-phase modulation gives rise to the generation of new frequencies as does self-phase modulation.

The instantaneous XPM-induced frequency chirps are obtained by differentiating Eqs. 3.9-c and 3.9-d according to the instantaneous frequency formula $\Delta\omega=-\partial\alpha/\partial\tau$. These are:

$$\Delta\omega_1(\tau,z)=2\frac{\omega_1}{c}n_2\frac{P_1}{A_{eff}}\frac{z}{T_0}\tau\,e^{-\tau^2}+2\frac{\omega_1}{c}n_2\frac{P_2}{A_{eff}}\frac{L_w}{T_0}\left[e^{-\left(\tau-\tau_d-z/L_w\right)^2}-e^{-\left(\tau-\tau_d-z/L_w\right)^2}\right] \tag{3.10-a}$$

$$\Delta\omega_2(\tau, z) = 2\frac{\omega_2}{c} n_2 \frac{P_2}{A_{eff}} \frac{z}{T_0} \tau e^{-\left(\tau - \tau_d - z/L_w\right)^2} + 2\frac{\omega_2}{c} n_2 \frac{P_1}{A_{eff}} \frac{L_w}{T_0} \left[e^{-\tau^2} - e^{-\left(\tau - z/L_w\right)^2} \right]$$

(3.10-b)

where $\Delta\omega_1=\omega-\omega_1$, and $\Delta\omega_2=\omega-\omega_2$. The first and second terms on the right sides of Eq. 3.10-a and 3.10-b are contributions arising from SPM and XPM, respectively. It is interesting to notice in Eq. 3.10 than the maximum frequency chirp arising from XPM is inversely proportional with the group velocity mismatch $L_w/T_0=1/(1/v_{g1}-1/v_{g2})$ rather than with the pump pulse time duration or distance traveled z like for SPM. Therefore, the time duration of pump pulses does not have to be as short as the time duration of probe pulses for XPM applications.

More generally, spectral profiles affected by XPM can be studied by computing the Fourier transform:

$$S(\omega-\omega_0, z) = \frac{1}{2\pi} \int_{-\infty}^{+\infty} a(\tau, z) e^{i\,\alpha(\tau, z)} e^{i(\omega-\omega_0)\tau} d\omega$$

(3.11)

where $|S(\omega-\omega_0, z)|^2$ represents the spectral intensity distribution of the pulse. Eq. 3.10 is readily evaluated numerically using fast Fourier transform algorithms.

Analytical results of Eqs. 3.9 take in account XPM, SPM and group velocity mismatch. These results are used in the Sec. 3.2.2 to isolate the specific spectral features arising from the nonlinear interaction of copropagating pulses. Higher order effects due to group velocity dispersion broadening are discussed in Sec. 3.2.3.

3.2.2 Spectral Broadening Enhancement.

The spectral evolution of ultrashort pulses interacting in a nonlinear Kerr medium is affected by the combined effects of XPM, SPM and pulse walk-off. For a negligible group velocity mismatch, XPM causes the pulse spectrum to broaden more than expected from SPM alone.[3-4] The pulse phase of Eq. 3.9-c and 3.9-d reduces to:

$$\alpha_i(\tau, z) = \frac{\omega_i}{c} n_2 \frac{(P_i + 2P_j)}{A_{eff}} z\, e^{-\tau^2} \tag{3.12}$$

The maximum spectral broadening of Gaussian pulses, computed using Eqs. 3-12, is given by:

$$\Delta\omega_i(z) \approx \frac{\omega_i}{c} n_2 \frac{(P_i + 2P_j)}{A_{eff}} \frac{z}{T_0} \tag{3.13}$$

Thus, the spectral broadening enhancement arising from XPM is given by:

$$\frac{\Delta\omega_{i_{SPM+XPM}}}{\Delta\omega_{i_{SPM}}} = 1 + \frac{2P_j}{P_i} \tag{2.14}$$

Therefore, XPM can be used to control the spectral broadening of probe pulses using strong command pulses. This spectral control is important for it is based on the electronic response of the interacting medium. It could be turned on and off in a few femtoseconds which could lead to applications such as the pulse compression of weak probe pulses, frequency-based optical computation schemes and the frequency multiplexing of ultrashort optical pulses with THz repetition rates.

The effect of pulse walk-off on XPM-induced spectral broadening can be neglected when wavelengths of pulses are in the low dispersion region of the nonlinear material, the wavelength difference or/and the sample length are small, and the time duration of pulses is not too short. For other physical situations, the group velocity mismatch and initial time delay between pulses affect strongly the spectral shape of interacting pulses.

Figure 3.2.1 shows how the spectrum of a weak probe pulse can be affected by the XPM generated by a strong copropagating pulse. The wavelength of the pump pulse had been chosen where the pump pulse travels faster than the probe pulse. Initial time delays between pulses at the entrance of the nonlinear medium had been selected to display the most characteristic interaction schemes. Fig. 3.2.1-a and Fig. 3.2.1-b are displayed for reference. They show the probe pulse spectrum without XPM interaction (3.2.1-a) and after the XPM interaction but for negligible group velocity mismatch (3.2.1-b). Fig. 3.2.1-c is for the case of no initial time delay and total walk-off. The probe spectrum is shifted and broadened by XPM. The anti-Stokes shift is characteristic of the probe and pump pulse walk-off. The probe

pulse is blue-shifted because it is modulated only by the back of the faster pump pulse. When the time delay is chosen such as the pump pulse enter in the nonlinear medium after the probe and has just time to catch-up the probe pulse, one obtains a similar broadening than in Fig. 3.2.1-c but with a reverse Stokes shift (Fig. 3.2.1-d). The XPM broadening becomes symmetrical when the input time delay not only allows the pump pulse to catch-up but also to pass partially through the probe pulse (Fig. 3.2.1-e). However, if the interacting length is long enough to allow the pump pulse to completely overcome the probe pulse there is no XPM-induced broadening (Fig. 3.2.1-f).

The diversity of spectral features displayed in Figs. 3.2.1 can easily been understood by computing the phase and frequency chirp given by Eqs. 3.9 and 3.10 (Fig. 3.2.2). For reference, Fig. 3.2.2-a shows the locations of the pump pulse (solid line) and the probe pulse (dotted line) at the output of the nonlinear sample (case of no initial delay and total walk-off). In this case the XPM phase, which is integrated over the fiber length, has the characteristic shape of an error function whose maximum corresponds to neither the probe pulse maximum nor the pump pulse maximum (Fig. 3.2.2-b). The probe pulse (dotted line in Fig. 3.2.2-c) sees only the blue part of the frequency chirp (solid line in Fig. 3.2.2-c) generated by the pump pulse. As a result, the probe spectrum is simultaneously broadened and shifted toward the highest frequencies (Fig. 3.2.1-c). One should notice that opposite to the SPM frequency chirp, the XPM chirp in Fig. 3.2.2-c is not monotonic. The pulse leading edge and trailing edge have a positive chirp and negative chirp, respectively. As a result, dispersive effects (GVD, grating pair,...) are different for the pulse front and the pulse back. In the regime of normal dispersion

($\beta^{(2)}>0$), the pulse front would be broadened by GVD while the pulse back would be sharpened. Figs. 3.2.2-d and 3.2.2-e show XPM-induced phase and frequency chirp for the mirror-image case of Figs. 3.2.2-a 3.2.2-b. The probe spectrum is now shifted toward the smallest frequencies. Its leading edge has a negative frequency chirp, while the trailing edge has a positive one. A positive GVD would compress the pulse front and broaden the pulse back. The case of a partial symmetrical walk-off is displayed in Figs. 3.2.2-f and 3.2.2-g. In first approximation, the time dependence of the XPM phase associated with the probe pulse energy is parabolic (Fig. 3.2.2-f), and the frequency chirp is quasi-linear (3.2.2-g). This is the prime quality needed for the compression of a weak pulse by following the XPM interaction by a grating pair compressor. Figs. 3.2.2-f & 3.2.2-g show why there is almost not spectral broadening enhancement when the pump pulse passes completely through the probe pulse (Fig. 3.2.1-f): the part of XPM associated with the probe pulse energy is constant (Fig. 3.2.2-h). The probe pulse is phase modulated, but **the phase shift is time independent.** Therefore, there is neither frequency chirp (Fig. 3.2-i) nor spectral broadening enhancement by XPM.

The combined effects of XPM and walk-off on the spectra of weak probe pulses (negligible SPM) have been shown in Fig. 3.2.1 and 3.2.2. When the group velocity mismatch is large, the spectral broadening is not significant, and the above spectral features reduce to a tunable induced-frequency shift of the probe pulse frequency (see Sec. 3.3.1). When strong probe pulses are used, the SPM contribution has to be included in the analysis. Figure 3.2.3 shows how the results of Fig. 3.2.1 are modified when the probe power is the same as the pump power, i.e. the SPM has to be taken

in account. Fig. 3.3-a shows the spectral broadening arising from the SPM alone. Combined effects of SPM and XPM are displayed in Figs. 3.2.3-b to 3.2.3-e with the same initial delays than in Fig. 3.2.1. The SPM contribution to the spectral broadening is larger than the XPM contribution because the XPM interaction length is limited by the walk-off between pump and probe pulses.

The XPM spectral features described in this section have been obtained using first order approximation of the nonlinear polarization, propagation constant and nonlinearity in the nonlinear wave equation (Eq. 3.1). Moreover, plane wave solutions and peak powers below the stimulated Raman scattering threshold have been assumed. For practical purposes it is often necessary to include the effects of 1) first and second order group velocity dispersion broadening $\beta^{(2)}$ and $\beta^{(3)}$, 2) induced and self-steepening, 3) four wave mixing occuring when pump and probe pulses are coupled through $\chi^{(3)}$, 4) stimulated Raman scattering generation, and 5) the spatial distribution of interacting fields (i.e., induced and self-focusing, diffraction, Gaussian profile of beams...). In Sec. 3.2.3, the combined effect of XPM with group velocity dispersion broadening $\beta^{(2)}$ is shown to lead to a new kind of optical wave breaking.

3.2.3 Optical Wave Breaking and Pulse Compression due to Cross-phase Modulation in Optical Fibers.

When an ultrashort light pulse propagates through an optical fiber, its shape and spectrum changes considerably as a result of the combined effect of group-velocity dispersion $\beta^{(2)}$ and self-phase modulation. In the normal-dispersion regime of the fiber ($\lambda \leq 1.3$ μm), the pulse can develop rapid oscillations in the wings together with spectral side lobes as a result of a phenomenon known as optical wave breaking (Tomlinson et al. 1983). In this section, it is shown that a similar phenomenon can lead to rapid oscillations near one edge of a weak pulse that copropagates with a strong pulse. [30]

To isolate the effects of XPM from SPM, a pump-probe configuration is chosen ($P_2 \ll P_1$) so that the pulse P_1 plays the role of the pump pulse and propagates without being affected by the copropagating probe pulse P_2. The probe pulse P_2, however, interacts with the pump pulse through XPM. To study how XPM affects the probe evolution along the fiber, Eqs. 3.5-a and 3.5-b have been solved numerically using a generalization of the beam-propagation or the split-step method.[34] The numerical results depend strongly on the relative magnitudes of the length scales L_d and L_w, where $L_d = T_0^2 / |\beta_2|$ is the dispersion length, i.e. the distance at which GVD doubles the time duration of the pulse, and $L_w = v_{g1} v_{g2} T_0 / |v_{g1} - v_{g2}|$ is the walk-off length, i.e. the distance at which the pulses are separated by the delay T_0. If $L_w \ll L_d$, the pulses walk-off from each other before GVD has an opportunity to influence the pulse evolution. However, if L_w and L_d become comparable, both XPM and GVD can act together and modify the pulse shape and spectra with new features.

To show these features as simply as possible, a specific case is considered in which $L_w/L_d=0.1$ and $\lambda_1/\lambda_2=1.2$. Both pulses are assumed to propagate in the normal GVD regime with $\beta_1=\beta_2>0$. It is assumed that the pump pulse goes faster than the probe pulse ($v_{g1}>v_{g2}$). At the fiber input both pulses are taken to be a Gaussian of the same width with an initial delay τ_d between them. First, the case $\tau_d=0$ is considered so that the two pulses overlap completely at z=0. Figure 3.2.4 shows the shapes and spectra of the pump and probe pulses at $z/L_d=0.4$ obtained by solving Eqs. 3.2.5-a and 3.2.5-b numerically with the normalized pump power $N=(2\pi/\lambda_1 P_1 L_d)^{0.5}=10$, where N=1 corresponds to power of the fundamental soliton[34]. For comparison, Fig. 3.2.5 shows the probe and pump spectra under identical conditions but without GVD effects ($\beta_1=\beta_2=0$). The pulse shapes are not shown since they remain unchanged when the GVD effects are excluded.

From a comparison of Figs. 3.2.4 and 3.2.5 it is evident that GVD can substantially affect the evolution of features expected from SPM or XPM alone. Consider first the pump pulse for which XPM effects are absent. The pulse shape and the spectrum shown on the right column exhibit features expected from dispersive SPM for N=10. With further propagation, the pump pulse eventually develops rapid oscillations in the wings as a result of conventional SPM-induced optical wave breaking. Consider now the probe pulse for which SPM effects are absent, and probe pulse evolution is governed by dispersive XPM. In absence of GVD, the pulse shape would be a narrow Gaussian centered at $\tau=4$ (the relative delay at the fiber output because of group-velocity mismatch). The GVD effects not only broaden the pulse considerably but also induce rapid oscillations near the trailing edge of the

probe pulse. These oscillations are due to XPM-induced optical wave breaking.

To understand the origin of XPM-induced optical wave breaking, it is useful to consider the frequency chirp imposed on the probe pulse by the copropagating pulse. As there is total walk-off and no initial delay, maximum chirp occurs at the center of the probe pulse. Since the chirp is positive, blue-shifts components are generated by XPM near the pulse center. As a result of the normal GVD, the peak of the probe pulse moves slower than its tails. Since the peak lags behind as the probe pulse propagates, it interferes with the trailing edge. Oscillations seen near the trailing edge of the probe pulse in Fig. 3.2.4 result from such an interference. Since the basic mechanism is similar to the optical wave breaking phenomenon occuring in the case of dispersive XPM, we call it XPM-induced optical wave breaking.

In spite of the identical nature of the underlying physical mechanism, optical wave breaking exhibits different qualitative features in the case of XPM compared with the SPM case. The most striking difference is that the pulse shape is asymmetric with only one edge developing oscillations. For the case shown in Fig. 3.2.4 oscillations occur near the trailing edge. If the probe and pump wavelengths were reversed so that the pump pulse moves slower than the probe pulse. Oscillations would occur near the leading edge since the pump pulse would interact mainly with that edge. In fact, in that case the shape and the spectrum of the probe pulse are just the mirror images of those shown in Figs. 3.2.4 and 3.2.5.

The effect of initial delay between probe and pump pulses is now investigated. The effect of initial delay on XPM-induced spectral broadening has been discussed in the dispersionless limit ($\beta_1=\beta_2=0$) in Sec. 3.2. For example, if the pump pulse is delayed by the right amount so that it catches up with the probe pulse at the fiber output, the probe spectrum is just the mirror image of that shown in Fig. 3.2.4, exhibiting a red shift rather than a blue shift. Furthermore, if τ_d is adjusted such that the pump pulse catches up with the probe pulse halfway through the fiber, the probe spectrum is symmetrically broadened since the pump walks through the probe in a symmetric manner. Our numerical results show that the inclusion of GVD completely alters this behavior. Figure 3.2.6 shows the probe shape and spectrum under conditions identical to those of Fig. 3.2.4 except that the probe pulse is advanced ($\tau_d=-2$) such that the pump pulse would catch it halfway through the fiber in the absence of GVD effects. The lower row shows the expected behavior in the dispersionless limit showing the symmetrical spectral broadening in this case of symmetrical walk-off. A direct comparison reveals how much the presence of GVD can affect the SPM effects on the pulse evolution. In particular, both the pulse shape and spectra are asymmetric. More interestingly, the probe pulse is compressed, in sharp contrast to the case of Fig. 3.2.4 where GVD led to a huge broadening. This can be qualitatively understood from Eq. 3.10. For the case shown in Fig. 3.2.6, the XPM-induced chirp is negative and nearly linear across the trailing part of the probe pulse. Because of this chirp, the travelling part is compressed as the probe pulse propagates inside the fiber.

The experimental observation of XPM-induced optical wave breaking would require the use of femtosecond pulses. This can be seen by noting that for picosecond pulses with T_0=5-10 ps, typically $L_d \approx 1$ km while $L_w \approx$ 1m even if the pump-probe wavelengths differ by as little as 10 nm. By contrast if T_0=100fs, both L_d and L_w become comparable ($\approx$10 cm), and the temporal changes in the probe shape discussed here can occur in a fiber less than a meter long. Pulses much shorter than 100 fs should also not be used since higher-order nonlinear effects such as self-steepening and a delayed nonlinear response become increasingly more important. Although these effects are not expected to eliminate the phenomenon of XPM-induced optical wave breaking, they may interfere with the interpretation of experimental data.

3.3 Pump-Probe Cross-phase Modulation Experiments.

Cross-phase modulation is intrinsic to numerous schemes of ultrashort pulse interaction. The first observation of spectral effects arising from XPM was reported using a pump-probe scheme.[3] Strong infrared pulses were successfully used to enhance the spectral broadening of second-harmonic picosecond pulses at 527-nm. The phase modulation generated by the infrared pulse at the probe wavelength was refereed to as an induced-phase modulation (IPM). This phenomena is now be defined and called cross-phase modulation (XPM). More recently, we have observed the induced-frequency shift and spectral broadening enhancement of picosecond probe pulses using optical fibers as nonlinear media.[31] Pump-probe experiments of XPM are of prime importance for they could lead to applications for pulse compression, optical communication and optical computation purposes. Results of these pump-probe experiments of XPM are discussed in this section.

3.3.1 Induced-Frequency Shift of Copropagating Pulses.

Optical fibers are convenient to study nonlinear optical processes. The optical energy is concentrated into small cross-sections (typically 10^{-7} cm^2) for long interaction lengths. Thus, large nonlinear effects are possible with moderate peak powers (10-10^5 W) which lead to intensities up to 10^{12} W/cm^2. Optical fibers appear to be an ideal medium to investigate XPM effects. The first pump probe experiment using picosecond pulses propagating in optical

fibers demonstrated the importance of the pulse walk-off on XPM spectral effects.[31] It was shown that ultrashort pulses which overlap in a nonlinear and highly dispersive medium undergo a substantial shift of their carrier frequencies. This new "coherent effect", which was refereed to as an induced-frequency shift, resulted from the combined effect of cross-phase modulation and pulse walk-off. In the experiment, the induced-frequency shift was observed by using strong infrared pulses which shifted the frequency of weak picosecond green pulses copropagating in a 1-m-long single-mode optical fiber. Tunable red and blue shifts were obtained at the fiber output by changing the time delay between infrared and green pulses at the fiber input.

A schematic of the experimental set-up is shown in Fig. 3.3.1. A mode-locked Nd:YAG laser with a second-harmonic crystal was used to produce 33-ps infrared pulses and 25-ps green pulses. Theses pulses were separated using a Mach-Zender interferometer delay scheme made with wavelength-selective mirrors. The infrared and green pulses propagated in different interferometer arms. The optical path of each pulse was controlled using variable optical delays. The energy of infrared pulses was adjusted with neutral density filters in the range 1-100 nJ while the energy of green pulses was set to about 1 nJ. The nonlinear dispersive medium was a 1-m-long single-mode optical fiber (Corguide of Corning Glass). This length was chosen to allow for a total walk-off without losing control of the pulse delay at the fiber output. The group-velocity mismatch between 532-nm and 1064-nm pulses was calculated to be about 76 ps/m in fused silica. The spectrum of green pulses was measured using a grating spectrometer (1 meter-1200 lines/mm) and an optical multichannel analyzer (OMA2).

The spectra of green pulses propagating with and without infrared pulses are plotted in Fig. 3.3.2. The dashed spectrum corresponds to the case of green pulses propagating alone. The blue-shifted and red-shifted spectra are spectra of green pulses copropagating with infrared pulses after the input delays were set at 0 ps and 80 ps, respectively. The main effect of the nonlinear interaction was to shift the carrier frequency of green pulses. The induced-wavelength shift versus the input delay between infrared and green pulses is plotted in Fig. 3.3.3. The maximum induced-wavelength shift increased linearly with the infrared pulse peak power (Fig. 3.3.4). Hence, the carrier wavelength of green pulses could be tuned up to 4 Å toward both the red and blue sides by varying the time delay between infrared and green pulses at the fiber input. The solid curves in Figs. 3.3.3 and 3.3.4 are from theory.

When weak probe pulses are used the SPM contribution can be neglected in Eqs. 2.9 and 2.10. Thus, nonlinear phase shifts and frequency chirps are given by:

$$\alpha_1(\tau, z) = -\sqrt{\pi}\,\frac{\omega_1}{c}\,n_2\,\frac{P_2}{A_{eff}}\,L_w\left[\operatorname{erf}\left(\tau - \tau_d\right) - \operatorname{erf}\left(\tau - \tau_d + \frac{z}{L_w}\right)\right] \tag{3.1}$$

$$\delta\omega_1(\tau, z) = \frac{\omega_1}{c}\,n_2\,\frac{P_2}{A_{eff}}\,\frac{L_w}{T_0}\left[e^{-\left(\tau - \tau_d\right)^2} - e^{-\left(\tau - \tau_d + \frac{z}{L_w}\right)^2}\right] \tag{3.2}$$

When the pulses coincide at the fiber entrance (t_d=0) the point of maximum phase is generated ahead of the green pulse peak because of the group-velocity mismatch (Eq. 3.1). The green pulse sees only the trailing part of the XPM profile because it travels slower than the pump pulse. This leads to a blue induced-frequency shift (Eq. 3.2). Similarly, when the initial delay is set at 80 ps, the infrared pulse has just sufficient time to catch up with the green pulse. The green pulse sees only the leading part of the XPM phase shift, which gives rise to a red induced-frequency shift. When the initial delay is about 40 ps, the infrared pulse has time to pass entirely through the green pulse. The pulse envelope sees a constant dephasing and there is no shift of the green spectrum (Fig. 3.3.3).

Equations 3.1 and 3.2 can be used to fit our experimental data shown in Figs. 3.7 and 3.8. Assuming that the central part of the pump pulses provides the dominant contribution to XPM, we set t=0 in Eq. 3.2 and obtain:

$$\delta\omega_1(\tau, z) = \frac{\omega_1}{c} n_2 \frac{P_2}{A_{eff}} \frac{L_w}{T_0} \left[e^{-(\tau - \tau_d)^2} - e^{-\left(\tau - \tau_d + \frac{z}{L_w}\right)^2} \right] \tag{3.3}$$

The maximum induced-frequency shift occurs at τ_d=0 and τ_d=δ=z/L_w and is given by:

$$\left|\Delta\omega_{max}\right| = \frac{\omega_1}{c} n_2 \frac{P_2}{A_{eff}} \frac{L_w}{T_0} \tag{3.4}$$

Equations 3.3 and 3.4 have been plotted in Figs. 3.7 and 3.8, respectively. There is a very good agreement between this simple analytical model and experimental data. It should be noted that only a simple parameter (i.e., the infrared peak power at the maximum induced-frequency shift) has been adjusted to fit the data. Experimental parameters were: λ=532 nm, T_o=19.8 ps (33 ps FWHM), L_W=26 cm, and δ=4.

We have shown experimentally and theoretically that ultrashort optical pulses which overlap in a nonlinear and highly dispersive medium can undergo a substantial shift of their carrier frequency. This induced-frequency shift, has been demonstrated using strong infrared pulses to shift the frequency of copropagating green pulses. The results are well explained by an analytical model which includes the effect of cross-phase modulation and pulse walk-off. This experiment led to a conclusive observation of XPM spectral effects.

3.3.2 XPM-Induced Spectral Broadening and Optical Amplification in Optical Fibers.

This section presents additional features which can arise from the XPM interaction between a pump pulse at 630 nm and a probe pulse at 532 nm. With this choice of wavelengths, the group velocity dispersion between the pump pulse and the probe pulse is reduced and the XPM-interaction enhanced. The spectral width and the energy of the probe pulse were found to increase in presence of the copropagating pump pulse.

A schematic of the experimental set-up is shown in Fig. 3.3.5 A mode-locked Nd:YAG laser with a second harmonic crystal was used to produce 25-ps time duration pulses at 532-nm. Pump pulses were obtained through stimulated Raman scattering by focusing 90% of the 532-nm pulse energy into a 1-cm cell filled with Ethanol and using a narrow band filter centered at 630 nm. Resulting pump pulses at 630-nm were recombined with probe pulses, and coupled into a 3-m long singlemode optical fiber. Spectra of probe pulses were recorded for increasing pump intensities and varying input time delays between pump and probe pulses.

With negative delays (late pump at the optical fiber input), the spectrum of the probe pulse was red-shifted as in the 1064 nm/532 nm experiment (Fig. 3.3.6). A new XPM-effect was obtained when both pulses entered simultaneously into the fiber .The spectrum of the probe pulse not only shifted toward blue frequencies as expected but also broadened (Fig.

3.3.6). An spectral broadening as wide as 10 nm could be induced which was, surprisingly, at least one order of magnitude larger than predicted by the XPM theory. As shown in Fig. 3.3.6, the probe spectrum extended towards the blue-shifted frequencies with periodic resonant lines. These lines could be related to modulation instability sidelobes which have been theoretically predicted to occur with cross-phase modulation.

The optical amplification of the probe pulse is another new and unexpected feature arising from the XPM interaction. Pump-power-dependant gain factors of 3 or 7 were measured using probe pulses at 532 nm and pump pulses at 630 nm or 1064 nm, respectively. Fig. 3.3.7 shows the dependence of the XPM-induced gain for the probe pulse at 532 nm with the input time delay between the probe pulse and the pump pulse at 630 nm. The shape of the gain curve corresponds to the overlap function of pump and probe pulses. Fig. 3.3.8 shows the dependence of the gain factor with the intensity of pump pulses at 1064 nm. This curve is typical of a parametric amplification with pump depletion. The physical origin of this XPM-induced gain is still under investigation. It could originate from a XPM-phase-matched four-wave-mixing process.

The spectral distribution of probe pulses can be significantly affected by the XPM generated by a copropagating pulse. In real time, the probe pulse frequency can be tuned, its spectrum broadened and its energy increased. XPM appears as a new technique to control the spectral properties and regenerate ultrashort optical pulses with THz repetition rates.

3.4 Cross-Phase Modulation with Stimulated Raman Scattering.

When long samples are optically studied, stimulated Raman scattering (SRS) contribute to the formation of ultrafast supercontinua. In 1980, Gersten, Alfano and Belic predicted that ultrashort pulses should generate broad Raman lines due to the coupling among laser photons and vibrational phonons.[2] This phenomenon was called cross-phase modulation (XPM). It characterized the phase modulation of the Raman pulse by the intense pump laser pulse. Recently, a great deal of attention has been focused on the combined effects of SRS, SPM and group velocity dispersion for the purposes of pulse compression and soliton generation.[5-13] Schadt et al. derived and computed the coupled waves equations describing the changes of pump and Raman envelopes in nonlinear and dispersive optical fibers.[5-6] Manassah obtained analytical solutions for the phase and shape of a weak Raman pulse amplified during the pump and Raman pulse walk-off.[9-10] In this section, we review our measurements of XPM and SPM effects on stimulated Raman scattering.

3.4.1 Generation of Picosecond Raman Pulses in Optical Fibers.

Stimulated Raman scattering of ultrashort pulses in optical fibers attracts a great deal of interest because of its potential applications for tunable fiber-lasers and all-optical amplifiers. Temporal and spectral modifications of pump and Raman pulses are more complex to analyze when Raman pulses are generated in short lengths (i.e. high Raman threshold) of very dispersive

optical fibers. In addition to XPM and walk-off, one has to take in account of pump depletion, SPM of the Raman pulse, Raman-induced XPM of the pump pulse, group velocity dispersion broadening, higher order SRS and XPM-induced modulation instability. This section presents measurements on the generation of Raman picosecond pulses from the noise using short lengths of a singlemode optical fiber.

A mode-locked Nd:YAG laser was used to generate 25-ps time-duration pulses at λ=532 nm with a repetition rate of 10 Hz. The optical fiber was custom made by Corning Glass. It has a 2.5-μm core diameter, a 0.24% refractive index difference and a single-mode cut-off at λ=462 nm. Spectra of output pulses were measured using a grating spectrometer (1 meter-600 lines/mm) and recorded with an optical multichannel analyzer OMA2. Temporal profiles of pump and Raman pulses were measured using a 2-ps resolution Hamamatsu streak camera.

Spectra of pump and Raman pulses, which were measured for increasing pump energy at the output of short fiber lengths, are plotted in Fig. 3.4.1. The dashed line in Fig. 3.41-a is the reference laser spectrum at low intensity. Figures 3.4.1-a (solid line) and 3.4.1-b show spectra measured at the Raman threshold at the output of a 1-m and 6-m long optical fibers, respectively. The Raman line appears at λ=544.5 nm (about 440 cm^{-1}). The laser line is broadened by SPM and shows XPM-induced sidebands. For moderate pump intensities above the stimulated Raman scattering threshold, spectra of Raman pulses are broad, modulated, and symmetrical in both cases (Figs. 3.4.1-c & 3.4.1-d). For these pump intensities, the pulse walk-off (6 m

corresponds to 2 walk-off length) does not lead to an asymmetrical spectral broadening. For higher pump intensities, Raman spectra become much wider (Figs. 3.4.1-e & 3.4.1-f). In addition, spectra of Raman pulses generated in the long fiber are highly asymmetrical (Fig. 3.4.1-f). The intensity-dependent features observed in Fig. 3.4.1 are characteristic of spectral broadenings arising from nonlinear phase modulations such as SPM and XPM as predicted by the theory. At the lowest intensities, XPM dominates, while at the highest intensities, the SPM generated by the Raman pulse itself is the most important. However, it should be noted that the widths of Raman spectra shown in Fig. 3.4.1 are one order of magnitude larger than expected by the theory. Modulation instability induced by pump pulses could explain such a difference between measurements and theory.

Temporal measurements of the generation process were performed to test whether the spectral asymmetry originated from the pump depletion re-shaping as in the case of longer pulses.[5-6] Pump and Raman profiles were measured at the output of a 17-m long fiber (Fig. 3.4.2). The dotted line is for a pump intensity at the SRS threshold, and the solid line for a higher pump intensity. The leading edge of the pump pulse is partially "eaten", but not completely emptied because of the quick walk-off between pump and Raman pulses. Thus, the leading edge of the pump pulse does not become very sharp, and the contribution of pump-depletion effects on the spectral asymmetry of pump and Raman pulses does not seem to be significant.

Figure 3.4.2 shows a typical sequence of temporal profiles measured for input pump intensities strong enough to generate higher order stimulated

Raman scattering lines. The temporal peaks are the maxima of high-order SRS scatterings which satisfy the group-velocity dispersion delay of 6 ps/m for each frequency shift of 440 cm^{-1}. These measurements show that 1) the Raman process clamps the peak power of pulses propagating into an optical fiber to a maximum value, and 2) high-order stimulated Raman scatterings occur in cascade during the laser pulse propagation.

3.4.2 Generation of Femtosecond Raman Pulses in Ethanol .

Nonlinear phenomena such as supercontinuum generation and stimulated Raman scattering were first produced in unstable self-focusing filaments generated by intense ultrashort pulses in many liquids and solids.[1] Optical fibers are convenient media to study such nonlinear phenomena without the catastrophic features of collapsing beams. However, optical fibers are not suitable for certain applications such as high power experiments, the generation of large Raman shifts (> 1,000 cm^{-1}) and Raman pulses having high peak powers (> 1MW). In this section, spectral measurements of SRS generation in Ethanol are presented. Spectral shapes are shown to result from the combined effects of XPM, SPM and walk-off.

Spectral measurements of SRS in Ethanol have been performed using the output from a CPM ring dye amplifier system.[12] Pulses of 500 femtosecond duration at 625 nm were amplified to an energy of about 1mJ at a repetition rate of 20 Hz. Pulses were weakly focused into a 20 cm-long cell filled with Ethanol. Output pulses were imaged on the slit of a 1/2 m Jarell-Ash spectrometer and spectra were recorded using an optical multichannel analyzer OMA2.

Ethanol has a Raman line shifted by 2928 cm^{-1}. Figure 3.4.3 shows how the Stokes spectrum of the Raman line changes as a function of the pump intensity. Results are comparable to those obtained using optical fibers. At low-intensity the Stokes spectrum is narrow and symmetrical (Fig. 3.4.3). As the pump intensity increases the Raman spectrum broadens asymmetrically

with a long tail pointing towards the longer wavelengths. Spectra of the anti-Stokes Raman line were also measured (Baldeck, 1987). They were as wide as Stokes spectra but with tails pointing towards the shortest wavelengths as predicted by the sign of the walk-off parameter.

3.5 Cross-Phase Modulation and Stimulated Four Photon Mixing in Optical Fibers.

Stimulated Four Photon Mixing (SFPM) is an ideal process for designing parametric optical amplifiers and frequency converters. SFPM is produced when two high-intensity pump photons are coupled by the third-order susceptibility $\chi^{(3)}$ to generate a Stokes photon and an anti-Stokes photon. The frequency shifts of the SFPM waves are determined by the phase matching conditions which depend on the optical geometry. In 1970, SFPM was produced in glass by Alfano and Shapiro using picosecond pulses.[35] Later on, SFPM has been successfully demonstrated by a number of investigators in few mode, birefringent, and singlemode optical fibers.[36-38] Most of the earlier experiments using optical fibers have been performed with nanosecond pulses. In 1981, Lin and Bosch obtained large-frequency shifts; however, the spectral dependence on the input intensity was not investigated.[39] In the followings, measurements of the intensity dependence of SFPM spectra generated by 25-ps pulses in an optical fiber are reported.[40] For such short pulses, spectra are affected by the combined effects of SPM and XPM. The broadening of SFPM lines and the formation of frequency continua are investigated.

The experimental is described as follows. A Quantel frequency-doubled mode-locked Nd:YAG laser produced 25-ps pulses. A X20 microscope lens was used to couple the laser beam into the optical fiber. The spectra of the output

pulses were measured using an 1-m 1200/mm grating spectrometer. Spectra were recorded on photographic film and with an optical multichannel analyser OMA 2. Average powers coupled in the fiber were measured with a power meter at the optical fiber output. The 15-m long optical fiber had a core diameter of 8 mm and a normalized frequency V=4.44 at 532 nm. At this wavelength, the 4 first LP modes (LP_{01}, LP_{11}, LP_{21}, and LP_{02}) were allowed to propagate.

Typical intensity-dependent spectra are displayed in Figs. 3.5.1, 3.5.2, and 3.5.3. At low intensity, I< 10^8 W/cm^2, the output spectrum contains only the pump wavelength λ=532 nm (Fig. 6.1-a). At approximately 5X10^8 W/cm^2 3 sets of symmetrical SFPM lines (at Ω=50, 160, and 210 cm^{-1}) and the first SRS Stokes line (at 440 cm^{-1}) appear (Figs. 3.5.1-b and 3.5.1-c). As the intensity increases the SFPM and SRS lines broaden, and a Stokes frequency continuum is generated (Figs. 3.5.1-d and 3.5.1-e). Above an intensity threshold of 20X10^8 W/cm^2, new sets of SFPM lines appear on the Stokes and antistokes sides with frequency ranging from 2700 to 3865 cm^{-1}. finally, the large shift merge (Fig. 3.5.1-f). and contribute to the formation of a 4000 cm^{-1} frequency continuum (Fig. 3.5.1-g). Fig. 3.5.2 shows how the large Stokes-shift SFPM lines are generated and broaden when the pump intensity increases from 20 to 30 X10^8 W/cm^2. Fig. 3.5.3 gives two examples of complete spectra including the large-shift anti-Stokes and Stokes lines. The measured SFPM shifts correspond well with the phase-matching condition of SFPM in optical fibers.

Fig. 3.5.4 shows the development of a Stokes continuum from the combined effects of SFPM, SRS, SPM and XPM. As the pump intensity is increased, the pump, SFPM, and first SRS lines broaden and merge (Fig. 3.5.4-a). For stronger pump intensities, the continuum is duplicated by stimulated Raman scattering, and the continuum expands towards the lowest optical frequencies (Fig. 3.5.4-b). As shown, the maximum intensities of new frequencies are self-limited.

The broadening of the SFPM and SRS lines arises from self- and cross-phase modulation effects. It is established that spectral broadenings generated by SPM are inversely proportional to the pulse duration and linearly proportional to the pump intensity. In this experiment, SPM effects are important because of the pump pulse shortness (25 ps) and intensity (10^9 W/cm^2). Moreover, it has been predicted that XPM enhances the spectral broadening in the ratio $\Delta\omega_{Raman}/\Delta\omega_{Pump} = 2$. The experimental ratios for the SFPM and SRS broadenings are, respectively, 2.7 and 3.6 (Fig. 3.5.4-a). Furthermore, the modulation which is seen in the continuum spectrum fits well with the spectrum modulation predicted by phase modulation theories.

Fig. 3.5.5 shows the spectral broadening of the anti-Stokes SFPM line of λ=460 nm (Ω=2990 cm^{-1}). This line is a large-shift SFPM anti-Stokes line generated simultaneously with the λ=633 nm SFPM Stokes line by the laser pump of λ=532 nm (see Fig. 3.5.3). the corresponding frequency shift and mode distribution are W=2990 cm^{-1} and LP_{01} (pump)-LP_{11}(Stokes and anti-Stokes), respectively. From Fig. 3.5-a to 3.5-d, the peak intensity of the λ=460 nm line increases from approximately 20 to 30 X10^8 W/cm^2 in steps of

$2.5X10^8$ W/cm^2. In Fig. 3.5.5-a, the spectrum contains only the 460-nm SFPM line generated by the laser pump (λ=532 nm). In Fig. 3.5.5-b, the line begins to broaden and two symmetrical lines appear with a frequency shift of 100 cm^{-1}. This set of lines could be a new set of small-shift SFPM lines generated by the 460-nm SFPM line acting as a new pump wavelength. Fig. 3.5.5-c and 3.5.5-d shows significant broadening, by a combined action of SFPM, SPM, and XPM of the 460 nm into a frequency continuum. Similar effects were observed on the Stokes side as displayed in Fig. 3.5.2.

The intensity effects on SFPM spectra generated by 25-ps pulses propagating in optical fibers have been experimentally investigated. In contrast to SFPM lines generated by nanosecond pulses, spectra were broadened by self-phase modulation and cross-phase modulation. Intensity saturated wide frequency continua, covering the whole visible spectrum, were generated for increasing intensities. Applications are for the design of wide-band amplifiers, the generation of "white" picosecond pulses, and the generation by pulse compression of femtosecond pulses at new wavelengths.

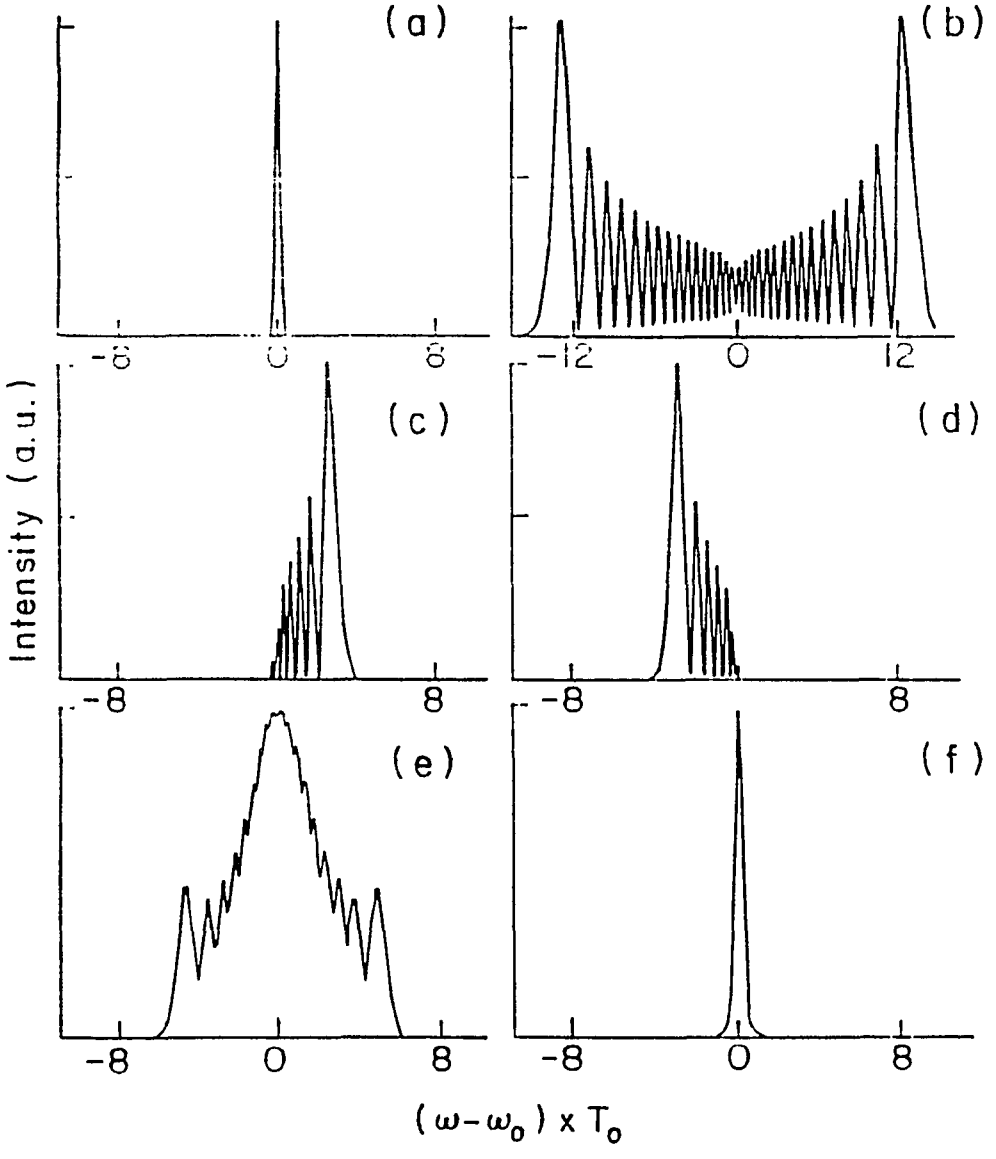

Fig. 3.2.1 Influence of cross-phase modulation, walk-off, and input time-delay on the spectrum of a probe pulse. $\phi=(\omega_1/c)n_2P_2L_W$, $\delta=z/L_W$, and τ_d are the XPM, walk-off and input time-delay parameters, respectively. a) Reference spectrum with no XPM; i.e. $\phi=0$. b) XPM in absence of walk-off; i.e. $\phi=50$ and $\delta=0$. c) XPM, total walk-off, and no initial time-delay; i.e. $\phi=50$, $\delta=-5$ and $\tau_d=0$. d) XPM, and initial time-delay to compensate the walk-off; i.e. $\phi=50$, $\delta=-5$ and $\tau_d=5$. e) XPM and symmetric *partial* walk-off; i.e. $\phi=50$, $\delta=-3$ and $\tau_d=1.5$. f) XPM and symmetric *total* walk-off; i.e. $\phi=50$, $\delta=-5$ and $\tau_d=2.5$.

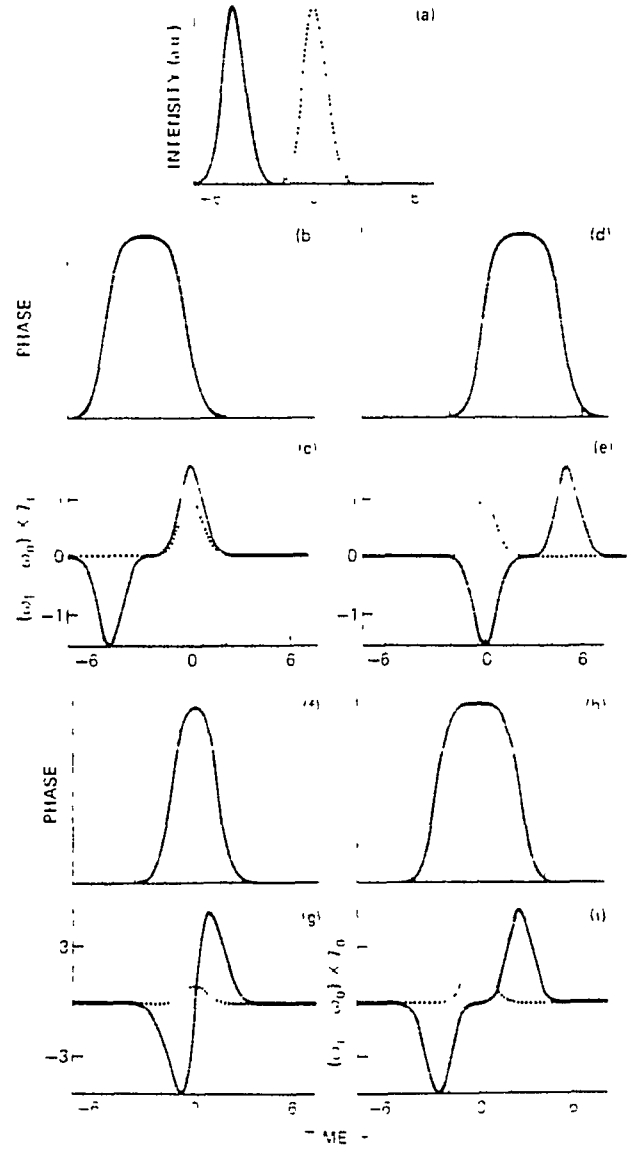

Fig. 3.2.2 Influence of cross-phase modulation (XPM), walk-off, and input time-delay on the phase and frequency chirp of a probe pulse. a) Locations of pump (solid line) and probe (dashed line) at the output of the nonlinear medium for a total walk-off, and no initial time-delay; i.e. δ=-5 and τ_d=0. b) XPM phase with a total walk-off, and no initial time-delay; i.e. ϕ=50, δ=-5 and τ_d=0. c) XPM-induced chirp (solid line) with a total walk-off, and no initial time-delay. Probe pulse intensity (dashed). d) XPM phase with an initial time-delay to compensate the walk-off; i.e. ϕ=50, δ=-5 and τ_d=5. e) XPM-induced chirp (solid line) with an initial time-delay to compensate the walk-off. Probe pulse intensity (dashed). f) XPM phase and symmetric *partial* walk-off; i.e. ϕ=50, δ=-3 and τ_d=1.5. g) XPM-induced chirp (solid line) and symmetric *partial* walk-off. Probe pulse intensity (dashed). h) XPM phase and symmetric *total* walk-off; i.e. ϕ=50, δ=-5 and τ_d=2.5. i) XPM-induced chirp (solid line) and symmetric *total* walk-off. Probe pulse intensity (dashed).

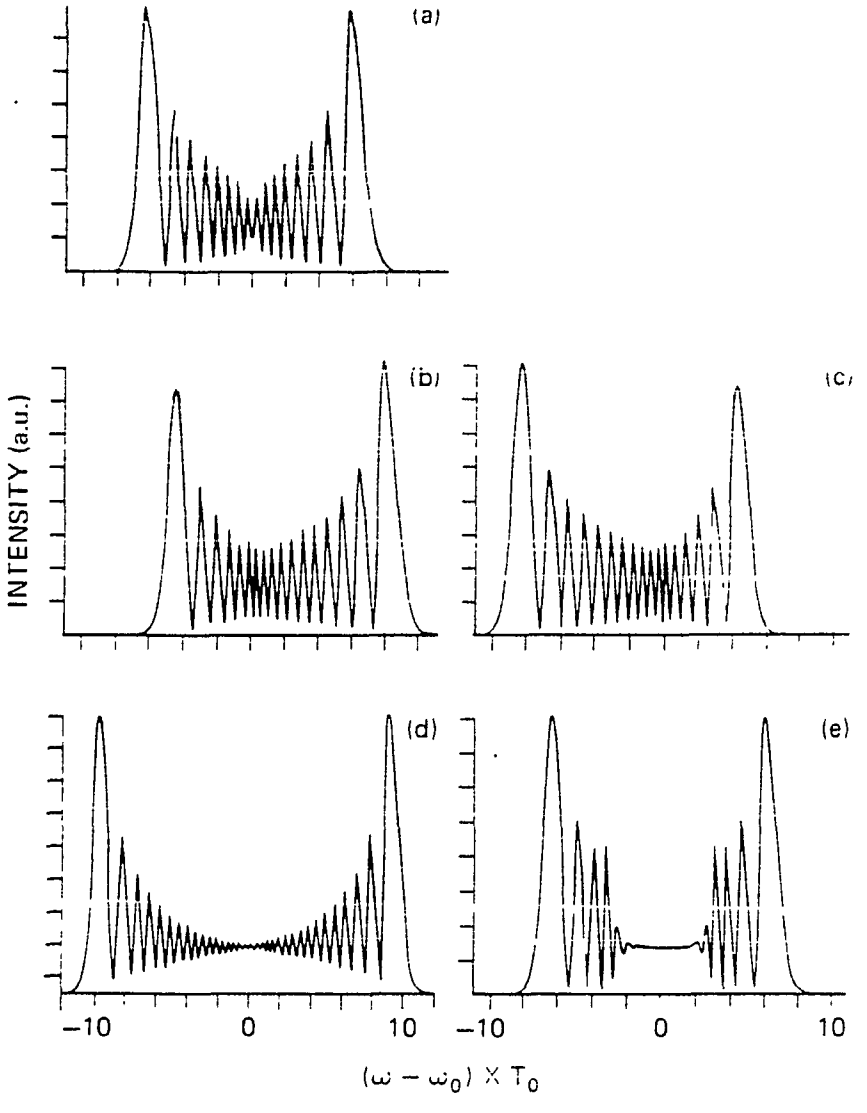

Fig. 3.2.3 Influence of self-phase modulation (SPM), cross-phase modulation (XPM), walk-off, and input time-delay on the spectrum of a probe pulse from Eqs. 2.9 and 2.11 with $P_1=P_2$. The same parameter values as in Fig. 3.2.1 are used.

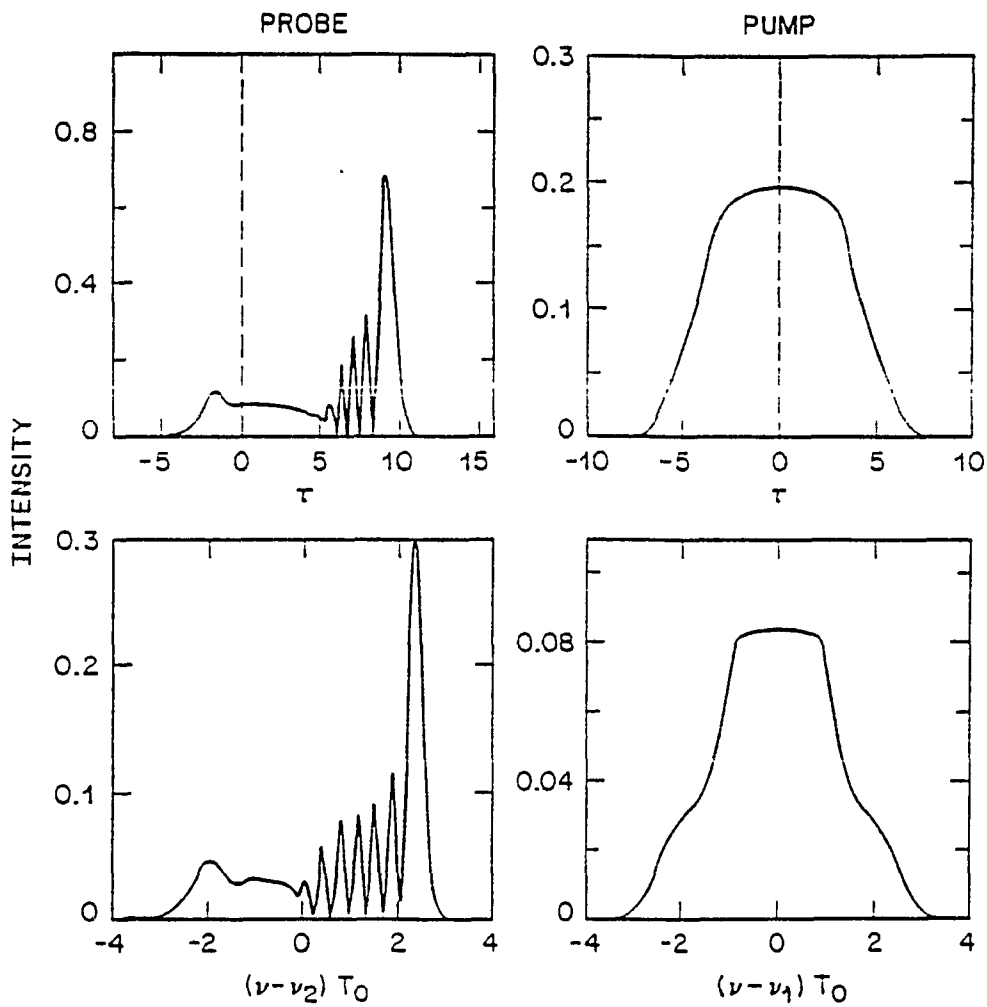

Fig. 3.2.4 Shape and spectrum of probe pulse (left column) and pump pulse (right column) at z/Ld=0.4 when the two pulses copropagate in the normal-dispersion regime of a single-mode fiber. The parameters are N=10, L_w/L_d=0.1, λ_1/λ_2=1.2, and τ_d=0. Oscillations near the trailing edge (positive time) of the probe pulse are due to XPM-induced optical wave breaking.

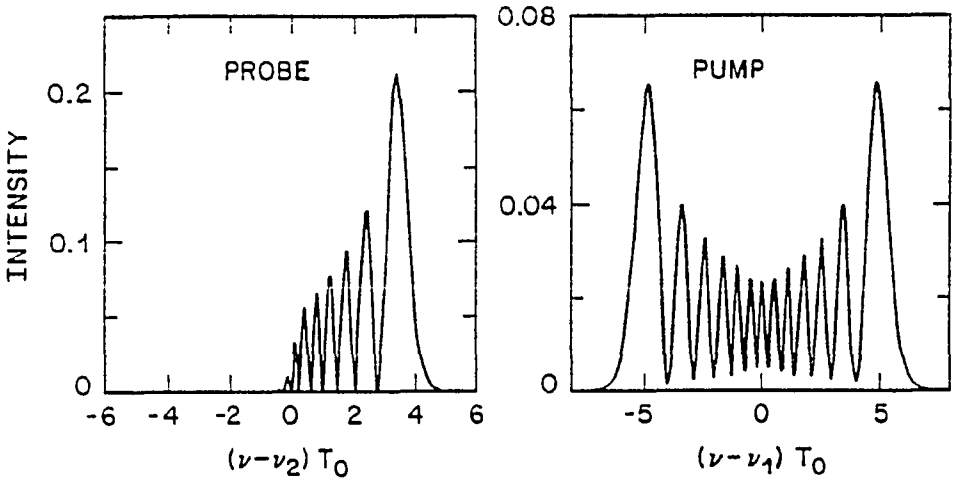

Fig. 3.2.5 Spectra of probe and pump pulses under conditions identical to those of Fig. 3.2.4 but without the GVD effects ($\beta_1=\beta_2=0$). Pulse shapes are not shown as they remain unchanged.

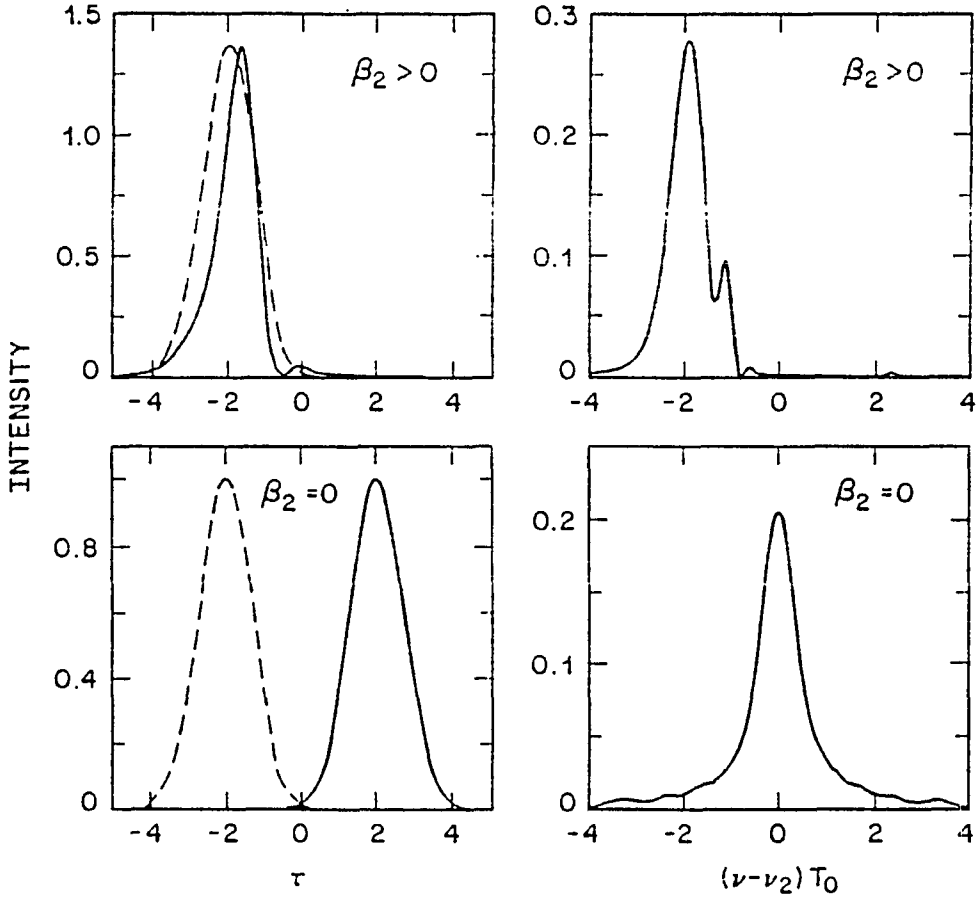

Fig. 3.2.6 Probe shape and spectrum with (upper row) and without (lower row) the GVD effects under conditions identical to those of Fig. 3.2.5 except the τ_d=-2. Note the important effect on pulse evolution of the initial time delay between the pump and probe pulses.

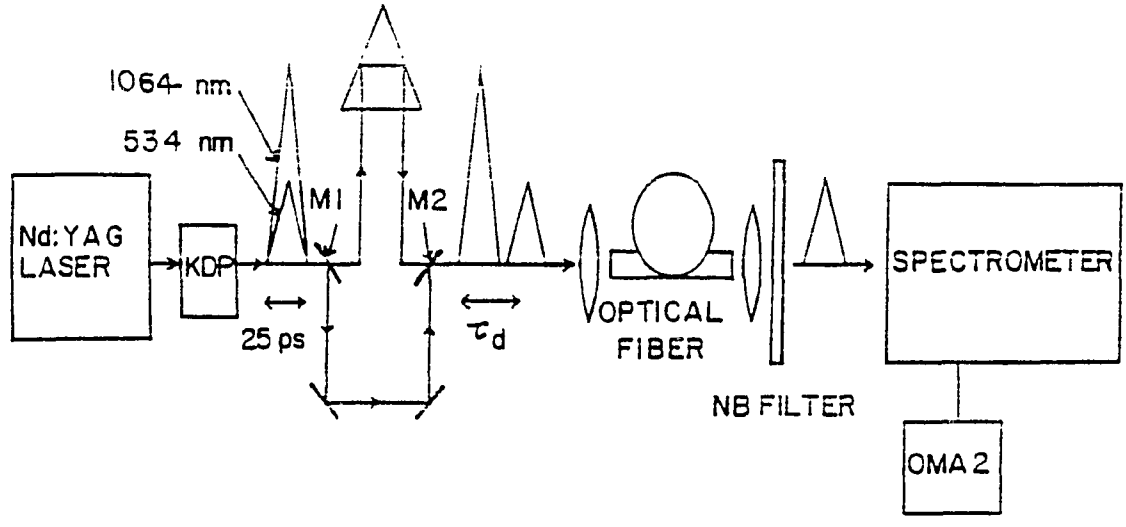

Fig. 3.3.1 Experimental set-up used to measure the induced-frequency shift of 532-nm pulses as function fo the time delay between pump and probe pulses at the optical fiber input. Mirrors M_1 and M_2 are wavelength selective, i.e., they reflect 532-nm pulses and transmit 1064-nm pulses.

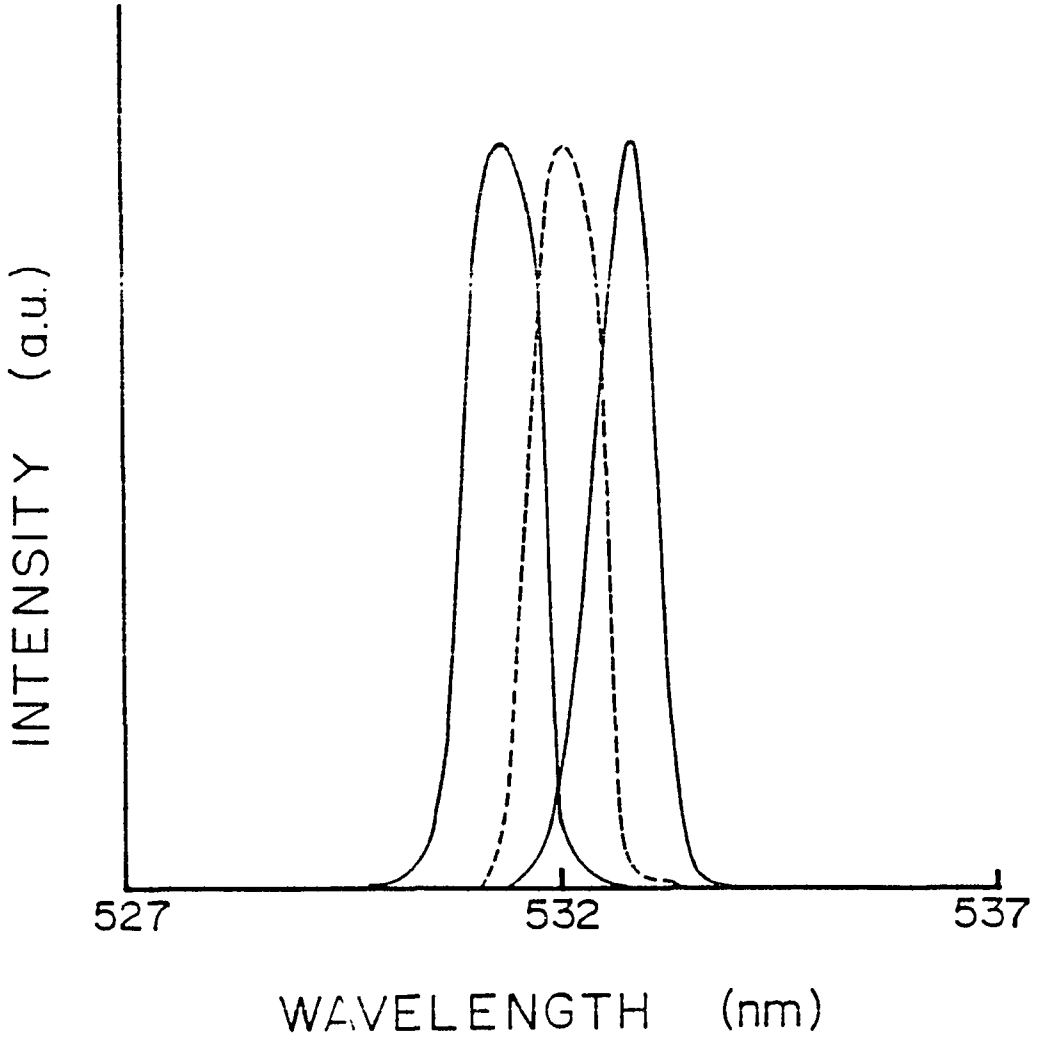

Fig. 3.3.2 Cross-phase modulation effects on spectra of green 532-nm pulses. a) Reference spectrum (no copropagating infrared pulse). b) Infrared and green pulses overlapped at the fiber input. c) The infrared pulse was delayed by 80-ps at the fiber input.

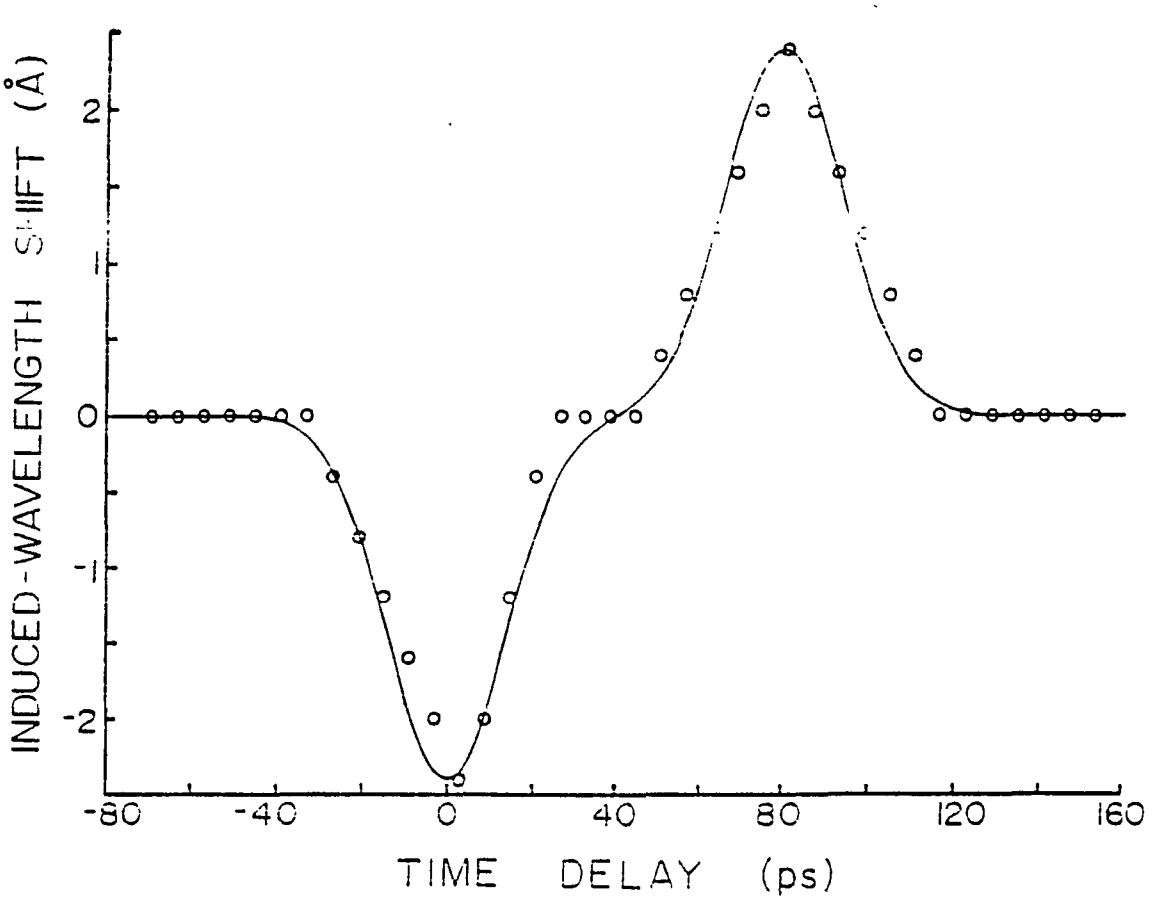

Fig. 3.3.3 Induced-wavelength shift of green 532-nm pulses as a function of the input time delay between 532-nm pulses and infrared 1064-nm pulses at the input of a 1-m-long optical fiber. Dots are experimental points. The solid line is the theoretical prediction.

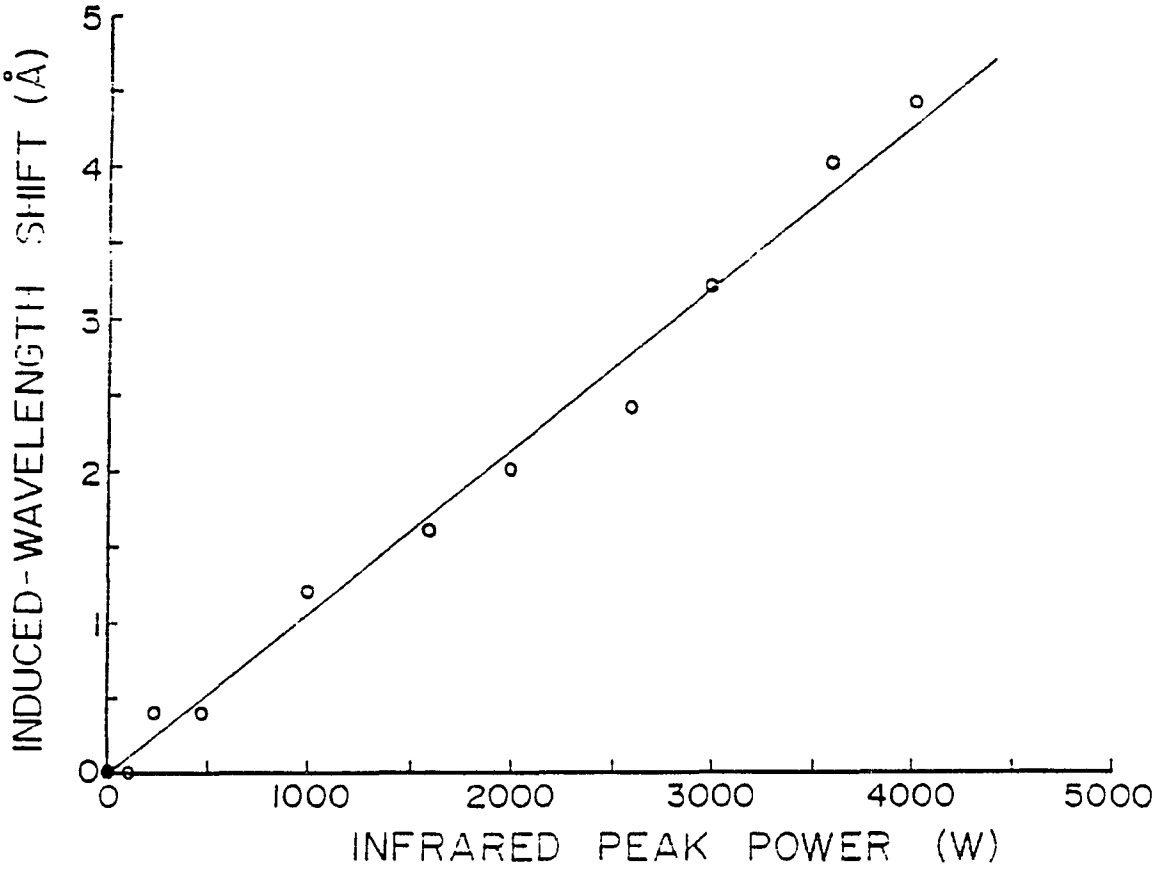

Fig. 3.3.4 Maximum induced-wavelength shift of 532-nm pulses versus the peak power of infrared pump pulses. Dots are experimental points. The solid line is the theoretical prediction.

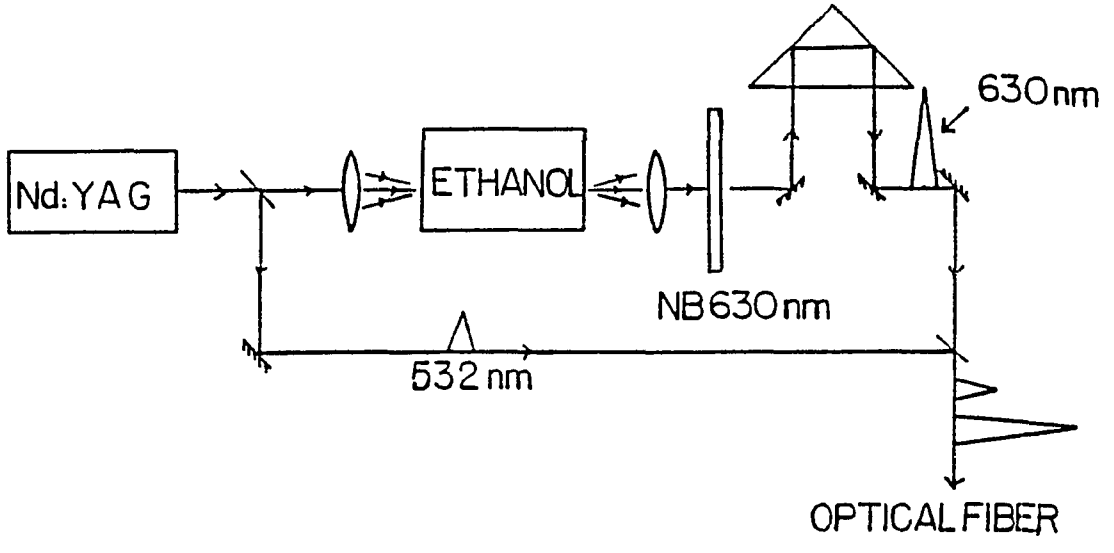

Fig. 3.3.5 Experimental set-up to generate copropagating picosecond pulses at 630 nm and 532 nm.

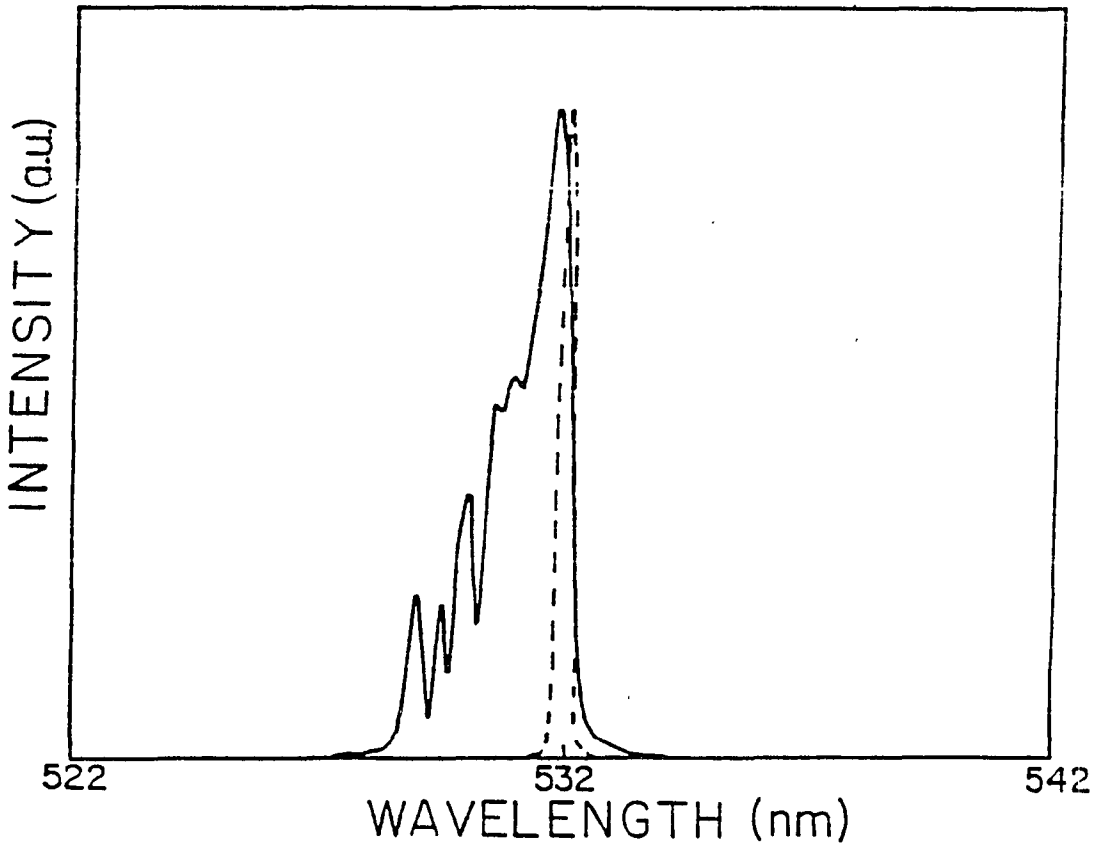

Fig. 3.3.6 Cross-phase modulation (XPM) effects on the spectrum of a probe picosecond pulse. Dashed line: reference spectrum without XPM. Solid line: with XPM and no time delay between pump and probe pulse at the optical fiber input.

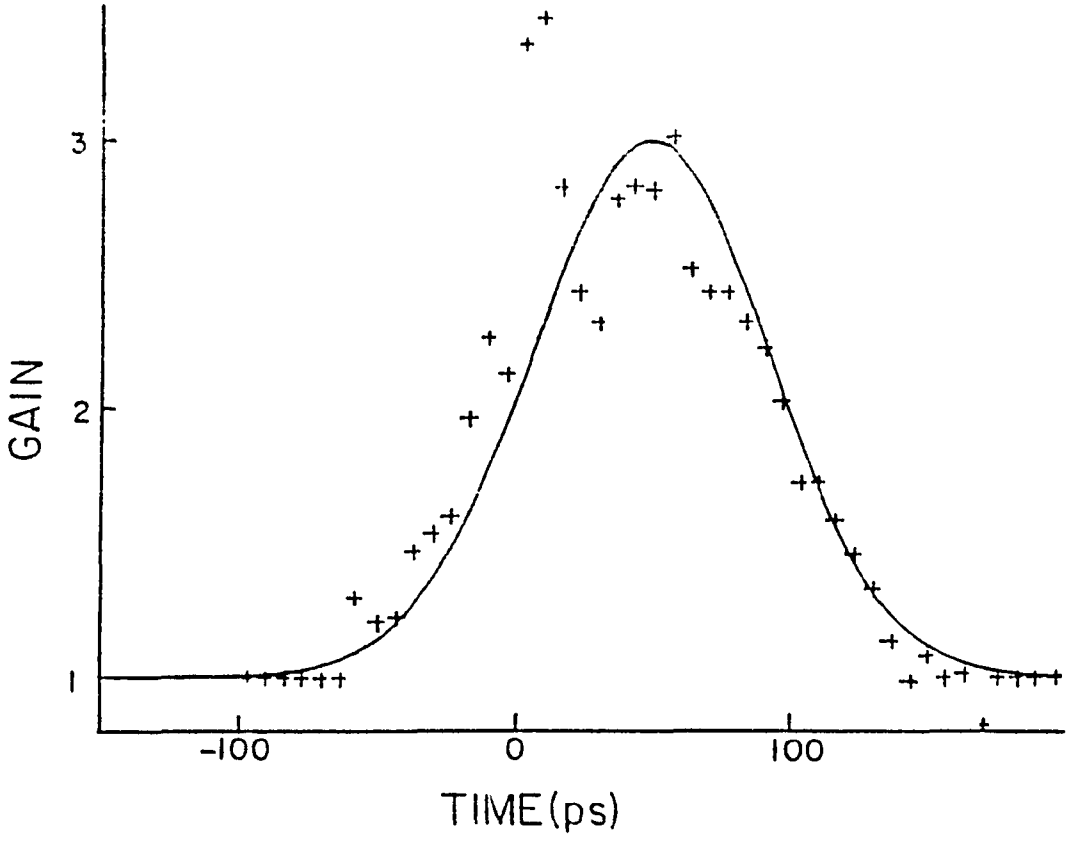

Fig. 3.3.7 XPM-induced optical gain $I_{532}(out)/I_{532}(in)$ *versus* input time delay between pump pulses at 630 nm and probe pulses at 532 nm. Crosses: experimental data. Solid line: fit obtained by taking the convolution of pump and probe pulses.

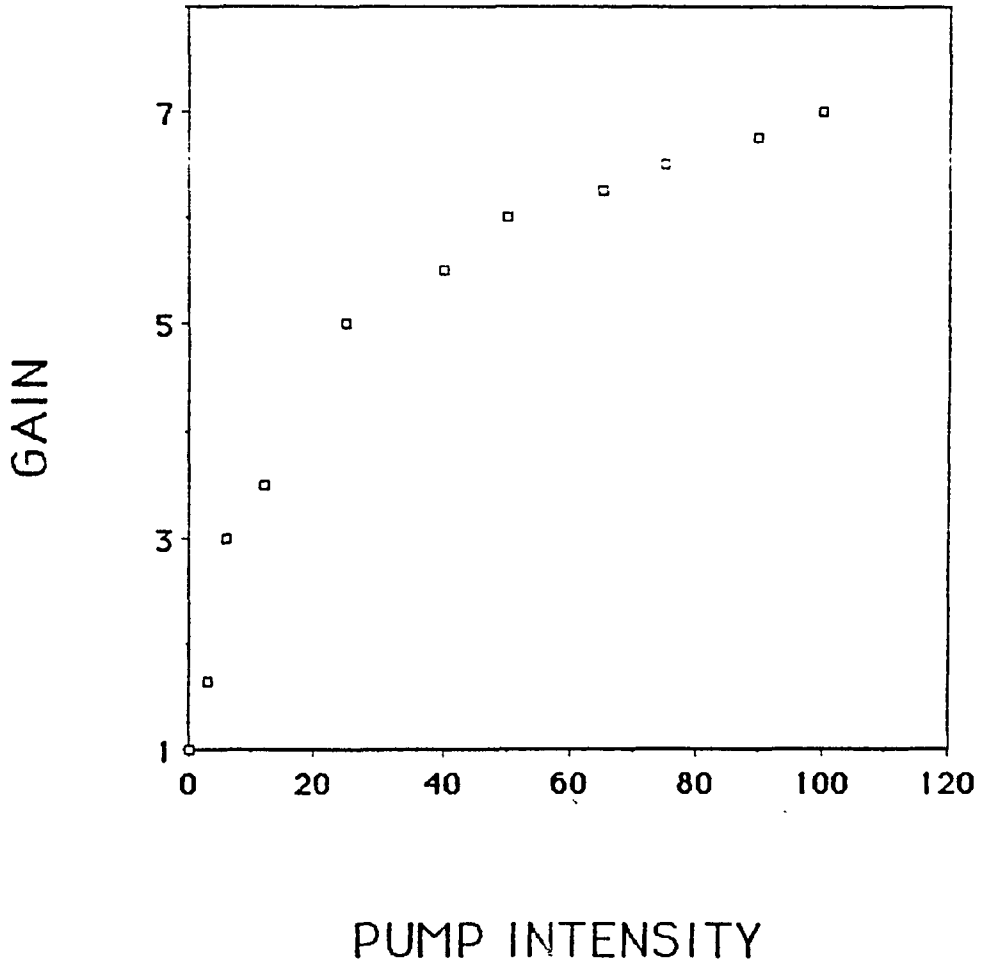

Fig. 3.3.8 XPM-induced optical gain $I_{532}(out)/I_{532}(in)$ *versus* intensity of pump pulses at 1064 nm.

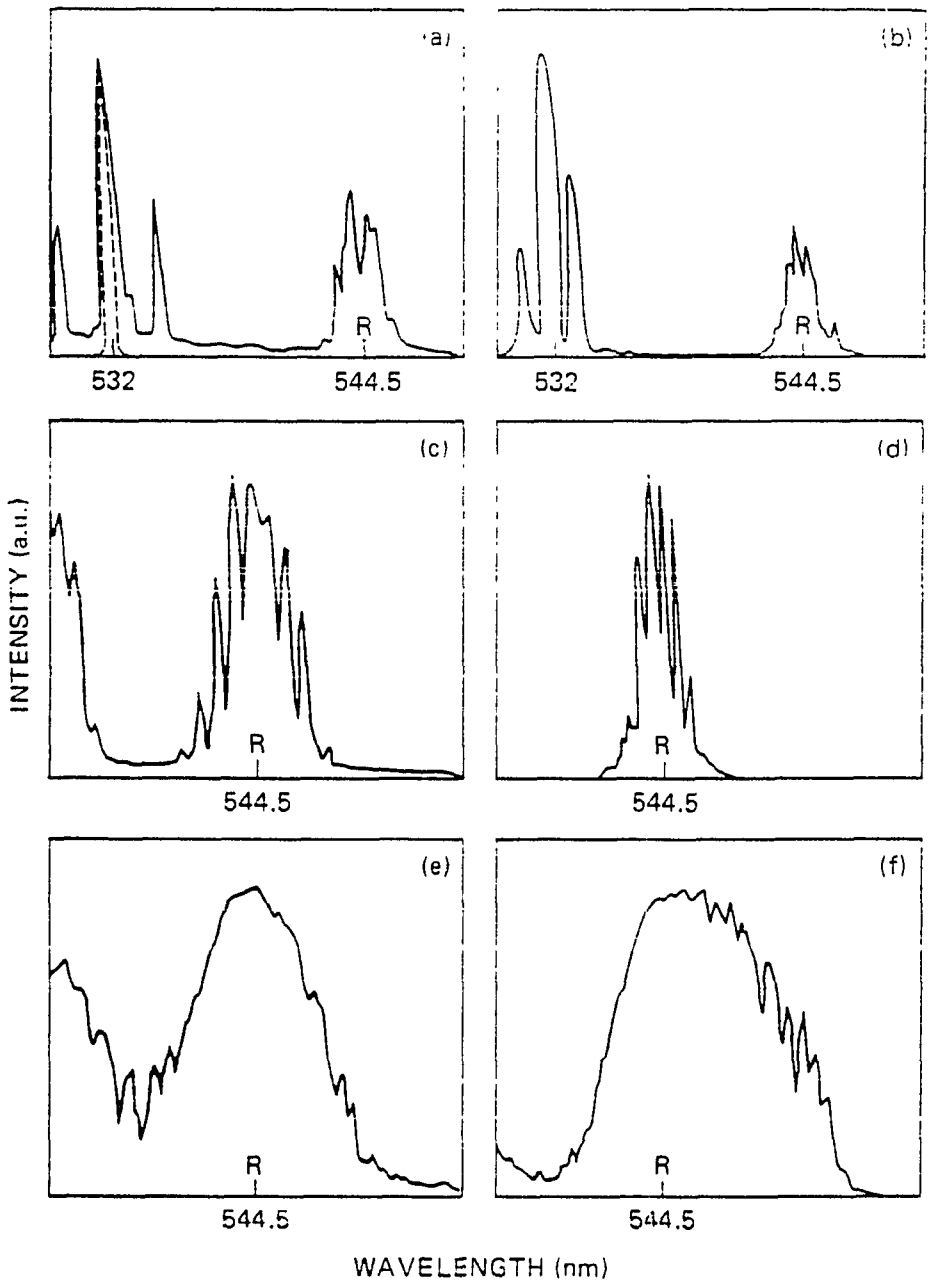

Fig. 3.4.1 Spectra of picosecond Raman pulses generated in short lengths of a single-mode optical fiber. The laser and Raman lines are at 532 nm and 544.5 nm, respectively. Results in the left column and right column were obtained with 1-m and 6-m long single-mode optical fiber, respectively. a) and b) dotted line: reference of laser spectrum at low intensity; solid line: pump and Raman lines near the stimulated Raman scattering threshold. Frequency sidebands about the laser line are XPM-induced modulation instability sidebands. c) and d) Raman spectra for moderate pump peak powers above threshold. e) and f) Raman spectra for higher pump peak powers.

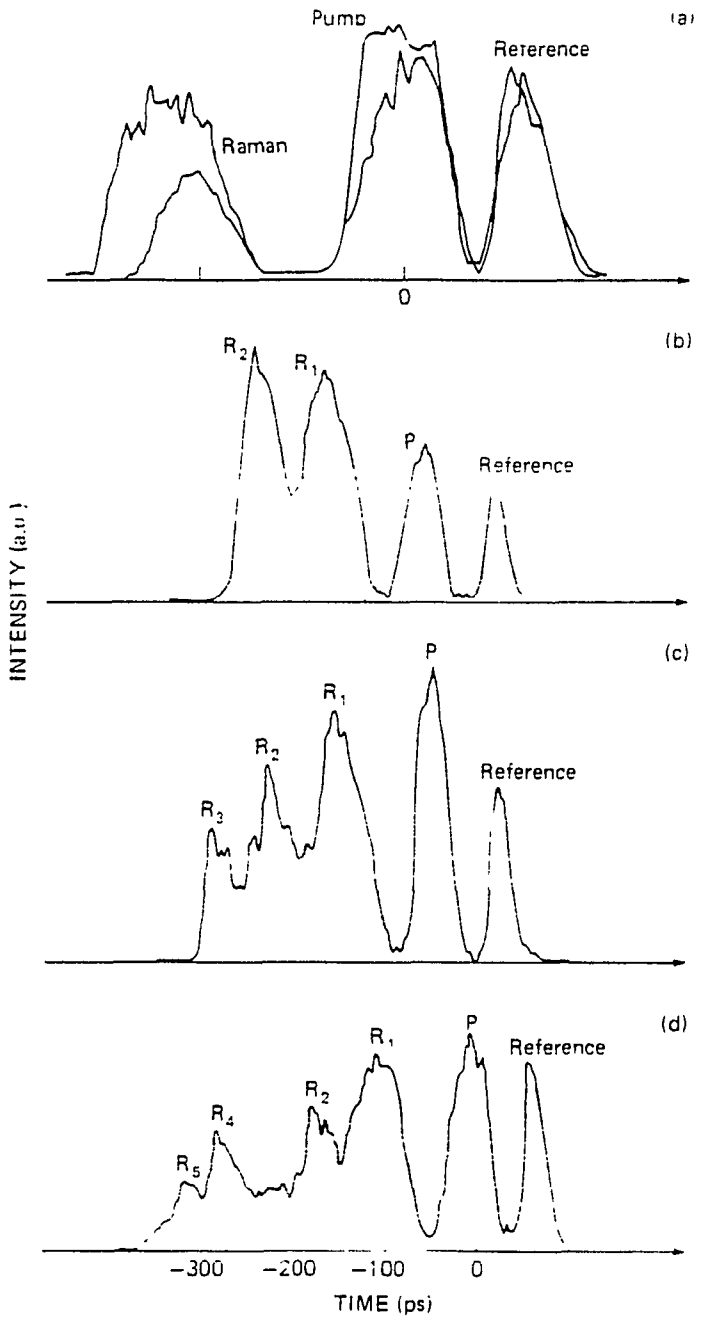

Fig. 3.4.2 Temporal shapes of reference pulse, pump pulse and stimulated Raman scattering (SRS) pulses at the output of a 17-m long single-mode optical fiber for increasing pump intensity. a) 1 st. order SRS for slightly different pump intensity near threshold. b) 1 st. and 2 nd. orders SRS. c) 1 st. - 3 rd. orders SRS. d) 1 st. - 5 th. orders SRS.

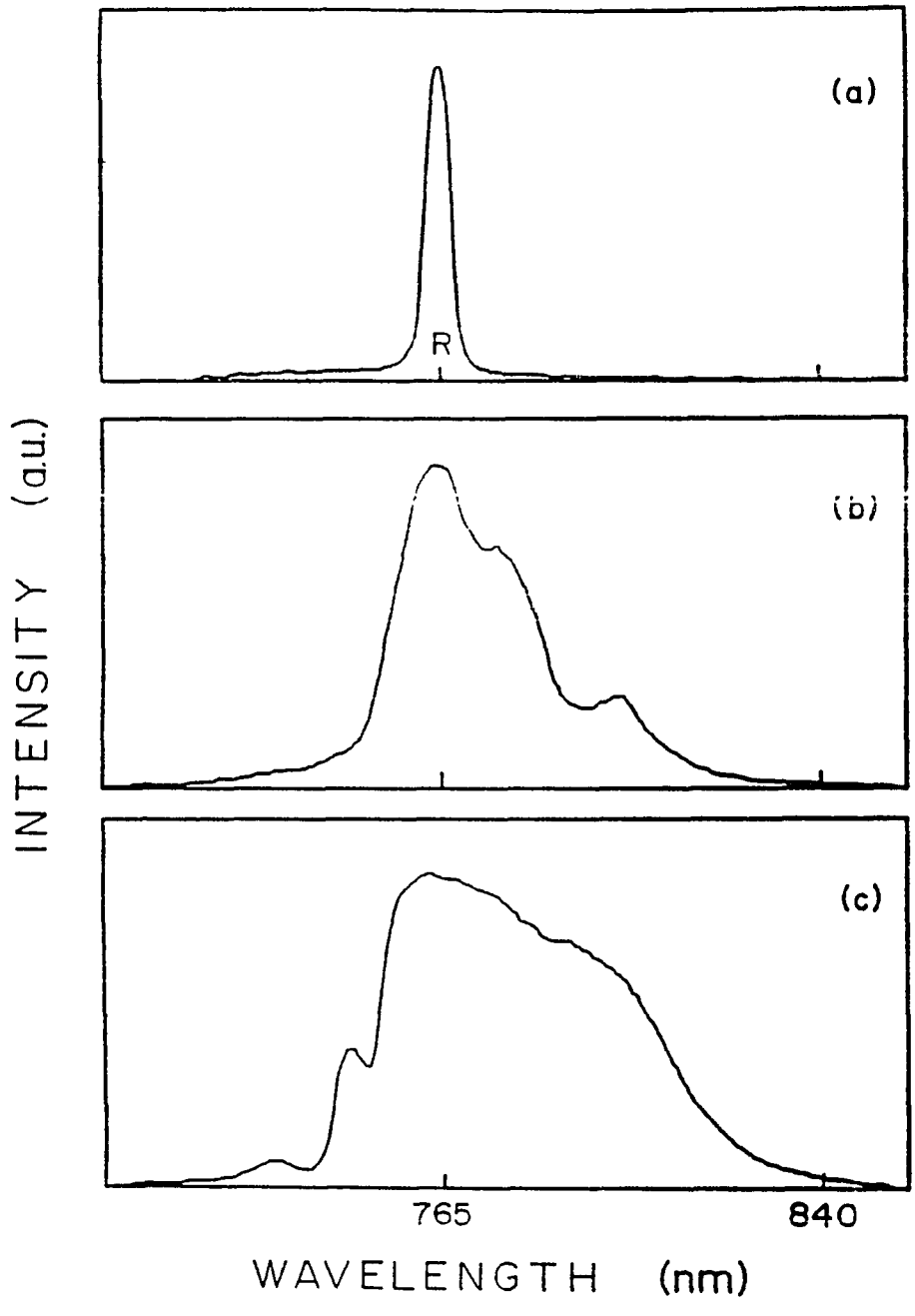

Fig. 3.4.3 Effects of cross- and self- phase modulations on the Stokes-shifted Raman line generated by 500-fs pulses in Ethanol. a) to c) are for increasing laser intensity.

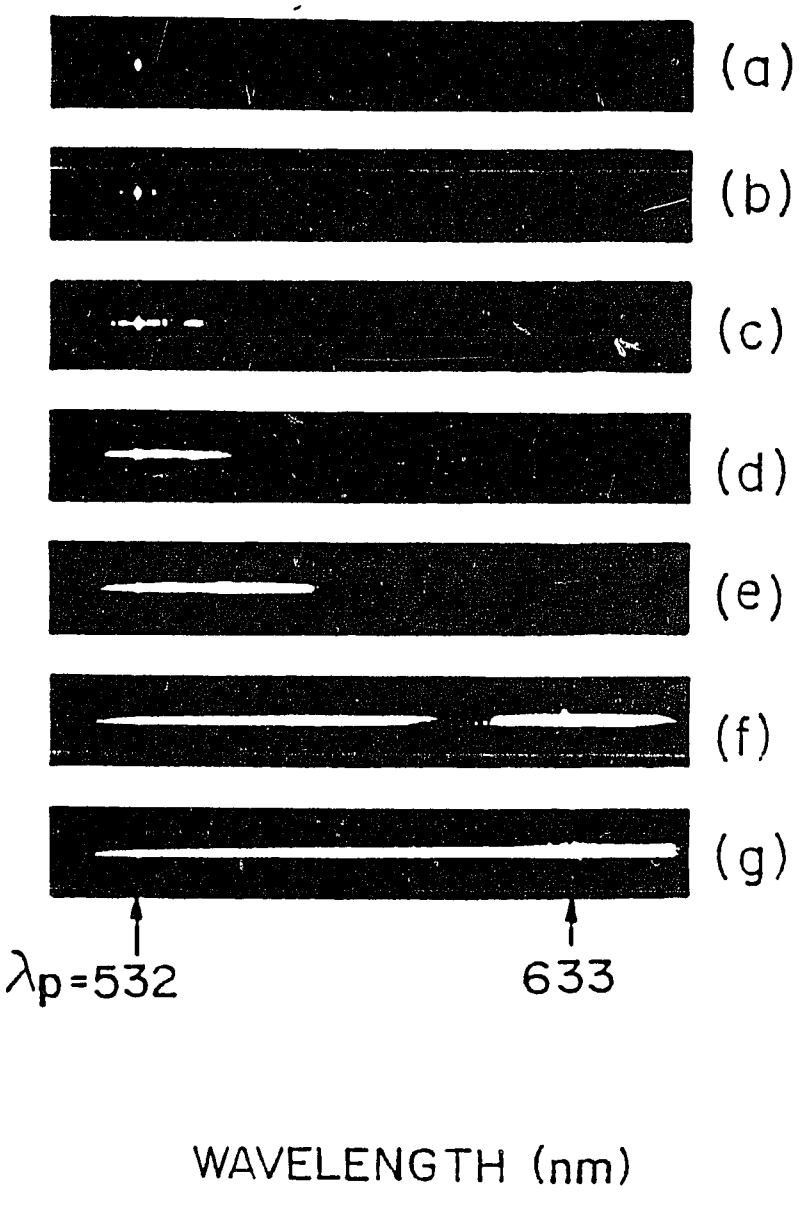

Fig. 3.5.1 Evolution of a stimulated four photon spectrum with the increase of the pulse intensity. a) $I<10^8$ W/cm^2. b) and c) $I=5X10^8$ W/cm^2. d) $I=10X10^8$ W/cm^2. e) $I=15X10^8$ W/cm^2. f) $I=30X10^8$ W/cm^2. g) $I=35X10^8$ W/cm^2.

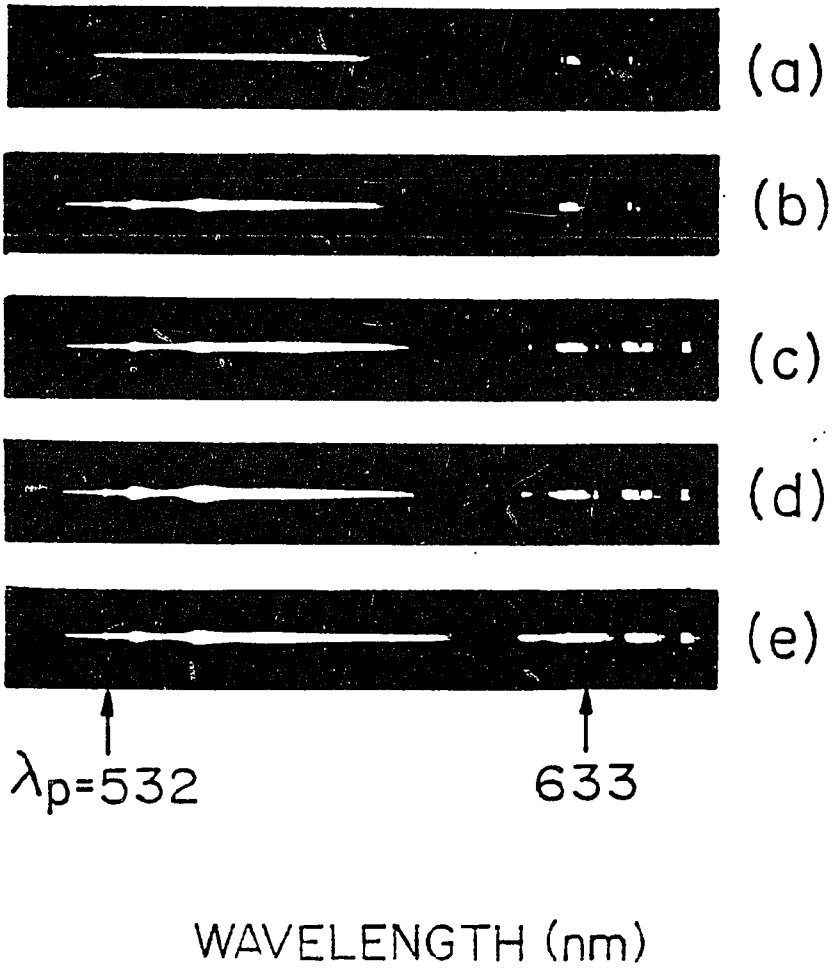

Fig. 3.5.2 a)-e) Sequence of the large-shift SFPM-lines broadening. The pulse peak intensity increases from I=20X10^8 W/cm^2 in a) to I=30X10^8 W/cm^2 in e) in steps of 2.5X10^8 W/cm^2.

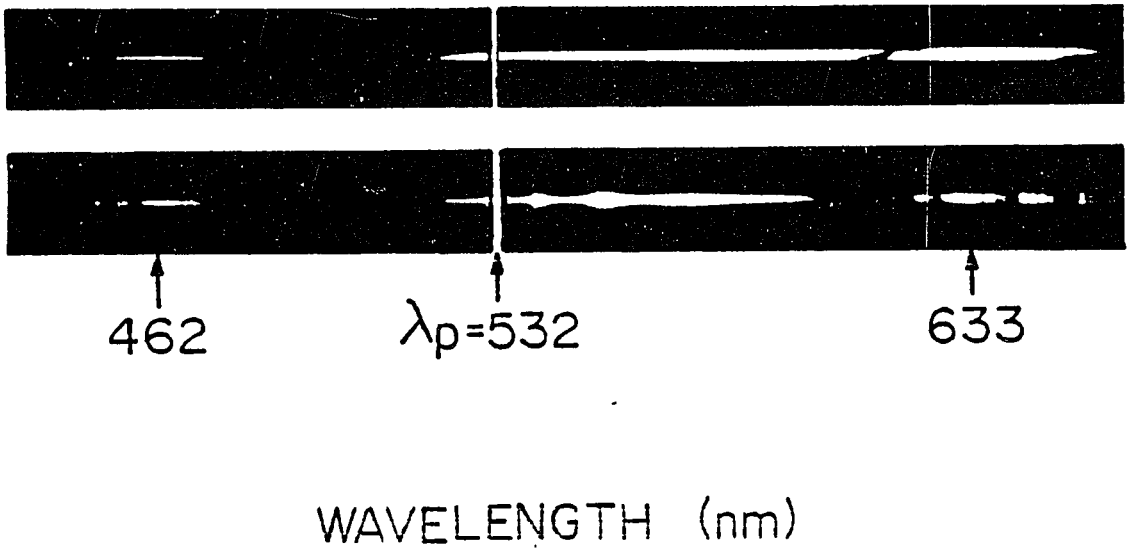

Fig. 3.5.3 Examples of large-shift Stokes lines with their corresponding anti-Stokes lines. Photographs of the Stokes and anti-Stokes regions were spliced together.

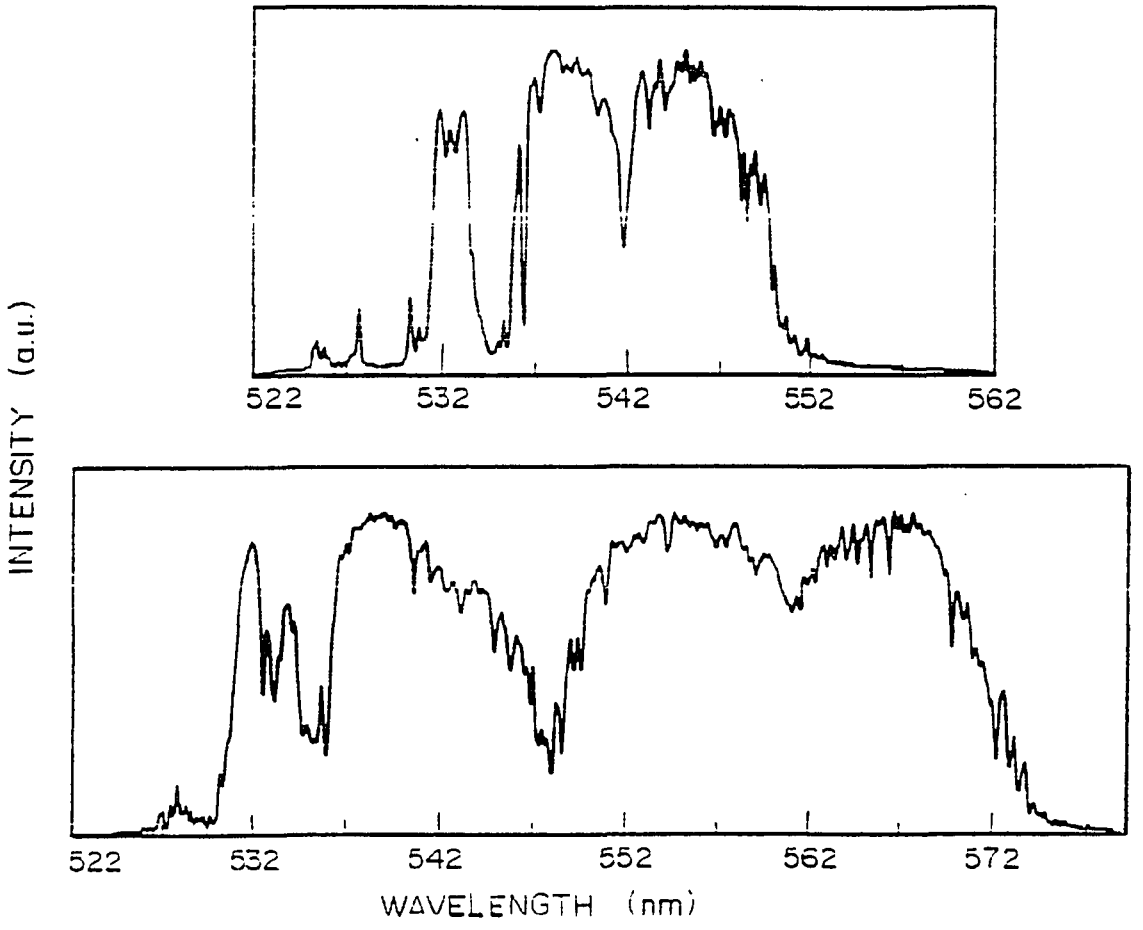

Fig. 3.5.4 Supercontinuum generation. a) The pump, SFPM, and first SRS Stokes lines are broadened at I=10X10^8 W/cm^2. b) The broadened second and third SRS Stokes lines appear and extend the spectrum toward the Stokes wavelengths at I=15X10^8 W/cm^2.

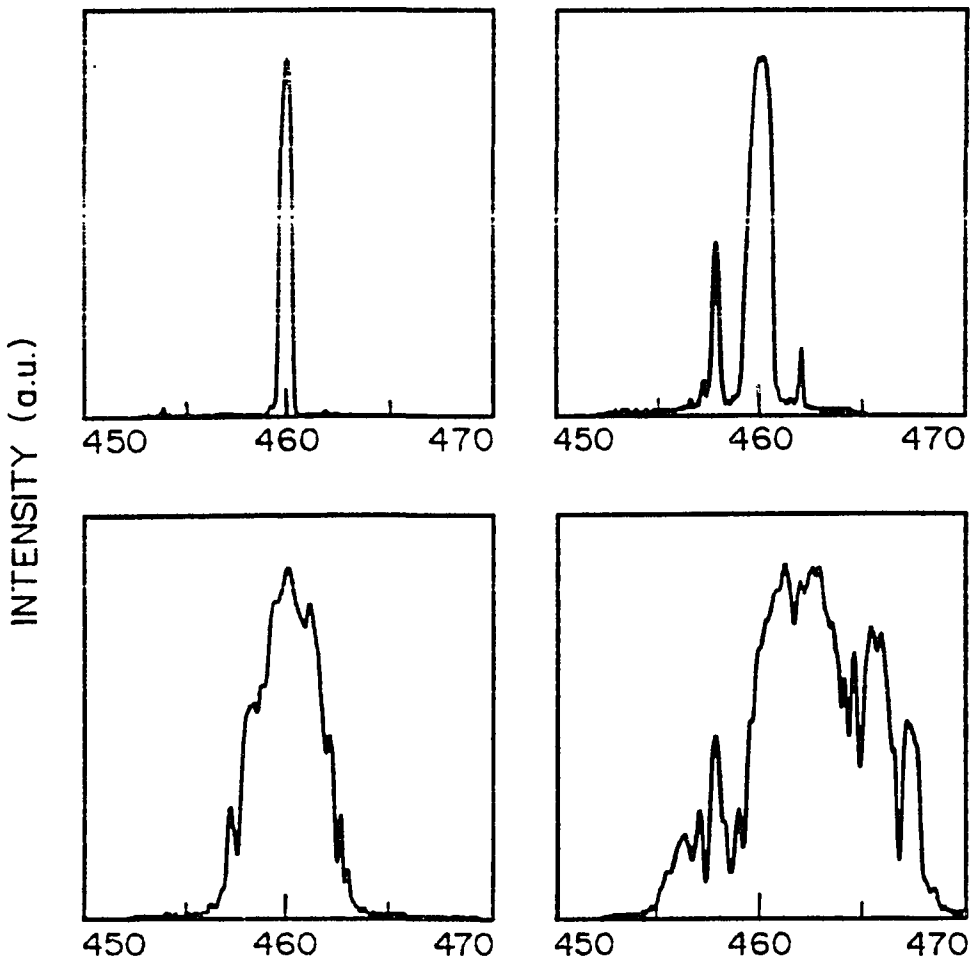

Fig. 3.5.5 The pulse peak intensity increases from I=20X10^8 W/cm^2 in a) to I=30X10^8 W/cm^2 in e) in steps of 2.5X10^8 W/cm^2.

3.7 References:

1. R.R. Alfano, Editor, *The Supercontinuum Laser Source,* (Springer-Verlag, Berlin, Heilderberg, 1989).

2. J. Gersten , R.R. Alfano, and M. Belic. Phys. Rev. **A21**, 1222-1224 (1980).

3. R.R Alfano, Q. Li, T. Jimbo, J. Manassah, and P.P. Ho. Op. Lett. **11**, 626-628 (1986).

4. Jamal T. Manassah, M. Mustafa, R.R. Alfano, and P.P. Ho. Phys. Lett. **113A**, 242-247 (1985).

5. D. Schadt, B. Jaskorzynska, and U. Osterberg. J. Opt. Soc. Am. **B3**, 1257-1260 (1986).

6. D. Schadt and B. Jaskorzynska. J. Opt. Soc. Am. **B4**, 856-862 (1987).

7. M.N. Islam, L.F. Mollenauer, R.H. Stolen, J.R. Simson, and H.T. Shang. Opt. Lett. **12**, 625-627 (1987).

8. M.N. Islam, L.F. Mollenauer, R.H. Stolen, J.R. Simson, and H.T. Shang. Opt. Lett. **12**, 814-816 (1987).

9. Jamal T. Manassah. Appl. Opt. **26**, 3747-3749 (1987).

10. Jamal T. Manassah. Appl. Opt. **26**, 3750-3751 (1987).

11. R.R., Alfano, P.L. Baldeck, F. Raccah, and P.P. Ho. Appl. Opt. **26**, 3491-3492 (1987).

12. P.L. Baldeck, P.P. Ho, and R.R. Alfano. Rev. Phys. Appl. **22**, 1677-1694 (1987).

13. A. Hook, D. Anderson, and M. Lisak. Opt. Lett. **13**, 1114-1116 (1988).

14. R.R. Alfano, Q. Z. Wang, T. Jimbo, and P.P. Ho. Phys. Rev. **A35**, 459-462 (1987).

15. R.R. Alfano and P.P. Ho. IEEE J. Quantum Electron. **24**, 351-364 (1988).

16. P.P. Ho, Q.Z. Wang, D. Ji, and R.R. Alfano. Appl. Phys. Lett. **53**, 111-113 (1988).

17. Jamal T. Manassah. J. Opt. Soc. Am. **B4**, 1235-1240 (1987).

18. Jamal T. Manassah and Orville R. Cockings. Opt. Lett. **12**, 1005-1007 (1987).

19. P.L. Baldeck and R.R. Alfano. J. Lightwave Technol. **L.T-5**, 1712-1715 (1987).

20. Govind P. Agrawal, P. L. Baldeck, and R. R. Alfano. Temporal and spectral effects of cross-phase modulation on copropagating ultrashort pulses in optical fibers. Submitted for publication.

21. Govind P. Agrawal. Phys. Rev. Lett. **59**, 880-883 (1987).

22. Govind P. Agrawal, P.L. Baldeck, and R.R. Alfano. Phys. Rev. **A39**, 3406-3413 (1989).

23. D. Schadt and B. Jaskorzynska. Electron. Lett. **23**, 1091-1092 (1987).

24. P.L. Baldeck, R.R. Alfano , and Govind P. Agrawal. Observation of modulation instability in the normal-dispersion regime of single-mode optical fibers. Submitted for publication.

25. A.S. Gouveia-Neto, M.E. Faldon, A.S.B. Sombra, P.G.J. Wigley, and J.R. Taylor. Opt. Lett. **13**, 901-903 (1988).

26. A.S. Gouveia-Neto, M.E. Faldon, and J.R. Taylor. Opt. Lett. **12**, 1029-1031(1988).

27. S. Trillo, S. Wabnitz, E.M. Wright, and G.I. Stegeman. Opt. Lett. **13**, 871-873 (1988).

28. B. Jaskorzynska and D. Schadt. IEEE J. Quantum Electron. **QE-24**, 2117-2120 (1988).

29. Jamal T. Manassah. Opt. Lett. **13**, 752-755 (1988).

30. Govind P. Agrawal, , P. L. Baldeck, and R. R. Alfano. Opt. Lett. **14**, 137 (1989).

31. P.L. Baldeck, R.R. Alfano, and Govind P. Agrawal. Appl. Phys. Lett. **52**, 1939 (1988).

32. D. Schadt and B. Jaskorzynska. J. Opt. Soc. Am. **B5**, 2374-2378 (1988).

33. Jamal T. Manassah. Opt. Lett. **14**, 396-397 (1989).

34. Govind P. Agrawal, *Nonlinear Fiber Optics* (Academic Press, London, 1989).

35. R.R. Alfano and S.L. Shapiro. Phys. Rev. Lett. **24**, 584-587 (1970).

36. R.H. Stolen. J. Quantum Electron. **QE-11**, 100-103 (1975).

37. R.H. Stolen, M.A. Bosh, and C. Lin. Opt. Lett. **6**, 213-215 (1981).

38. K. Washio, K. Innoue, and T. Tanigawa. Electron. Lett. **16**, 331-333 (1980).

39. C. lin and M.A. Bosh. Appl. Phys. Lett. **38**, 479-481 (1981).

40. P.L. Baldeck and R.R. Alfano. J. Lightwave Techn. **LT-5**, 1712-1715 (1987).

CHAPTER 4

TERAHERTZ PULSE GENERATION ARISING FROM MODULATION INSTABILITY IN OPTICAL FIBERS AND CPM DYE LASERS

4.1. Introduction:

The ultimate optical bandwidth of optical fibers is about 100 THz. This corresponds to the possibility to use 10-fsec time duration optical pulses to transmit information. The generation, propagation and coding of such pulses with terahertz repetition rates is one of the most challenging task of future optical communication engineering.

The direct generation of femtosecond pulses with terahertz repetition rates would required a candidate broadband (50 nm bandwidth) mode-locked laser to have a cavity length in the μm range. Such laser with the corresponding fast saturable absorbant has still to be discovered. Meanwhile, it has been proposed and demonstrated that modulation instability can be used to generate train of femtosecond pulses with up to 15 terahertz repetition rates.[1-12] As it will discussed in Chapter 6, cross-phase modulation effects can be used for the optical processing (phase, frequency, temporal and spatial coding) of such high repetition rate pulses.

Modulation instability refers to the sudden break-up in time of waves propagating in nonlinear dispersive media. It is a common nonlinear

phenomenon studied in several branches of physics (an overview on modulation instability can be find in [1-2]). Modulation instabilities occur when the steady state becomes unstable as a result of an interplay between the dispersive and nonlinear effects. Tai, Hasegawa and Tomita have observed the modulation instability in the anomalous-dispersion regime of silica fibers, i.e. for wavelengths greater than 1.3 μm.[3-5] Most recently, Agrawal has suggested that a new kind of modulation instability can occur even in the normal-dispersion regime when two copropagating fields interact with each other through the nonlinearity-induced cross-phase modulation.[6,8,9,11] This chapter summarizes the first observation of a modulation instability initiated by cross-phase modulation in the normal-dispersion regime of silica optical fibers (section 4.2) and in a femtosecond dye laser (section 4.3).

4.2 Observation of Modulation Instability in the Normal Dispersion Regime of Single-Mode Optical Fibers.

In this section we discuss our measurement of modulation instability in the normal dispersion regime of optical fibers.[9]

Optical pulses at 532 nm were generated either by a mode-locked Nd:YAG laser or a Q-switched Nd:YAG laser with widths of 25 ps or 10 ns, respectively. In both cases the repetition rate of pulses was 10 Hz. Pulses were coupled into a single-mode optical fiber using a microscope lens with a magnification of 40. The peak power of pulses into the fiber could be adjusted in the range 1 to 10^4 W by changing the coupling conditions and by using neutral density filters. The optical fiber was custom made by Corning Glass. It has a 2.5-μm core diameter, a 0.24% refractive index difference and a single-mode cut-off at λ=462 nm. Spectra of output pulses were measured using a grating spectrometer (1 meter-600 lines/mm) and recorded with an optical multichannel analyzer OMA2.

Figures 4.2.1 & 4.2.2 show spectra of intense 25-ps pulses recorded for different peak powers and fiber lengths. Figure 4.2.1-a is the reference spectrum of low-intensity pulses. Figures 4.2.1-b and 4.2.1-c show spectra measured at about the modulation-instability threshold for fiber lengths of 3 m and 0.8 m, respectively. They show modulation-instability sidebands on both sides of the laser wavelength at 532 nm and the first-order stimulated Raman scattering line at 544.5 nm. Notice that the frequency shift of sidebands is larger for the shorter fiber. Secondary sidebands were also

observed for pulse energy well above the modulation instability threshold and longer optical fiber lengths as shown in Fig. 4.2.2.

Similar to spectra in Tai et al's experiment,[4] spectra shown in Figs. 4.2.1 and 4.2.2 are undoubtfull signatures of modulation instability. A major salient difference of spectra in Figs. 4.2.1 and 4.2.2 is that they show modulation instability about 532 nm, a wavelength in the **normal-dispersion regime** of the fiber. According to the theory, modulation instability at this wavelength is possible only if there is a cross-phase modulation interaction.[6,11] As shown in Fig. 4.2.1, modulation-instability sidebands were observed only in presence of stimulated Raman scattering light. It has been recently demonstrated that cross-phase modulation is intrinsic to the stimulated Raman scattering process. Therefore, sideband features observed in Figs. 4.2.1 & 4.2.2 are conclusively a result of the cross-phase modulation induced by the simultaneously generated Raman pulses. To rule-out the possibility of multimode or single-mode stimulated four-photon mixing process as the origin of the sidebands, we note that the fiber is truly single-mode (cut-off wavelength at 462 nm) and that the sideband separation changes with the fiber length.

To strengthen the conclusion that the sidebands are due to modulation instability induced by cross-phase modulation, we have measured and compared with theory the dependence of sideband shifts on the fiber length. For this measurement, they used 10-ns pulses from the Q-switched Nd:YAG laser to ensure the quasi CW operation. The spectra were similar to those obtained with 25-ps pulses (Fig. 4.2.1). As shown in Fig. 4.2.3, the sidelobe

separation, defined as the half-distance between sideband maxima, varied from 1.5 nm to 8.5 nm for fiber lengths ranging from 4 m to 0.1 m, respectively. The energy of input pulses was approximately set at the modulation instability threshold for each fiber length. The solid line in Fig. 4.2.3 corresponds to the theoretical fit. As discussed in ,[6,11] the maximum gain of modulation instability sidebands is given by $g_{max}=k''\Omega_m^2$, where $\Omega_m=2\pi f_m$ is the sideband shift. Thus, the power of a sideband for an optical fiber length L is given by:

$$P(\Omega_m,L) = P_{noise}\exp(k''\Omega_m^2 L) \tag{4.1}$$

where P_{noise} is the initial spontaneous noise and $k''= \partial(v_g)^{-1}/\partial\omega$ is the group velocity dispersion at the laser frequency.

For such amplified spontaneous emission, it is common to define a threshold gain g_{th} by:

$$P_{th}(L) = P_{noise}\exp(g_{th}) \tag{4.2}$$

where P_{th} is the sideband power near threshold such as each sideband contains about 10% of the input energy. A typical value for g_{th} is 16.[4]

From Eqs. 4.1 and 4.2, the dependence of the sideband shift with the fiber length near threshold is given by:

$$\Omega_m = (g_{th}/k''L)^{1/2} \tag{4.3}$$

At λ=532 nm, the group velocity dispersion is $k'' \approx 0.06$ ps^2/m. The theoretical fit shown in Fig. 4.2.3 (solid line) is obtained using this value and g_{th} = 18.1 in Eq. 4.3. The good agreement between the experimental data and the theory of modulation instability supports our belief that we have observed cross-phase-modulation-induced modulation instability, as predicted in [6,11].

Tai et al. have shown that modulation instability leads to the breakup of long quasi-CW pulses in trains of picosecond subpulses.[4] The data described in Fig. 4.2.3 shows that the maximum sideband shift is $\Delta\lambda_{max} \approx 8.5$ nm or 8.5 THz which corresponds to the generation of femtosecond subpulses within the envelope of the 10-ns input pulses with a repetition time of 120 fs. Despite, autocorrelation measurements were not possible yet because of the low repetition rate (10 Hz) needed to generate pulses with kW peak powers, we believe that they have generated for the first time modulation instability subpulses shorter than 100 fs.

We observed modulation instability in the normal-dispersion regime of optical fibers. Modulation-instability sidebands appear about the pump frequency as a result of cross-phase modulation induced by the simultaneously generated Raman pulses. Sideband frequency shifts were measured for many fiber lengths and were found to be in good agreement with theory. In this experiment, cross-phase modulation originated from an optical wave generated inside the nonlinear medium, but similar results are

expected when both waves are incident externally. Modulation instability induced by cross-phase modulation represents a new kind of modulation instability that occurs not only in normally dispersive materials, but also, most importantly, has the potential to be controlled in real time by switching on or off the copropagating pulse responsible for the cross-phase modulation. Using optical fibers, such modulation instabilities could lead to the design of a novel source of femtosecond pulses at visible wavelengths.

4.3 15 Terahertz Pulse Generation Arising from Modulation Instability Oscillation in a Colliding Pulse Mode-Locked Dye Laser

In this section, we report on the first observation of modulation instability oscillation in a colliding-pulse mode-locked dye laser (Fig. 4.3.1).[12] Trains of a few tens of femtosecond pulses with 15 terahertz repetition rates were obtained by operating the laser in the negative dispersion regime with a low concentration of DODCI saturable absorber. To our knowledge, this is the highest repetition rate for well separated optical pulses reported to date.

In this design both astigmatic distortions and frequency shift introduced by oblique angles of incidence are avoided. Rhodamine 590 was used as the gain medium with concentration of 1.4×10^{-3} M/l in a jet with thickness of about 120 μm. The modulation instability oscillation regime was obtained when DODCI was used as the saturable absorber medium with a rather low concentration of $0.5 \sim 2 \times 10^{-4}$ M/l in a jet thickness of about 50 μm. Using a low concentration of DODCI can increase the saturation parameter.Therefore, the negative chirp from the absorber saturation shifts to the beginning of the pulse and the amount of negative chirp reduces. As a result, the pulse chirping originates mainly from the nonlinear refractive index of the solvent. This chirp rearrangement of the frequency components, i.e. chirp linearization, is very important for the generation of modulation instability and, similarly, for soliton shaping. The amount of negative group-velocity dispersion in the cavity was controlled by a four-prism sequence with

a separation of about 30 cm. The time evolution of the laser pulse was monitored by a dispersionless noncollinear autocorrelator driven by a shaker with a 0.1mm thick KDP crystal.

Typical autocorrelation traces of the terahertz pulse trains are presented in Figs. 4.3.2 and 4.3.3. It is shown that 1) trains of femtosecond subpulses are generated within a pulse envelope of about 600 femtosecond time-duration, and 2) the subpulse repetition rate depends critically on the saturable absorber thickness, the intracavity glass path and the input pump power (Fig. 4.3.4). In Fig. 4.3.2, the modulation period decreases from 140 fs to 80 fs when the thickness of the absorber dye jet is increased from about 40 to 50 μm by moving the jet vertically. This is because the total amount of (negative) dispersion decreases (see equation 4.4). For the same argument, figure 4.3.3 (from a to c) shows a decrease of the modulation period when the intracavity glass path is increased a few microns by translating one of the intracavity prisms. The modulation period changes from 160 fs to 64 fs, which corresponds to a 15.6 terahertz repetition rate. The modulation period was also found to decrease with the input pump power (see equation 4.4).

It is apparent from Fig. 4.3.3-c that the autocorrelation shape is modulated by as much as 60 % indicating that the subpulses are separated completely in the real time.[7] The autocorrelation shape and envelope of the laser output power were simultaneously measured. In the regime of modulation instability oscillation, we did not observe the strong regular modulation (5-200 kHz) which is a characteristic of high-order soliton shaping

process. It is worth noting that the overall pulse duration of the pulse envelope remains about the same in Figs. 4.3.2 and 4.3.3.

The modulation instability oscillation in CPM dye laser appeared after the soliton state. When the intracavity glass path is increased the soliton state is obtained first.Then, when the intracavity glass path is increased further, the soliton state pulse suddenly breaks up into a new state with regular periodic modulation---modulation instability oscillation.Increasing the intracavity glass path further from the state which corresponds to the highest subpulse repetition rate, the periodic modulation on the pulse envelope suddenly turns into a random modulation regime (Fig. 4.3.3-d). This behavior resembles the transition from a soliton state to a periodic state to a chaotic state .

In the following, the generation of terahertz subpulses which is described in Figs. 4.3.2 and 4.3.3 is interpreted as a modulation instability oscillation which has been predicted to arise from the propagation of intense optical pulses in a nonlinear dispersive cavity. Modulation instability is the temporal result of a colinear four-photon-mixing process which is phase matched by the intensity-dependence of the nonlinear refractive index (see appendix 2 for details). Once the phase-matching condition is achieved, the modulation instability grows exponentially from an initial frequency background which can originate from quantum noise, fluorescence, and/or self-phase modulation. In a CPM dye laser cavity, if the intracavity peak power and negative group-velocity dispersion conditions are satisfied, an intense soliton-like pulse propagating through the absorber dye jet can generate simultaneously the nonlinear refractive index which is needed to

satisfy the phase matching condition, and the self-phase modulation spectral broadening which is necessary to seed the process at the four-wave mixing frequencies. As a result, collinear Stokes- and anti-Stokes waves are generated, and interfere in time with the un-shifted laser pulse. In addition, the gain medium of the CPM dye laser can amplify the modulation which repeats for each round trip in the cavity. Therefore, the soliton-like initial optical pulse can break-up into an internal pulse structure which develops a deep amplitude modulation. Such modulation instability process which is seeded by the self-phase modulation spectral broadening has been observed in optical fibers. This process has been called self-amplitude modulation.[7]

In first approximation, the nonlinear propagation of ultrashort pulses in a CPM dye laser can been described by using the formalism of pulse propagation in nonlinear dispersive optical fibers in which the repetition rate of modulation instability subpulses is given by the ratio of chirp to dispersion (a simple derivation can be find in appendix 2):[6,11]

$$\nu_{max} = \frac{1}{2\pi}\left(\frac{\omega_0}{c}\frac{n_2|E|^2}{|\beta^{(2)}|}\right)^{1/2} \tag{4.4}$$

where n_2 is the nonlinear refractive index of the saturable absorber solvent, E^2 is the pulse intensity at the dye jet focus, and $\beta^{(2)}$ is the effective group velocity dispersion in the CPM dye laser cavity.

To compare our experimental results with the modulation instability theory, we have studied the dependence of the subpulse repetition rate with

the Ar^+ laser pump power which was found to be linearly dependant with the intracavity pulse peak power in the regime of modulation instability oscillation (Fig. 4.3.4). The "zero" pump power in Fig. 4.3.4 corresponds to the situation where the shortest pulse is obtained but no modulation on the pulse envelope is achieved. Dots in Fig. 4.3.4 are the experimental data points. The solid line is a data fit obtained by a least mean square algorithm. The data fit gives a relationship $\nu_{max} \sim (|E|^2)^{0.503}$ which is in a surprisingly good qualitative agreement with the modulation instability theory. A quantitative comparison of our experimental results with Eq. 4.4 is not possible as the intracavity group velocity dispersion $\beta^{(2)}$ is difficult to evaluate. Figures 4.3.2 and 4.3.3 show also a qualitative agreement of our experimental data with Eq. 4.4. Increasing the intracavity glass path or jet thickness, the amount of the negative dispersion in the laser cavity is decreased, and so the subpulse repetition rate is increased.

In conclusion, we have observed modulation instability oscillation which is a new operating regime for the CPM femtosecond dye laser. Trains of a few tens of femtosecond pulses with 15 terahertz repetition rates were obtained by operating the laser in the negative dispersion regime with a low concentration of DODCI saturable absorber. Modulation instability oscillation in the CPM laser could originate from self-amplitude modulation initiated by self-phase modulation during the pulse formation process. Experimental results are in a good qualitative agreement with the modulation instability theory.

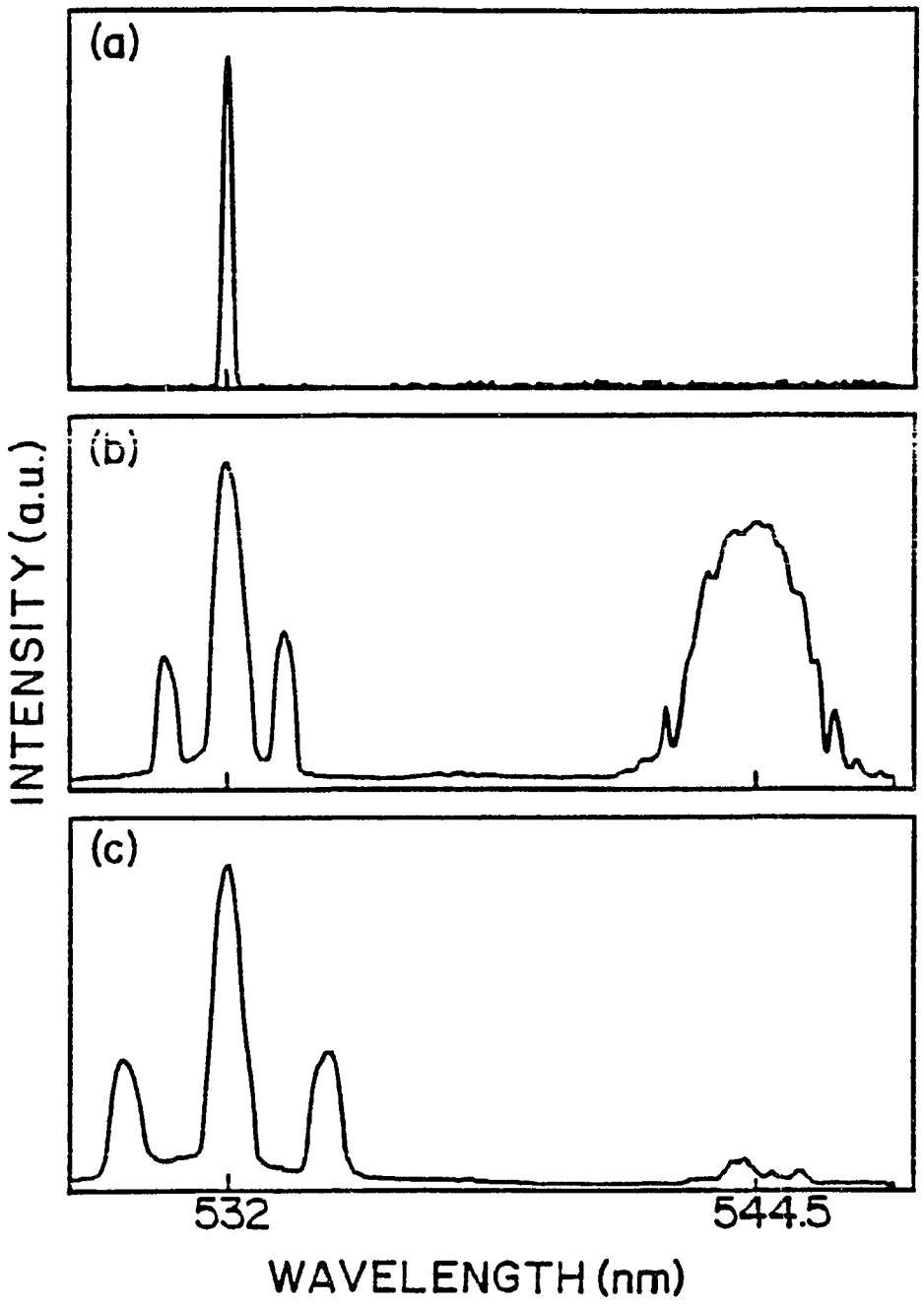

Fig. 4.2.1 Characteristic frequency sidebands of modulation instability resulting from cross-phase modulation induced by the simultaneously generated Raman pulses in lengths L of a single-mode optical fiber. The laser line is at λ=532 nm and the Raman line at λ=544.5 nm. The time duration of input pulses is 25 ps. a) Reference spectrum at low intensity. b) Spectrum at about the modulation instability threshold and L=3 m. c) same as b) for L=0.8 m.

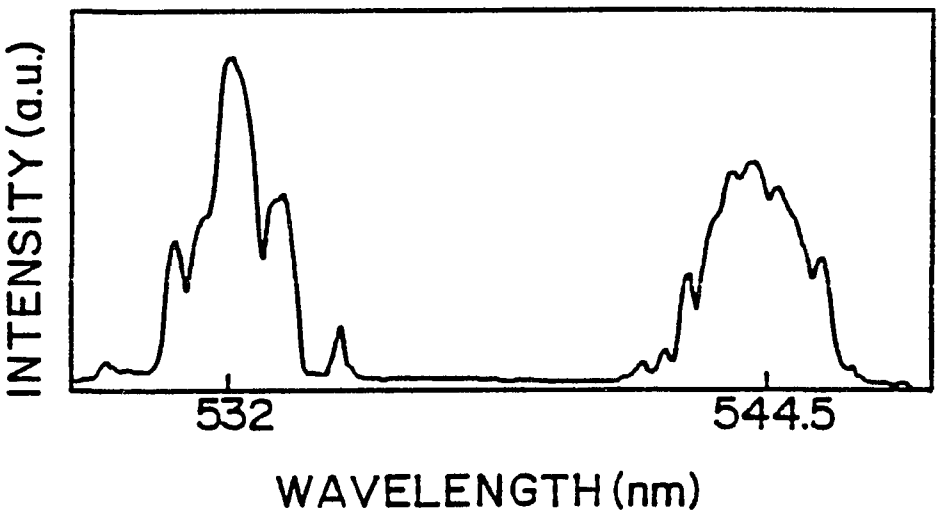

Fig. 4.2.2 Secondary sidebands which were observed for pulse energy well above the modulation instability threshold.

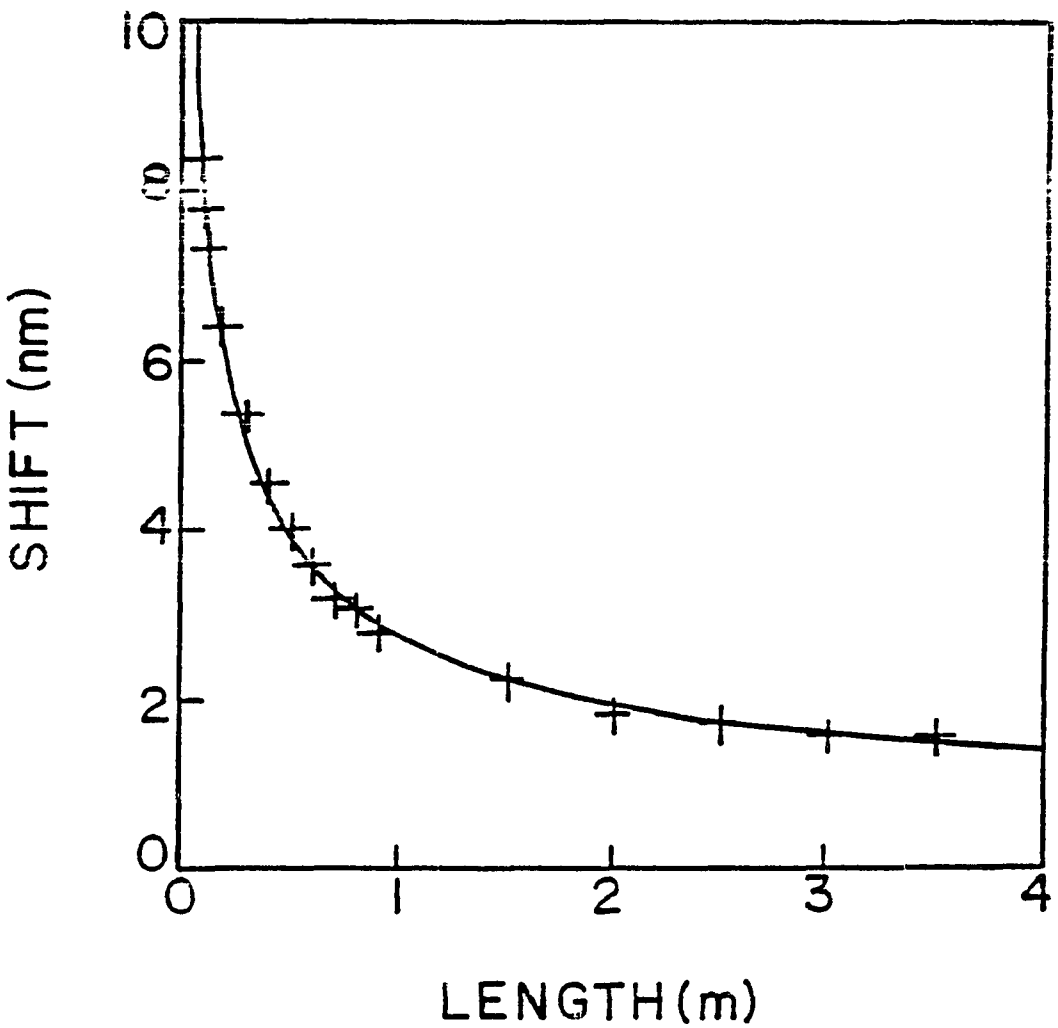

Fig. 4.2.3 Sideband shifts *versus* fiber length near the modulation instability threshold. The time duration of input pulses is 10 ns. Crosses are experimental points. The solid line is the theoretical fit.

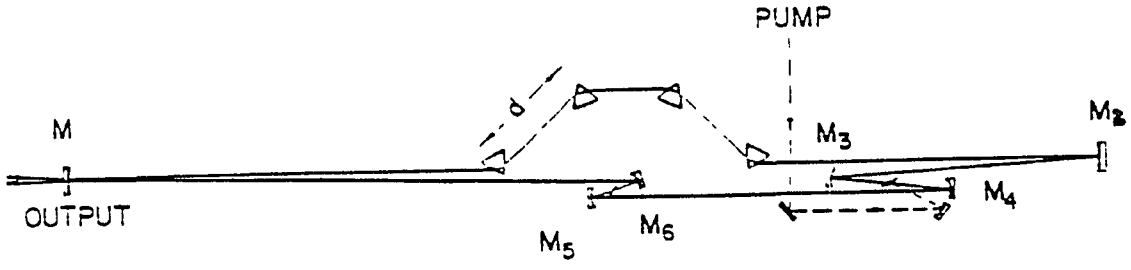

Fig. 4.3.1 Schematic diagram of the CPM dye laser.

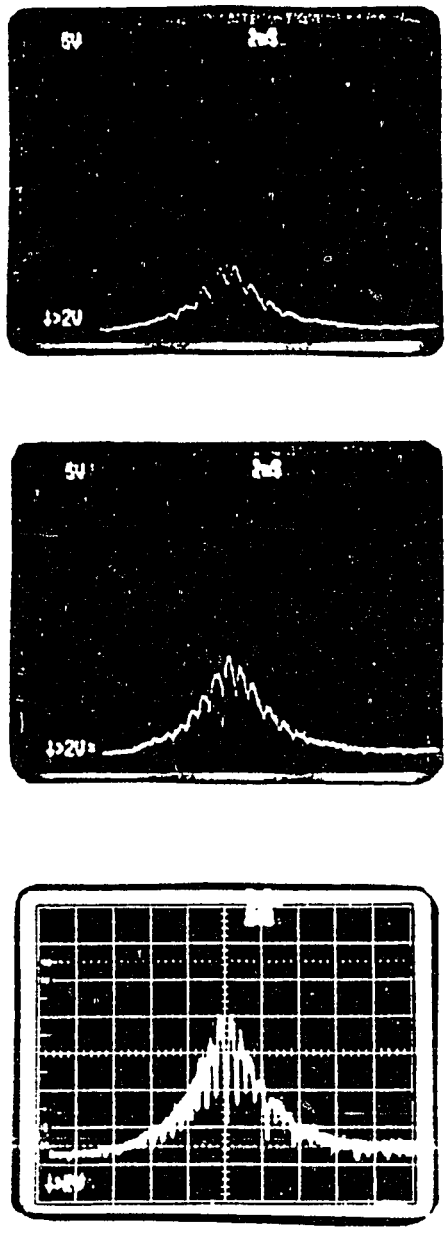

Fig. 4.3.2 Autocorrelation traces of the modulation instability oscillation in the CPM dye laser for different jet thicknesses.The thickness of the absorber jet was increased from about 40 to 50 μm. The period of modulation instability subpulses changes from 140 fs (Fig. 3.6.5-a) to 80 fs (Fig. 3.6.5.c). One division corresponds to 320 fs in time.

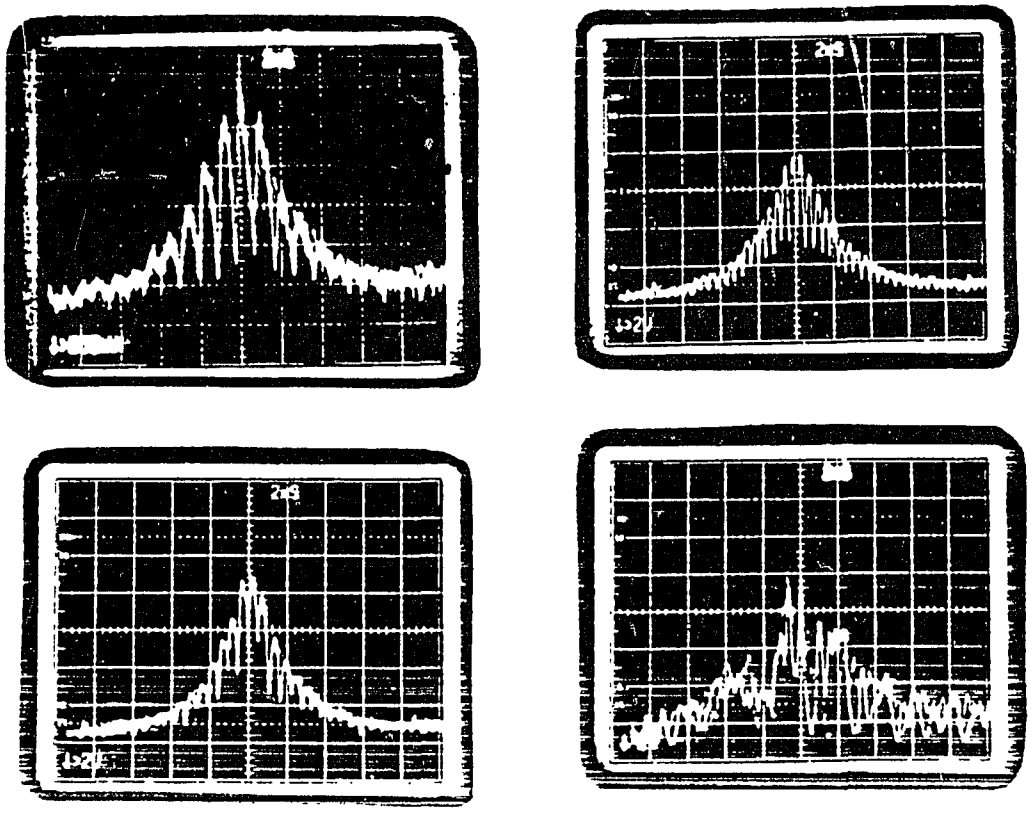

Fig. 4.3.3 Autocorrelation traces of the modulation instability oscillation in the CPM dye laser for different amount of intracavity glass. The period of modulation instability subpulses changes from 160 fs to 64 fs due to the increased of intra-cavity glass. This corresponds to subpulse repetition rates up to 15.6 terahertz. One division corresponds to 320 fs in time.

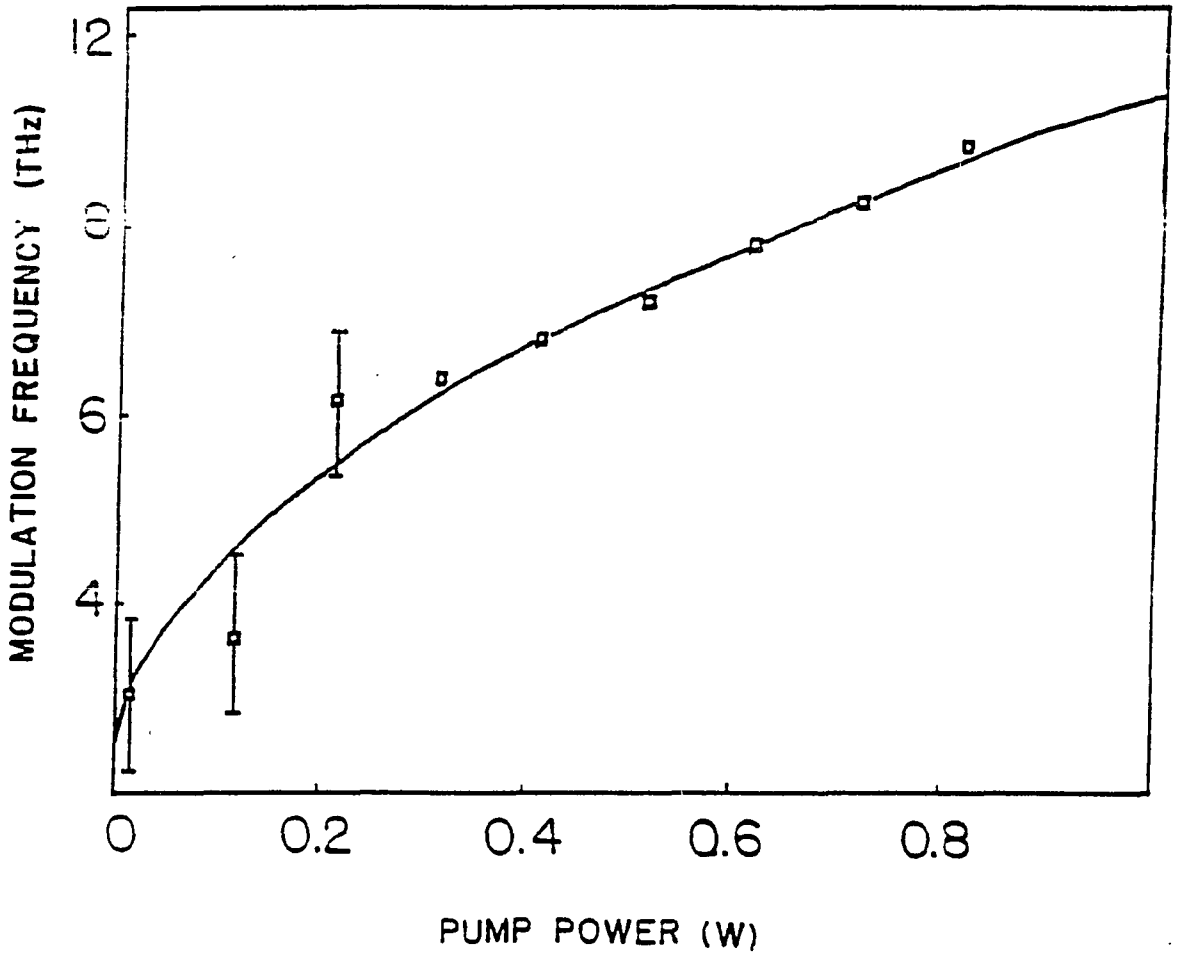

Fig. 4.3.4 Dependence of the subpulse repetition rate on the Ar^+ laser pump power. The solid line is a theoretical fit from the modulation instability theory.

4.5 References

1. A. Hasegawa. *Plasma Instabilities and Nonlinear Effects* (Springer-Verlag, Heildelberg, 1975).

2. Govind P. Agrawal. *Nonlinear Fiber Optics* (Academic Press, Boston, 1989).

3. K. Tai and A. Tomita, Appl. Phys. Lett. **48**, 1033 (1986).

4. K. Tai, A. Hasegawa, and A. Tomita, Phys. Rev. Lett. **56**, 135 (1986).

5. K. Tai and A. Tomita, J. L. Jewell, and A. Hasegawa, Appl. Phys. Lett. **49**, 236 (1986).

6. G. P. Agrawal, Phys. Rev. Lett. **59**, 880 (1987).

7. M. J. Potasek and G. P. Agrawal, Phys. Rev. **A 36**, 3862 (1987).

8. A. S. Gouviea-Neto, M. E. Faldon, A. S. B. Sombra, P. G. J. Wigley, and J. R. Taylor, Opt. Lett. **13**, 901 (1988).

9. P. L. Baldeck, R. R. Alfano, G. P. Agrawal. In *Ultrafast Phenomena 6* (Springer-Verlag, Berlin, Heilderberg 1988), pp. 53-54.

10. M. Nakazawa, K. Suzuki, and H. A. Haus. Phys. Rev. **A48**, 5193 (1988).

11. Govind P. Agrawal, P.L. Baldeck, and R.R. Alfano. Phys. Rev. **A39**, 3406-3413 (1989).

12. Ching-Yue Wang, P.L. Baldeck, Y. Budansky, and R.R. Alfano. Opt. Lett. **14**, 497-499 (1989).

CHAPTER 5

SPATIAL EFFECTS OF NONLINEARITIES IN LARGE CORE OPTICAL FIBERS

5.1 Observation of Beam Focusing in Multimode Optical Fibers

Self-phase modulation originates from the nonlinear refractive index $\Delta n(r, t)=n_2 E_0^2(r, t)$ which is generated by the pulse propagating in the nonlinear medium. Consequently, SPM has not only temporal and spectral effects but also spatial effects. Self-focusing corresponds to the focusing of the beam due the radial change of the refractive index induced by the nonlinear propagation. Self-focusing has been observed in many liquids and solids since the 60's. [1-4]

In this section I report on the focusing of picosecond pulses propagating in an optical fiber.[5] Focusing occurred at Raman frequencies for which the spatial effect of the nonlinear refractive index was enhanced by cross-phase modulation. This work might be important for communication links based on multimode optical fibers.

The experimental set-up is shown in Fig. 5.1.1. A Quantel frequency-doubled mode-locked Nd:YAG laser produced 25-ps pulses at 532-nm. The

laser beam was coupled into the optical fiber with a 10X microscope lens. A stable modal distribution was obtained with a Newport FM-1 mode scrambler. Images of the intensity distribution at the output face were magnified by 350X and recorded on photographic film. Narrow-band (NB) filters were used to select frequencies of the output pulses. The optical fiber was a commercial multimode step-index fiber (Newport F-MLD). Its core diameter was 100 μm, its numerical aperture 0.3, and its length 7.5 m.

Several magnified images of the intensity distributions that were observed at the output face of the fiber for different input pulse energies are shown in Fig. 5.1.2. The intensity distribution obtained for low pulse energies (E<1 nJ) is shown in Fig. 5.1.2-a. It consists of a disk profile with a speckle pattern. The intensity distribution of the disk covers the entire fiber-core area. The disk diameter, measured by comparison with images of calibrated slits, is 100 μm, which corresponds to the core diameter. The characteristics of this fiber allow for the excitation of about 200,000 modes. The mode scrambler distributed the input energy to most of the different modes. The speckle pattern is due to the interference of these modes on the output face. Figure 5.1.2-b shows the intensity distribution in the core for intense pulses (E> 10 nJ). At the center of the 100-μm-diameter disk image, there is an intense smaller (11 μm) ring of a Stokes-shifted frequency continuum of light. About 50% of the input energy propagated in this small-ring pattern. The corresponding intensities and nonlinear refractive indices are in the gigawatts per square centimeter and 10^{-6} ranges, respectively. For such intensities, there is a combined effect of stimulated Raman scattering, self-phase modulation, and cross-phase modulation (XPM) that generates the observed frequency

continuum. In Fig. 5.1.2-c, a NB filter selected the output light pattern at 550 nm. This clearly shows the ring distribution of the Stokes-shifted wavelengths. Such a ring distribution was observed for a continuum of Stokes-shifted wavelengths up to 620 nm for the highest input energy before damage.

The small-ring intensity profile is a signature of induced-focusing at the Raman wavelengths. There are many salient features. First, the small ring is speckleless, which is characteristic of single-mode propagation. This single-mode propagation means that the guiding properties of the fiber are dramatically changed by the incoming pulses. Second, SRS, SPM, and XPM occur only in the ring structure, i.e. where the maximum of input energy has been concentrated. This shows induced focusing of these beams. Our experimental results may be explained by an induced-gradient-index model for self-focusing. For high input energies, the Gaussian beam induces a radial change of the refractive index in the optical-fiber core. The step-index fiber becomes a gradient-index fiber, which modifies its light-guiding properties. There is further enhancement of the nonlinear refractive index at Raman frequencies because of XPM. Thus, Stokes-shifted light propagates in a well marked induced-gradient-index fiber. The ray-propagation characteristics of a gradient-index fiber are shown schematically in Fig. 5.1.3.[6] The cross-sectional view of a skew-ray trajectory in a graded-index fiber is shown. For a given mode u, there are two values for the radii, r_1 and r_2, between which the mode is guided. The path followed by the corresponding ray lies completely within the boundaries of two coaxial cylindrical surfaces that form a well-defined ring. These surfaces are known as the caustic surfaces. They have inner and

outer radii, r_1 and r_2, respectively. Hence, Fig. 5.1.3 shows that skew rays propagate in a ring structure that is comparable with the one shown in Fig. 5.1.2-c. This seems to support the induced-gradient-index model for induced-focusing of probe beams in optical fibers.

Self-focusing of Raman picosecond pulses have been observed in optical fibers. Experimental results may be explained by an induced-gradient-index model. An immediate application of this observation could be the single-mode propagation of high-bit-rate optical signals in large core optical fibers.

In recent similar experiment the Raman pulse, propagating in the anomalous regime of a 500-m multimode fiber, has been shown to form a femtosecond soliton (width 70-100 fs) which carried its energy in the fundamental fiber mode even though the 150-ps pump pulse excited a large number of the fiber modes.[7] It is though that this behavior is a consequence of a nonlinear mode coupling, which prevents a diffusion of energy to higher-index modes. However, the physical mechanism for this coupling is not yet clear.[7] In addition to this important experimental report Ref. 7 brought to our attention a previous paper[8] which has found results very similar to ours.

The following sections describes theoretical results on nonlinear effects associated with the spatial dependence of the nonlinearity $\chi^{(3)}$ in graded-index and homogeneous media.

5.2 Theory of Self-Focusing and Self-Phase Modulation in a Parabolic Graded-Index Optical fiber

In the process to explain our experimental results presented in the previous section, we have developed the following model of self-phase modulation and self-focusing in a graded-index optical fiber with Pr. Jamal T. Manassah of CCNY.[9] Afterwards, we found that this theoretical analysis does not give any insight into the self-focusing measurements performed in ref. 9 which might involve the nonlinear coupling and energy transfer between modes.[7] However, this theoretical study lead us to a better understanding of the combined effects of self-phase modulation, diffraction, and self-focusing.

The theoretical computation described in this section shows that the characteristics of self-phase modulated pulses are affected by the spatial distribution of the pulse intensity. The conventional self-phase modulation theory described in section 2.1 is based on the plane wave approximation. When there is diffraction or focusing of pulses, like in graded-index waveguides, the plane wave theory of self-phase modulation does not hold as discussed below. For example, we will see that in certain cases, the sign of self-phase modulation is reversed by the spatial effects.

The propagation of Gaussian beams in a graded-index waveguide structure leads to the appearance of a sequence of maxima and minima in the field intensity along the length of the fiber.[10] In this section, we examine the combined effects of the Kerr nonlinearity, diffraction and graded-index

waveguiding on the spatial and spectral profiles of an intense pulse propagating in a parabolic graded-index optical fiber. The beam transverse geometrical shape, radius of curvature, phase and spectrum are computed as function of the fiber parameters and pulse peak power. Approximate analytical results are derived for the beam waist, radius of curvature and phase.

In the case of low-intensity pulses propagating in a graded-index waveguide one can show that the longitudinal phase is given by $\phi = -kz + \eta(z)$. Where -kz is the plane-wave phase and $\eta(z)=\text{arctg}(z/z_0)$ is a corrective phase arising from the spatial distribution of the refractive index. In this section, we will show that the self-phase modulation generated by an intense pulse propagating in a graded-index waveguide not only has a plane wave contribution arising from the intensity-dependent refractive index of -kz, but also has a contribution arising from the intensity-dependent refractive index of $\eta(z)$. The key point is that the signs of kz and $\eta(z)$ are different. Therefore, the sign of self-phase modulation can be reversed by making the plane wave contribution of SPM smaller than the contribution of the corrective phase. This change of sign of SPM might have important consequences for the propagation of optical solitons in waveguides, and the spectral broadening and compression of ultrashort pulses.

In the following theoretical analysis, the approximations that we will make are that: 1) the graded index profile is approximated by[11] $n=n_0(1-Ar^2/2n_0)$, 2) the fiber core-cladding boundary conditions are neglected , we are assuming that the beam diameter a is much smaller than the core radius r_c, 3)

effects of group velocity dispersion are neglected, 4) the self-steepening of the amplitude is neglected, 5) the quadratic index of refraction n_2 is not modified by the radial variation in the ordinary index of refraction, 6) one component of the electric field is kept, i.e. we are neglecting the vector nature of the electric field, and 7) the gradient index of refraction is of the order required to guide the beam. Under these assumptions, ε the envelope of the electric field obeys the equation:

$$\nabla_T^2 \varepsilon - 2ik\varepsilon' - k k_2 r^2 \varepsilon + \frac{n_2 k^2}{n_0} |\varepsilon|^2 \varepsilon = 0 \qquad (5.2.1)$$

where ∇^2_T is the transverse component of the Laplacian, $\varepsilon' = \partial\varepsilon/\partial z$, $k_2 = kA = 2kn_0\Delta/r_c^2$, Δ is the relative index difference between the core center and the cladding.

If the initial condition is written as:

$$\varepsilon(r, 0, u) = \varepsilon_0 \exp\left(-\frac{r^2}{a^2}\right) \exp\left(-\frac{u^2}{2\tau^2}\right) \qquad (5.2.2)$$

The initial pulse is assumed to be Gaussian both in the transverse plane and in the comoving coordinate system $u=(z/v_g - t)$, where v_g is the pulse group velocity, a the initial beam radius, τ the pulse duration, and ε the magnitude of the pulse amplitude. This initial condition assumes that the beam radius is much smaller than the core radius.

In the following, the product $\varepsilon_o \exp(-u^2/2\tau^2)$ is denoted by $\tilde{\varepsilon}_o$. Then, an approximate solution to Eq. 5.2.1, with the boundary condition given by Eq. 5.2.2, correct to order r^2/a^2 can be obtained through the trial solution: [11]

$$\mathcal{E}(r, z, u) = \frac{\tilde{\mathcal{E}}_0}{\omega(z, u)} \exp\left[-\frac{r^2}{a^2 \omega^2(z, u)} - i \frac{k}{2} \rho(z, u) r^2 + ik\alpha(z, u) \right] \tag{5.2.3}$$

where the different functions can be interpreted as follows: ω is the normalized beam radius, ρ is the inverse of the beam radius of curvature, and $k\alpha$ is the longitudinal phase on the fiber axis. This approximation of self-similarity of the beam is well justified for powers smaller than the critical power, in particular for instances where ω_{max} and ω_{min} are not too far apart.

The equations satisfied by these subsidiary functions are:

$$\rho = \frac{1}{\omega} \frac{\partial \omega}{\partial z} \tag{5.2.4}$$

$$\frac{\partial \alpha}{\partial z} = \frac{a^2}{2\omega^2}[B - C] \tag{5.2.5}$$

$$\frac{\partial^2 \omega}{\partial z^2} + A\omega + [2C - B]\frac{1}{\omega^3} = 0 \tag{5.2.6}$$

where $A=1/L_w^2$, $B=4/a^4k^2=1/L_d^2$, $C=n_2\varepsilon_o^2/n_oa^2$, and L_w and L_d are the characteristic lengths for waveguiding and diffraction, respectively.

The solutions to Eqs. 5.2.5-5.2.6, satisfying the boundary conditions $\omega=1$, $\rho=0$, and $\alpha=0$ at $z=0$, are:

1) the normalized beam waist:

$$\omega = [\beta \cos(\gamma z) + \delta]^{\frac{1}{2}} \tag{5.2.7}$$

2) the inverse of the radius of curvature:

$$\rho = -\frac{1}{2}\frac{\beta\gamma \sin(\gamma z)}{\left[\beta \cos(\gamma z) + \delta\right]} \tag{5.2.8}$$

3) the longitudinal phase:

$$k\alpha = k\frac{a^2(B - C)}{2\left[B - 2C\right]^{\frac{1}{2}}} \operatorname{arctg}\left[\left(\frac{B - 2C}{A}\right)^{\frac{1}{2}} \operatorname{tg}\left(A^{\frac{1}{2}}z\right)\right] \tag{5.2.9}$$

where $\gamma=2A^{1/2}$, $\beta = (2C - B + A)/2A$ and $\delta = (A - 2C + B)/2A$. The above solutions are valid for $\beta \leq \delta$ or equivalently $B-2C \geq 0$. For negative n_2, (defocusing medium), $\beta<\delta$ is satisfied for all values of ε. For positive n_2 (focusing medium), $\beta=\delta$ for the critical field ε_c which is given by $\varepsilon_c^2=2n_o/a^2k^2n_2$. In the low intensity limit, Eqs. 5.2.7 to 5.2.9 lead to the usual results of Gaussian beams propagating in lens-like media. [13-14]

Equation 5.2.7 shows that the normalized beam waist ω varies periodically along the optical fiber length. The period of variation depends only on the waveguiding characteristic length L_w. The magnitude of ω_{min}, the minimum normalized beam waist, depends on all three characteristic lengths. In Fig. 5.2.1, the minimum beam waist is plotted as a function of the pulse normalized peak power $p=P/P_c=\varepsilon_0^2/\varepsilon_c^2$ for different graded-index

parameters Δ, where P_c is the critical power for self-focusing. The minimum beam diameter decreases for increasing peak powers and collapses at $P=P_c$.

The inverse of the radius of curvature (ρ) is plotted in Figure 5.2.2 as a function of the normalized fiber length $2z/(\pi L_W)$. For increasing peak powers, the curvature is clearly enhanced periodically by self-focusing at the beam waist locations.

The total phase of the electric field can be computed using Eqs. 5.2.3, 5.2.8 and 5.2.9. This phase, and consequently the spectral broadening arising from self-phase modulation, is radially-dependent. It is worth noting that the time-dependent part of the phase ϕ' (denoted ϕ'_t) =total phase $-\omega_o t$ reduces to that of the traditional SPM theory in the case of a homogeneous medium ($k_2=0$), and for an incoming plane wave ($a \rightarrow \infty$).

Furthermore, for weak waveguiding ($k_2 \rightarrow 0$), but finite initial beam diameter, the time-dependent phase ϕ'_t reduces to:

$$\lim_{k_2 \rightarrow 0} \phi'_t = \phi_{spm}\left(1 - \frac{2r^2}{a^2}\right) \tag{5.2.10}$$

Thus, in this limit the spectral extent as function of the radius varies as $(1-2r^2/a^2)$. Eq. 5.2.11 is valid for $r/a << 1$.

In figure 5.2.3, the longitudinal phase contribution $k\alpha(z,u=0)$, denoted α-phase, is plotted as function of the normalized fiber length for different power levels. As shown, the a-phase mostly increases by steps at z locations corresponding to the periodical positions of the minimum beam waist. As a result, the total amount of the longitudinal phase yielded by the pulse is often much larger than the usual SPM, and it depends strongly on the waveguiding diffraction and nonlinear parameters. It is worth noting that for $z<<L_W$ the regularized α-phase, defined as the value of the α-phase at a certain power minus its value for zero intensity, has the same sign as ϕ_{SPM}; however, this sign changes for $z>L_W$. The change of sign can be understand as follows: 1) for $z<< L_W$ the beam diameter is maximum and the plane-wave approximation - kz hold; therefore, we have the conventional result of SPM derived from the plane-wave theory. 2) for $z=\pi L_W/2$ the beam diameter passes by a minimum and the phase front is curve; therefore, the contribution from the corrective phase $\eta(z)$ is more important than the one from the plane-wave contribution kz, and there is change of the SPM sign. Moreover, as the beam intensity is very high (small beam diameter) there is a lot of SPM created. Physically, the change of sign of SPM leads to the reverse of the red leading the blue in the supercontinuum. Finally, one notices that α-phase approaches a ladder function for values of ε that equalize B and 2C (i.e., $P \rightarrow P_c$).

The temporal distribution of the longitudinal phase, the α-phase, can be studied using Eq. 5.2.9. If we define the parameter s as:

$$C = s\,B\,e^{-\frac{u^2}{\tau^2}} \tag{5.2.11}$$

where s=1/2 corresponds to $P=P_c$. Then,

$$\frac{(\alpha\text{-phase})_{regul}}{\phi_{spm}(u=0)} \approx \left(\frac{A}{B}\right)^{\frac{1}{2}} \frac{1}{s} \frac{\left[\left(1-2s\exp\left(-\frac{u^2}{\tau^2}\right)\right)^{\frac{1}{2}} + s\exp\left(-\frac{u^2}{\tau^2}\right) - 1\right]}{\left(1-2s\exp\left(-\frac{u^2}{\tau^2}\right)\right)^{\frac{1}{2}}} \tag{5.2.12}$$

In figure 5.2.5, the α-phase normalized to its maximum value (Eq. 5.2.12) is plotted as function of time for different power levels. For small peak powers, the width of the phase envelope is $\sqrt{2}$ smaller than the conventional SPM phase as predicted by Eq. 5.2.12. As the pulse peak power increases and tends to the critical power the phase width significantly decreases, and the value of the phase at its maximum increases dramatically.

The spectral distribution of intense ultrafast pulses propagating in a gradient-index fiber is computed by taking the Fourier transform of the field envelope defined by Eq. 5.2.3 and Eqs. 5.2.7-9. For small peak powers ($P<<P_c$) SPM spectra generated in graded-index fibers (Fig. 5.2.5-a) are similar to the conventional SPM-broadened spectra.[15] For peak powers near the critical

power for self-focusing ($P \approx P_c$) new SPM features appears (Fig. 5.2.5-b). SPM spectra in the presence of self-focusing are quite distinct from that predicted by the conventional self-phase modulation theory. There is an intense peak at the laser wavelength over a much weaker background of white light. This supercontinuum broadening is due to the narrowing of the a-phase, as observed in Fig. 5.2.4. This is because most of the pulse energy is not modulated. It is reminiscent of frequency supercontinua generated much earlier by self-focusing filaments.[4]

In conclusion, the beam transverse shape and the radius of curvature in the presence of waveguiding, self-focusing and diffraction in a parabolic index material have been derived. The phase is qualitatively different from that predicted by the conventional self-phase modulation theory. The most important result is the reverse of the SPM sign when there is a lot of focusing and diffraction. This occurs at the periodic minima of the beam propagating in a graded-index optical fiber. In this case the plane-wave contribution -kz of SPM is less important than the corrective phase contribution $\eta(z)$. The change of sign of SPM may have important consequences on the propagation of solitons in graded-index fibers and on pulse compression processes. The soliton propagation designates the nonlinear propagation regime for which the effect of SPM (red-shifted frequencies are generated at the pulse front and blue-shifted at the pulse back) compensates the temporal broadening of pulses in the negative group-velocity dispersion regime (blue-shifted frequencies propagates faster than red-shifted). The change of sign of SPM implies that in graded-index fibers solitons can propagates only in the normal dispersion regime ($\lambda < 1.3$ μm). Similarly, for pulse compression schemes the reverse of

sign of SPM implies that in graded-index fibers the blue-shifted frequencies are generated at the pulse front and the red-shifted frequencies are generated at the pulse back. Hence, the spectral broadened pulse must be compressed by a normal-dispersion element which can be the optical fiber itself (if $\lambda<1.3$ μm) or a sequence of prisms. Therefore, in theory, femtosecond pulses could be spectrally broadened and compressed by the combined effect of SPM and group-velocity dispersion in a graded-index fiber. This effect should be investigated experimentally.

5.3 Theory of Self-Focusing, Self-Phase Modulation and Diffraction in Bulk Homogeneous Material

In the previous section, we addressed the problem of the propagation of a pulse in a medium with nonlinearity and with a parabolic graded index profile. In this section, we will use our results to study the competing effects of self-focusing and diffraction on the spectral distribution of the supercontinuum generated by the propagation of an ultrafast pulse in a homogeneous medium. This case applied to optical fibers when the boundary conditions of the cladding are negligible. The spectral distribution is shown to differ from those predicted by the conventional plane wave theory of SPM. This work was done in collaboration with Pr. Jamal T. Manassah of CCNY.[16]

In the slowly varying approximation the envelope of the electrical field can be written for r<a as:

$$\mathcal{E}(r, z, u) = \frac{\tilde{\mathcal{E}}_0}{\omega(z, u)} \exp\left[-\frac{r^2}{a^2 \omega^2(z, u)} - i \frac{k}{2} \rho(z, u) r^2 + ik\alpha(z, u) \right] \tag{5.3.1}$$

where $u=(z/v_g - t)$ is the comoving coordinate, v_g is the group velocity, a is the initial beam radius assuming a Gaussian spatial distribution, $\varepsilon_0=\varepsilon_0 \exp(-$

$u^2/2\tau^2$), ε_o is the electric field initial amplitude, and τ is the pulse duration assuming an initial Gaussian temporal distribution. The physical parameters in Eq. 5.3.1 are : ω the normalized beam radius, ρ the inverse radius of curvature and $k\alpha$ the longitudinal phase.

The solutions for ω, ρ, α, with the boundary conditions ω=1, ρ=0 and α=0 at z=0 for r/a<<1, are given by:

$$\omega = \left[\beta \cos(\gamma z) + \delta\right]^{1/2} \tag{5.3.2}$$

$$\rho = -\frac{1}{2}\frac{\beta\gamma \sin(\gamma z)}{\left[\beta \cos(\gamma z) + \delta\right]} \tag{5.3.3}$$

$$\alpha = \frac{a^2(B - C)}{2[B - 2C]^{1/2}} \operatorname{arctg}\left[\left(\frac{B - 2C}{A}\right)^{1/2} tg\left(A^{1/2} z\right)\right] \tag{5.3.4}$$

for B>2C, and

$$\alpha = \frac{a^2}{4}\frac{(B-C)}{(2C-B)^{1/2}} \ln\left\{\frac{1+\left(\frac{2C-B}{A}\right)^{1/2} tg\left(A^{1/2}z\right)}{1-\left(\frac{2C-B}{A}\right)^{1/2} tg\left(A^{1/2}z\right)}\right\} \qquad (5.3.5)$$

for B<2C

where $\gamma=2A^{1/2} \equiv 2/L_w$, L_w is the waveguiding length of the lens-like material, the graded index material index of refraction is $n=n_o(1-A\, r^2/2n_o)$, $\beta=(2C-B+A)/2A$, $\delta=(A-2C+B)/2A$, $B=4/a^4k^2=1/L_d^2$, L_d is the Rayleigh's diffraction length, $C=n_2\varepsilon_o^2/n_o a^2$, n_o is the material linear index of refraction and n_2 is its quadratic nonlinear index of refraction.

In the case of a homogeneous medium (A→0), the above solutions can be rewritten as:

$$w = [1 + y^2 (1 - p')]^{1/2} \qquad (5.3.6)$$

$$L_d \rho = \frac{y\,[1 - p']}{[1+y^2(1 - p')]} \qquad (5.3.7)$$

$$k\alpha = \frac{[1-\frac{1}{2}p']}{[1 - p']^{1/2}} \operatorname{arctg}\,[(1 - p')^{1/2} y] \qquad (5.3.8)$$

for p'<1, and

$$k\alpha = \frac{[1-\frac{1}{2}p']}{[p'-1]^{1/2}} \ln\left\{\frac{1+y(p'-1)^{1/2}}{1-y(p'-1)^{1/2}}\right\} \qquad (5.3.9)$$

for p'>1.

where $p'=pexp(-u^2/t^2)$, $p=\varepsilon_0^2/\varepsilon_c^2$, $y=z/L_d$, and

$\varepsilon_c^2=n_o a^2/2n_2 L_d^2=n_o\lambda^2/2n_2 p^2 a^2$. ε_c is the critical field for self-focusing. In the above notation the normalized self-focusing distance is $y_{foc}=1/(p-1)^{1/2}$.

In the following, the analysis is limited to $y<y_{foc}$, where the above solutions are valid.

The solutions of ω, ρ, α in the linear regime ($\varepsilon_0\rightarrow 0$), reduce to the standard formula of a Gaussian pulse propagating in a homogeneous medium, specifically:

$$w = (1+y^2)^{1/2} \qquad (5.3.10)$$

$$r\,L_d = y/(1+y^2) \qquad (5.3.11)$$

$$k\alpha = \text{arctg}(y) \equiv h(z) \tag{5.3.12}$$

The expression for the time dependent portion of the phase for the plane wave approximation ($a\to\infty$), reduces to that of the conventional self-phase modulation theory, specifically:

$$\lim_{a\to\infty} k\alpha_t = -\frac{1}{2} p'y = -\frac{kn_2}{2n_0} \tilde{\mathcal{E}}_0^2 z = \phi_{spm} \tag{5.3.13}$$

Next, the general features of the beam diameter scaling factor, inverse radius of curvature, phase and spectral distributions are examined for different physical regimes.

In fig. 5.3.1 the normalized beam radius is plotted for u=0 as a function of the normalized length (z/L_d) and for different electric field intensities $p=\varepsilon_0^2/\varepsilon_c^2$. For weak fields (p<1) diffraction is the dominant effect, while for the most intense fields (p>1) the nonlinearity is dominant, there is self-focusing and w approaches zero as the length approaches the self-focusing distance.

In fig. 5.3.2 the normalized inverse radius of curvature ($L_d/R=\rho L_d$) is plotted for u=0 as a function of the normalized length. For p<1, this quantity is positive, has a maximum for $y=1/(1-p)^{1/2}$ and goes to zero for very large

distances, i.e diffraction is the dominant effect. For p>1, this quantity is negative, monotonically decreasing and approaches - ∞ at the self-focusing distance.

In fig. 5.3.3 the regularized longitudinal phase, i.e its value for a specific p minus its value for p=0, is plotted for u=0 as a function of the normalized length. For 0<p<2 the longitudinal phase changes sign in the total length interval, when positive it is the reverse sign of that predicted by the conventional self-phase modulation theory. For 1<p<2 this phase has a positive asymptote for the sample length equal to the self-focusing distance. For p>2 this phase is everywhere negative, admits the conventional self-phase modulation curve as a tangent at the origin, however decreases much faster than the result as the length increases until it reaches a negative asymptote at the self-focusing distance.

In fig. 5.3.4, the electric field intensity (ε_0^2/w^2) is plotted for p≈1 as function of the normalized time (u/τ) for different normalized length of the sample, as can be observed the pulse compresses with increasing length. Physically it should be noted that, for very large distances the dispersion effects will impose a limit on the value of this compression. In fig 5.3.5, the regularized longitudinal phase is plotted for p<1 as function of the normalized time for different normalized length of the sample. As can be observed, for small length the phase has the same sign as conventional SPM theory, for intermediate length the phase changes sign in its width interval, and for large length the phase is always positive leading to the reverse of the red leading the blue in the supercontinuum. In fig. 5.3.6, the spectral

distribution for p≈1 and large z is plotted, it should be noted that a central peak appears in the spectrum. This has been observed in earlier work.[3]

The electric field intensity, phase and spectral distribution are plotted as function of U for length close to the self focusing distance in the figures 5.3.7, 5.3.8, 5.3.9, respectively. Both the field intensity and the phase narrow, albeit at different rates. The magnitude of the maxima of both intensity and phase increase dramatically from those of the conventional SPM theory because of the strong self-focusing effect. If the electric field can still be supported by the medium, i.e. no breakdown occurs, fig. 5.3.5-c shows the dramatic change in the spectral extent over an infinitesimal change in the sample length.

In conclusion, the simultaneous effects of self-focusing, self phase-modulation and diffraction on the amplitude, phase and spectral distribution in a $\chi^{(3)}$ medium is computed. Our theoretical results reduce to those of diffraction theory for low intensity pulse and to conventional SPM theory for large transverse diameter pulse. In general, the competing effects of diffraction and self-focusing lead to novel features of the pulse shape and generated supercontinuum.

5.4 Theory of Thermal Focusing Effects of the Supercontinuum

It has long been recognized that the propagation of a laser beam in a material produces a local heating in the beam vicinity due to absorption and that the temperature gradient in the material induces a transverse gradient of the refractive index which leads to a lensing effect.[17] In section 5.1 we have shown that the phase shape and spectral distribution of a pulse propagating in a parabolic graded index material differ significantly from conventional self-phase modulation results.[9] This temperature gradient can in the case of supercontinuum generation with high repetition rate produce significant variations in the spectral extent and shape.[18] Properly controlled, for example by using a CW heating beam, it is also possible to use this effect in some optical fibers, lead glass, and certain semiconductors where $dn/dT>0$ [19-21] to control the sign of the pulse phase such as to reverse the red leading the blue in the supercontinuum and possibly to compress pulses within $\chi^{(3)}$ materials without the need for external gratings or prisms. In this section, we find the normalized beam diameter, the pulse phase and the supercontinuum spectral shape in the presence of such temperature gradients. This work was done in collaboration with Pr. Jamal T. Manassah.[22]

Gordon et al.[17] results can essentially be summarized that due to heating the index of refraction in the material is given by:

$$n = n_0 \left[1 + \frac{\delta'}{r_H^2} r^2 \right] \tag{5.4.1}$$

where r_H is the heating beam spot size, n_0 is the material linear index of refraction and

$$\delta' = - \frac{0.12\, P\, b}{n_0\, \kappa\, \pi} \left(\frac{dn}{dT} \right) \frac{8\, D\, t}{r_H^2 + 8\, D\, t} \tag{5.4.2}$$

where

$$D = \frac{\kappa}{\rho\, C_p} \tag{5.4.3}$$

P is the heating laser power (in Watts), b is the fractional power dissipation in the medium per centimeter, k is the thermal conductivity (cal/cm s ^{0}K), r is the density (g/cm^3), C_p is the specific heat (cal/g ^{0}K), and dn/dT measures the change in the material index of refraction for a change in its temperature.

A pulse whose envelope is given by:

$$\mathcal{E}(r, 0, u) = \mathcal{E}_0 \exp\left(-\frac{r^2}{a^2}\right)\exp\left(-\frac{u^2}{2\tau^2}\right) \tag{5.4.4}$$

at the entrance of a $c^{(3)}$ - nonlinear material, where $u = z/v_g - t$, v_g is the group velocity, a is the initial beam radius, t is the pulse duration, r is the cylindrical radius, and $\mathcal{E}_0$ is the magnitude of the pulse, will develop through the nonlinear material to give an envelope $\mathcal{E}(r,z,u)$ at the space-time point (r,z,u). The functional form of $\mathcal{E}(r,z,u)$ is given by:

$$\mathcal{E}(r, z, u) = \frac{\tilde{\mathcal{E}}_0}{\omega(z, u)} \exp\left[-\frac{r^2}{a^2\omega^2(z, u)} - i\frac{k}{2}\rho(z, u)r^2 + ik\alpha(z, u)\right] \tag{5.4.5}$$

where $\mathcal{E}_0=\mathcal{E}_0\exp(-u^2/2t^2)$ and the functions ω, ρ, α are given for focusing materials (i.e. $dn/dT>0$) by:

$$\omega = \left[\beta\cos(\gamma z) + \delta\right]^{1/2} \tag{5.4.6}$$

$$\rho = -\frac{1}{2}\frac{\beta\gamma \sin(\gamma z)}{\left[\beta \cos(\gamma z) + \delta\right]} \tag{5.4.7}$$

$$k\alpha = \frac{ka^2(B - C)}{2[B - 2C]^{1/2}} \operatorname{arctg}\left[\left(\frac{B - 2C}{A}\right)^{1/2} tg\left(A^{1/2} z\right)\right] \tag{5.4.8}$$

where $\gamma=2[2n_0 |\delta'| /r_H^2]^{1/2}=2A^{1/2}$, $\beta=(2C-B+A)/2A$, $\delta=(A-2C+B)/2A$, and

$$B = \frac{4}{a^4 k^2} = \frac{1}{(\text{Rayleigh Length})^2} \tag{5.4.9}$$

$$C = \frac{n_2 \tilde{\mathcal{E}}_0^2}{n_0 a^2} \tag{5.4.10}$$

If we use the critical field $\mathcal{E}_c$ for the medium, i.e. the field for which the self-focusing distance is equal to infinity, C can be written as:

$$C = \frac{B}{2} p \exp\left(-\frac{u^2}{\tau^2}\right) \tag{5.4.11}$$

where

$$p = \frac{\varepsilon_0^2}{\varepsilon_c^2} \qquad \text{and} \qquad \varepsilon_c^2 = \frac{2 n_0}{a^2 k^2 n_2} \tag{5.4.12}$$

physically p represents the power of the incoming pulse in units of the critical power of the nonlinear medium. The main features of the solutions [5.4.6-8] are that:

1) The normalized beam diameter is a periodic function in z. The wavelength of this periodicity is proportional to $|\delta'|^{-1/2}$. In figure 5.4.1, ω is plotted for selected values of $|\delta'|$.

2) The longitudinal phase, for u=0, as function of z mostly increases by steps at z locations corresponding to the periodical positions of the minimum beam diameter. As a result this phase is not linear in z as the conventional self-phase modulation theory phase. Furthermore, its magnitude can be much larger. In fig. 5.4.2, this phase is plotted for different values of the δ'-parameter.

3) The time dependent portion of the longitudinal phase may have the reverse sign than that of conventional SPM. Physically, this result leads to the reverse of the read leading the blue in the supercontinuum. Furthermore, as the pulse peak magnitude increases and tends to the critical field of the nonlinear medium, the phase width decreases significantly. Therefore, for w close to its maximum only a short period over the pulse duration is modulated, this portion increases as w approaches its minimum.

In fig. 5.4.3, the spectral intensity is plotted for the same length z but for different δ' parameters. For larger δ' the spectral extent is larger.

In fig. 5.4.4, the spectral intensity is plotted for the same δ' as of the curve in fig. 5.4.3-b, but for a slightly different sample length. As can be observed the spectral extent does not significantly change with a small variation in z, however the spectral shape can be dramatically altered. Actually, the two lengths chosen correspond to a maximum and a minimum positions of the normalized beam diameter.

In conclusion, we have shown in this letter that by heating the path of a probe pulse, by a heating beam (or alternately through a high repetition rate of the probe beam) it is possible to waveguide the probe pulse and to alter significantly its spectral intensity distribution. Uncontrolled, this heating phenomenon can lead to random characteristics in supercontinuum generation. Controlled, it may find a number of interesting applications.

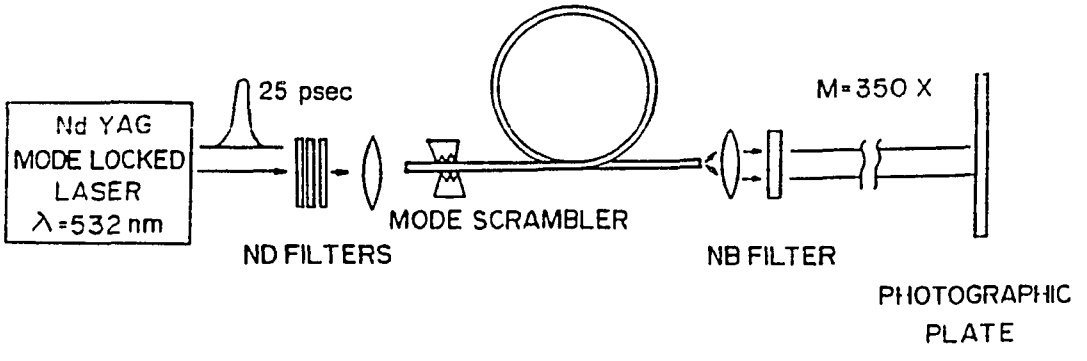

Fig. 5.1.1 Experimental set-up for the observation of self-focusing in a large core optical fiber.

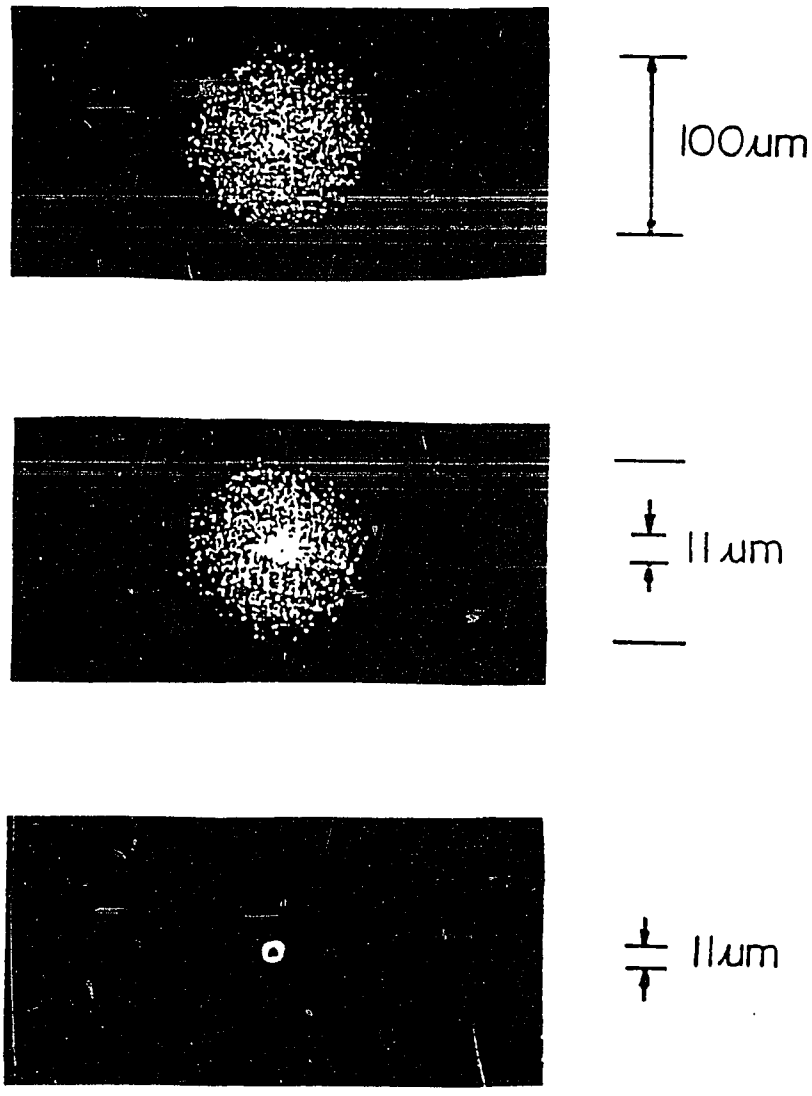

Fig. 5.1.2 Images of the intensity distributions at the optical fiber output: a) input pulses of low energies (E<1nJ), b) input pulses of high energies (E>10 nJ), same as b) with an additional narrow-band filter centered at λ=550 nm. (M=350X).

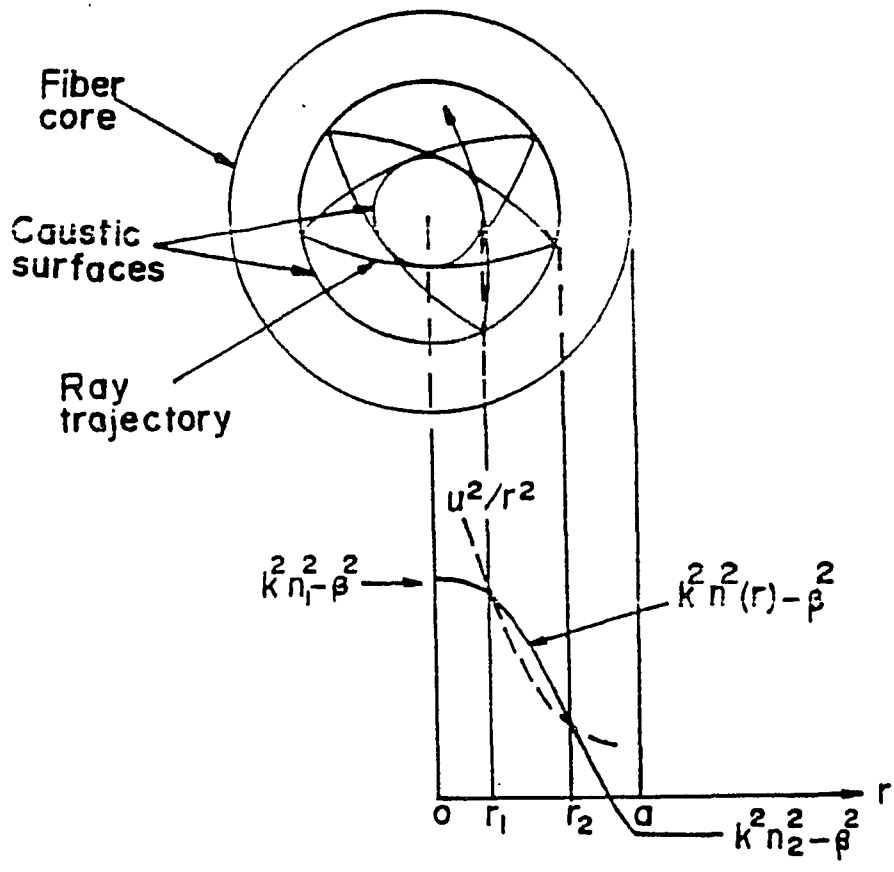

Fig. 5.1.3 Cross-sectional projection of a skew ray in a gradient-index fiber and the graphical representation of its mode solution from the WBK method. The field is oscillatory between the turning points r_1 and r_2 and is evanescent outside this region.

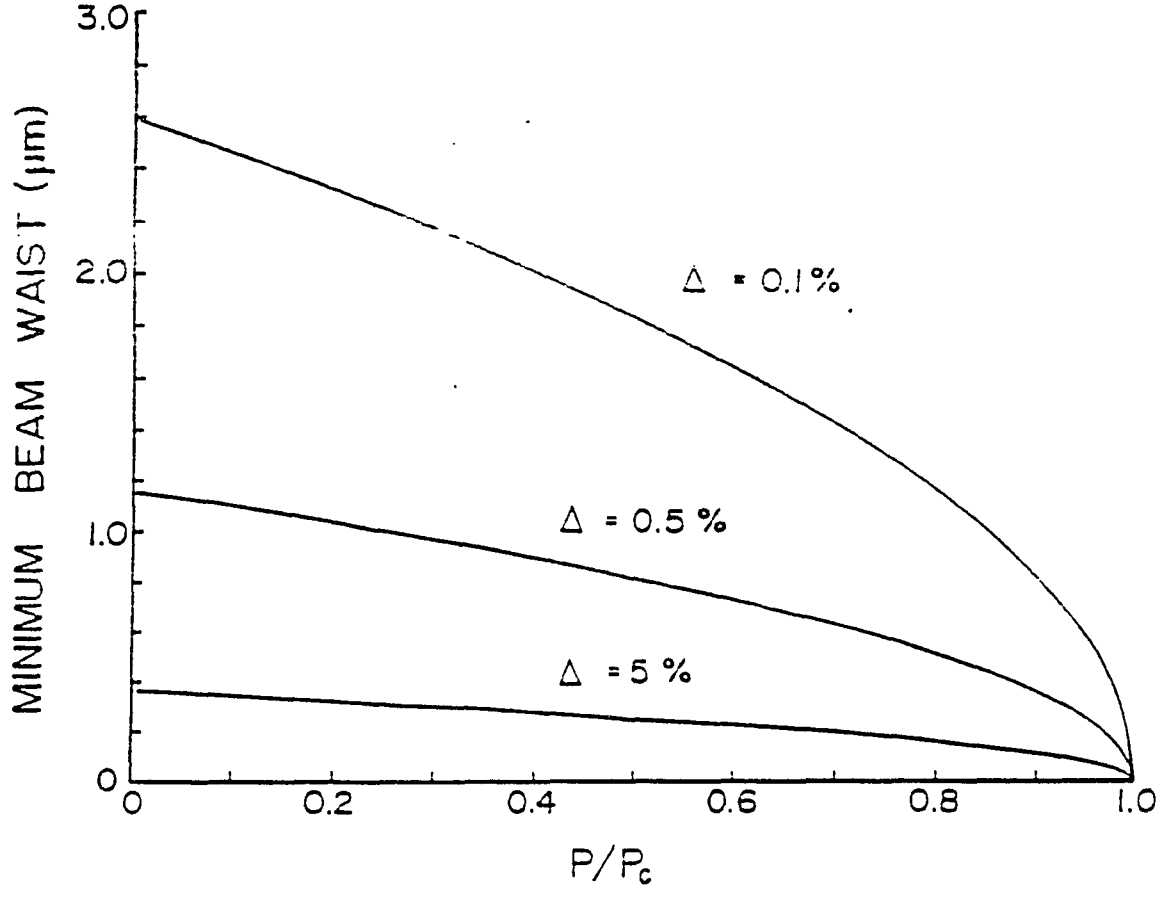

Fig. 5.2.1 Minimum beam waist as function of normalized peak power P/P_C. Δ is the relative refraction index difference between the core center and the cladding. In silica fibers $P_C \approx 10^6$ W.

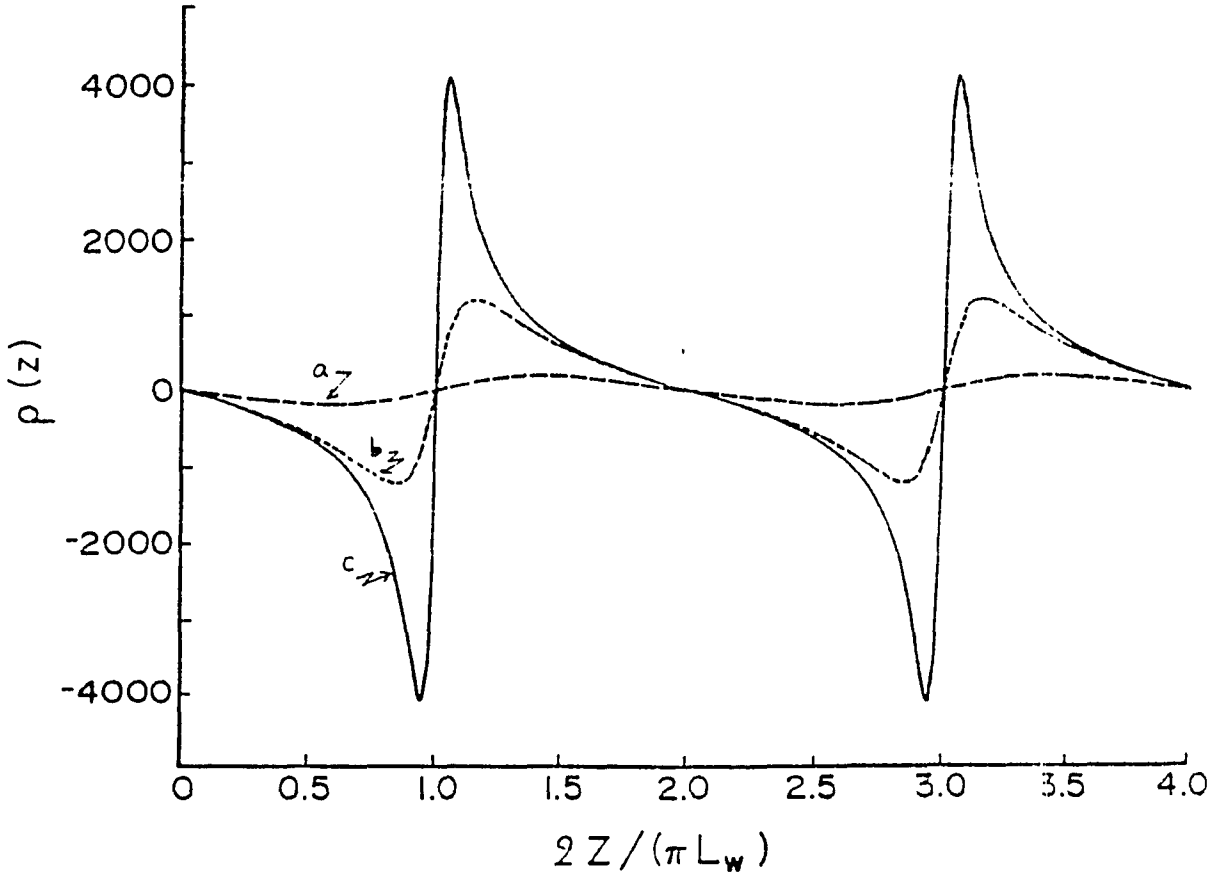

Fig. 5.2.2 Inverse of radius of curvature as function of normalized length $2z/pL_W$ for a graded-index fiber (a =1.5m, Δ=0.48%, and L_W=15.3 mm). (a) P/P_c=0.1; (b) P/P_c=0.9 and (c) P/P_c=0.99.

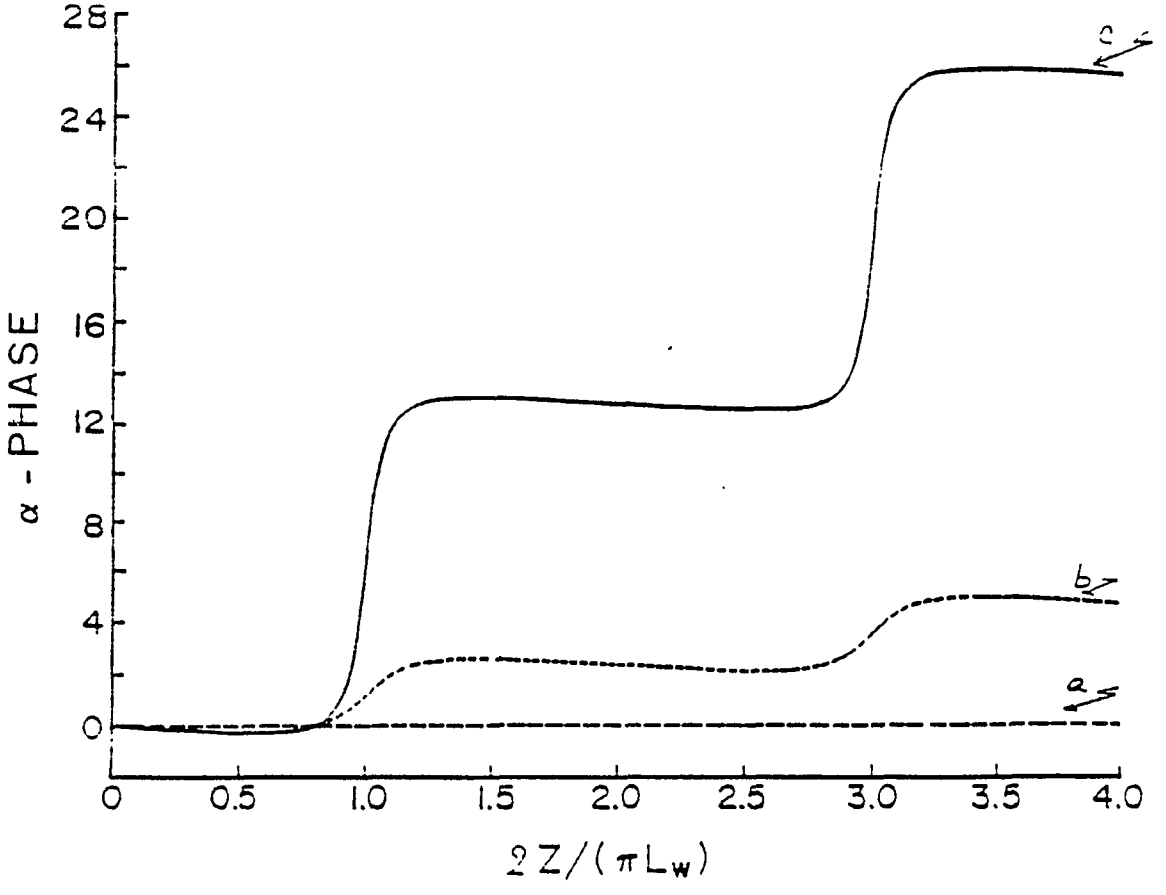

Fig. 5.2.3 α-phase as function of the normalized length $2z/pL_W$. (a) P/P_c=0.1; (b) P/P_c=0.9 and (c) P/P_c=0.99.

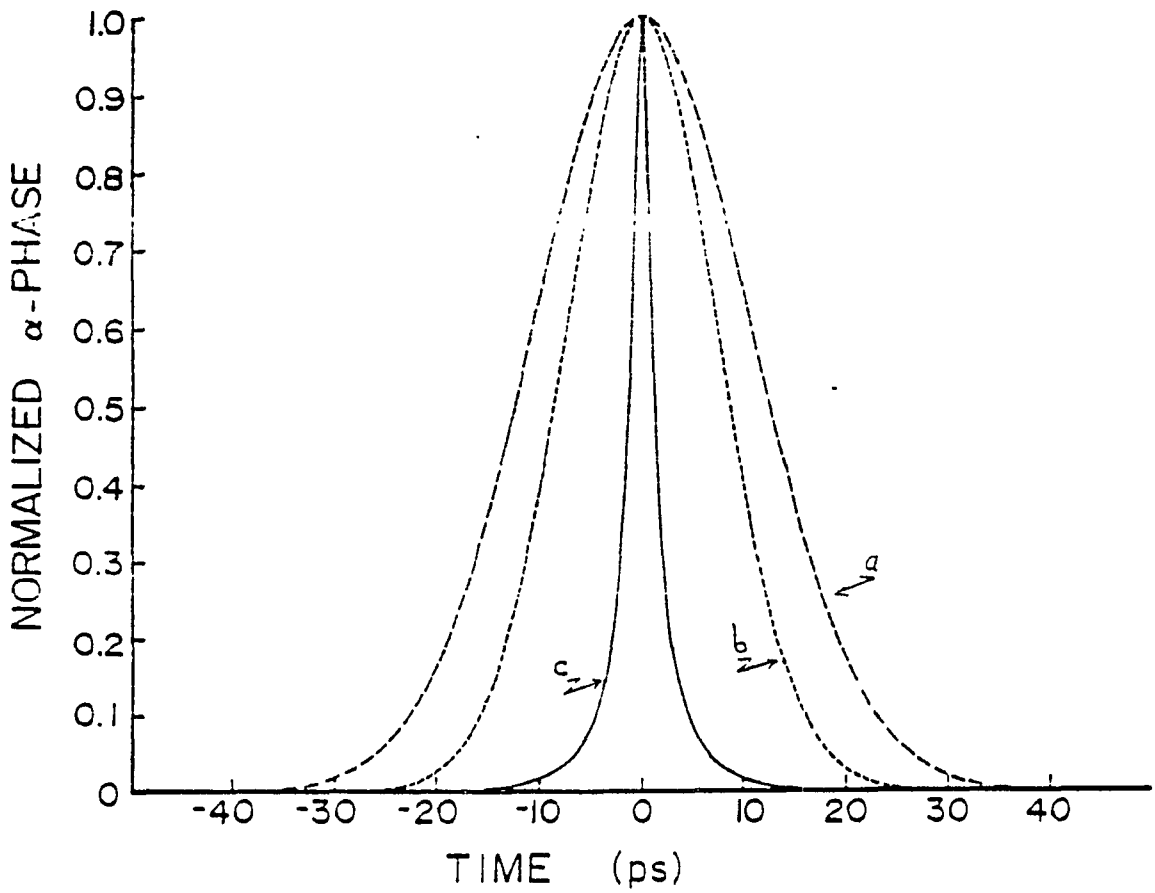

Fig. 5.2.4 α-phase normalized to its maximum value plotted versus time. (a) conventional SPM phase for P/P_c=0.1; (b) P/P_c =0.1 and (c) P/P_c=0.992. Maximum phase are -0.92, +0.55 and +1880 radians, respectively. (a=25 mm, Δ=0.48%, z=10 cm, and t=15ps).

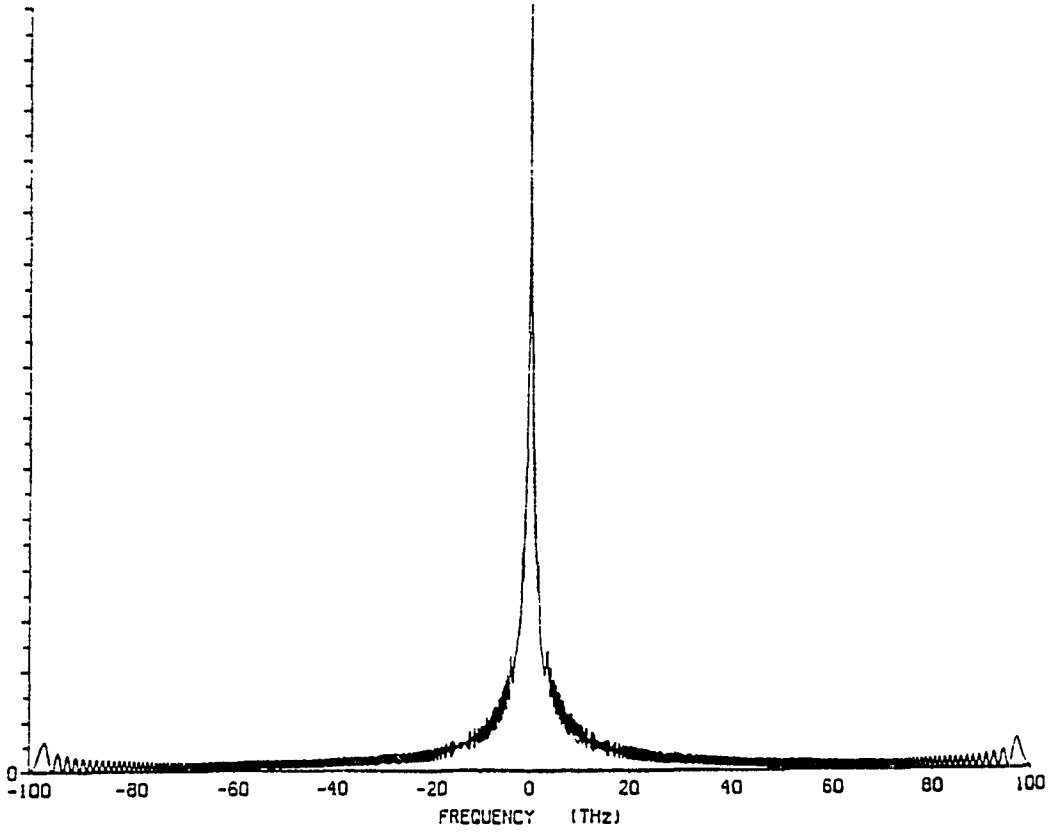

Fig. 5.2.5 Spectral broadening of a Gaussian pulse (t=15 ps) outgoing from a graded-index fiber (a=25 mm, Δ=0.48%). (a) P/P_c=0.1 and z=5m; (b) P/P_c= 0.997 and z=0.1m.

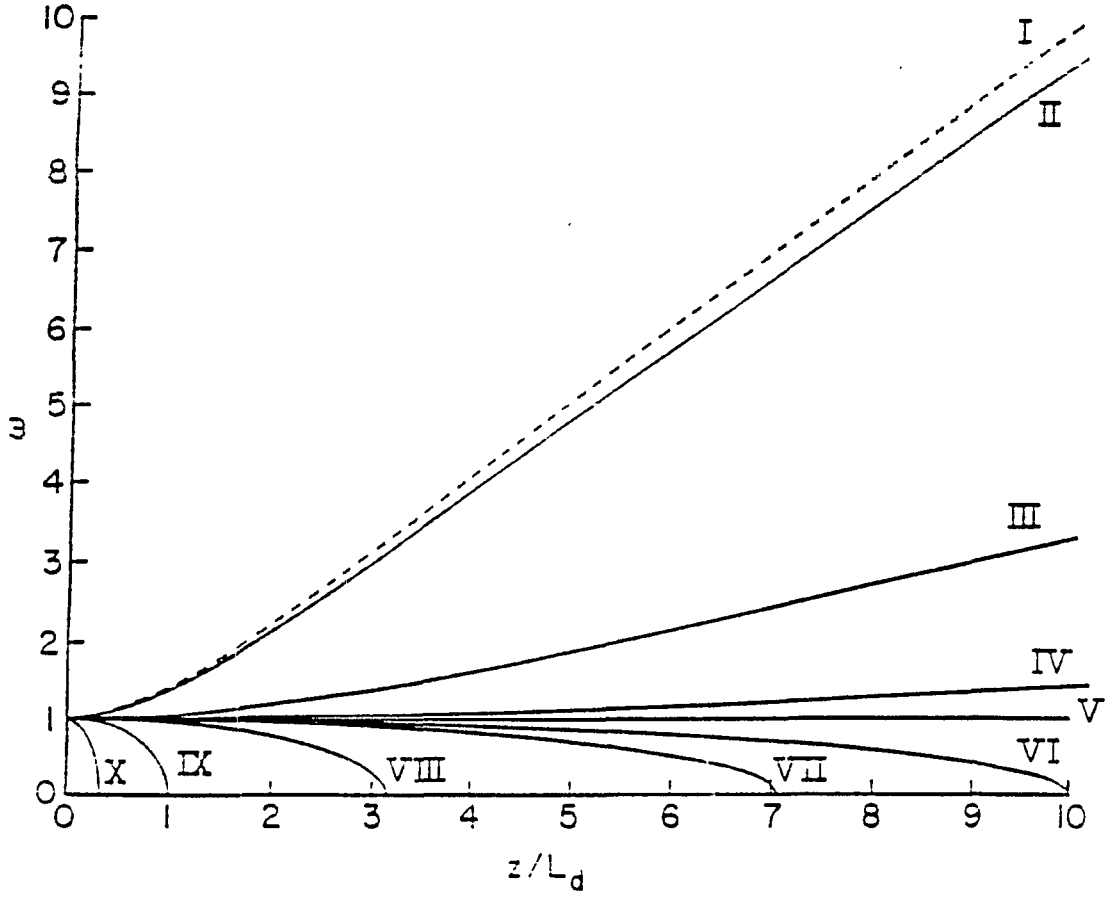

Fig. 5.3.1 The normalized beam radius for U=0 as function of the normalized length (z/L_d). (i) $p<<1$; (ii) p=0.1; (iii) p=0.9; (iv) p=0.99; (v) p=1; (vi) p=1.01; (vii) p=1.02; (viii) p=1.1; (ix) p=2; (x) p=10.

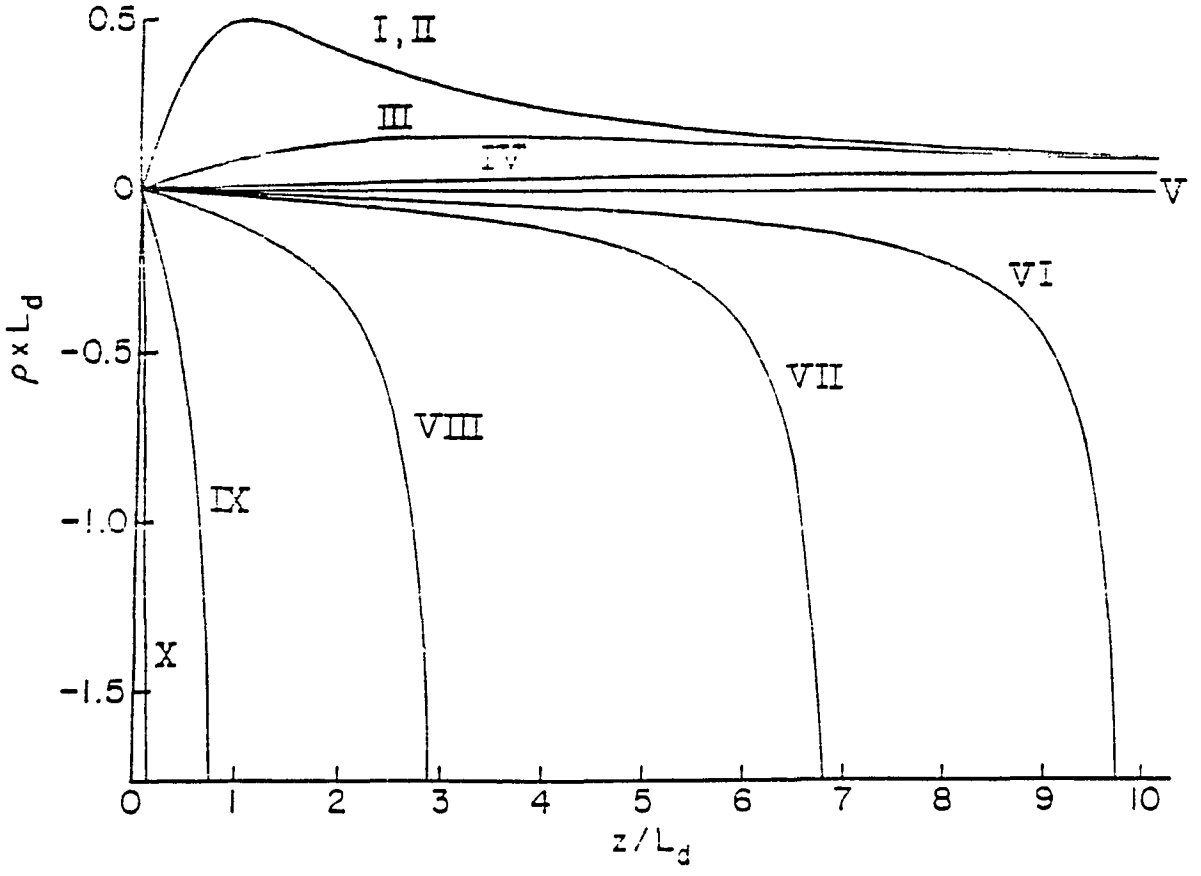

Fig. 5.3.2 The normalized inverse radius of curvature (rL_d), for U=0 as function of the normalized length (z/L_d). (i) $p<<1$; (ii) p=0.1; (iii) p=0.9; (iv) p=0.99; (v) p=1; (vi) p=1.01; (vii) p=1.02; (viii) p=1.1; (ix) p=2; (x) p=10.

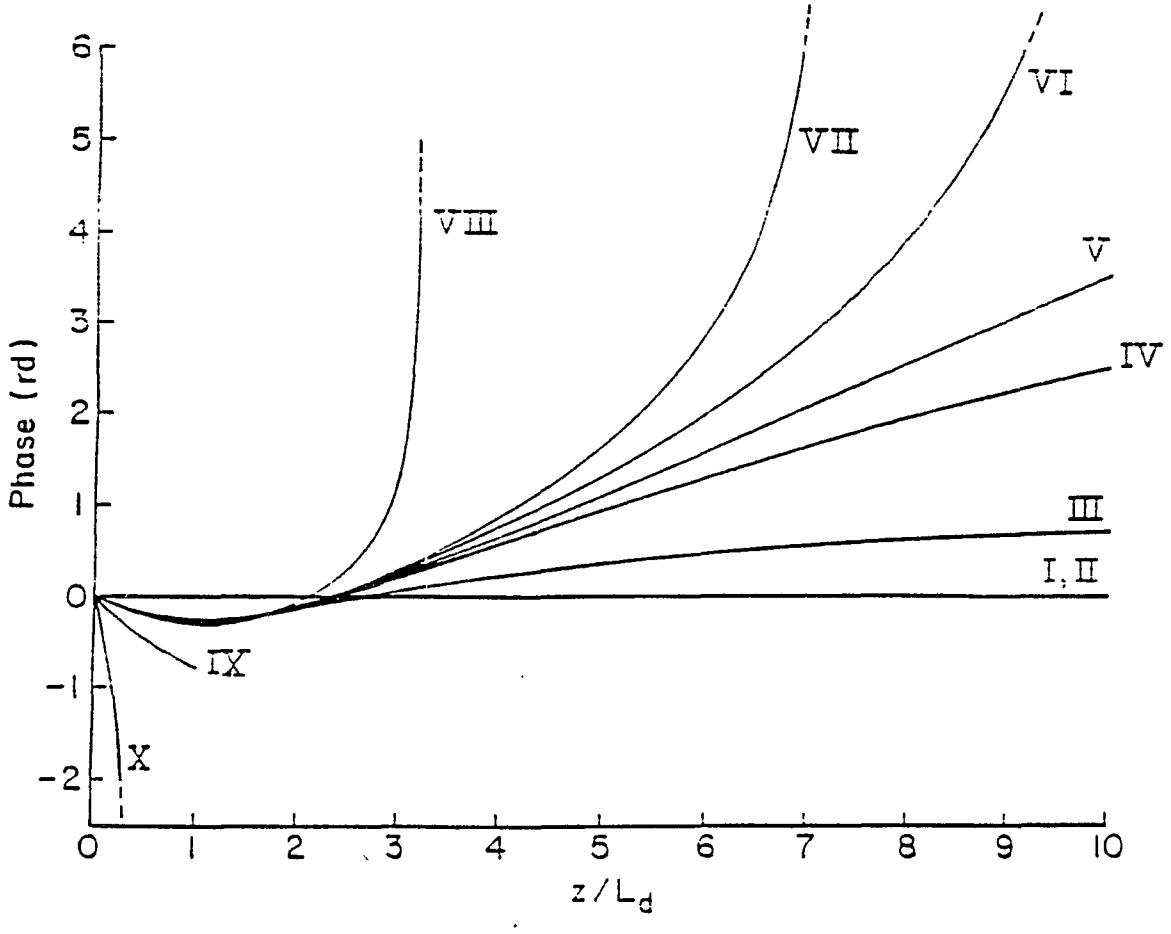

Fig. 5.3.3 The regularized longitudinal phase for U=0, as function of the normalized length (z/L_d). (i) $p<<1$; (ii) p=0.1; (iii) p=0.9; (iv) p=0.99; (v) p=1; (vi) p=1.01; (vii) p=1.02; (viii) p=1.1; (ix) p=2; (x) p=10.

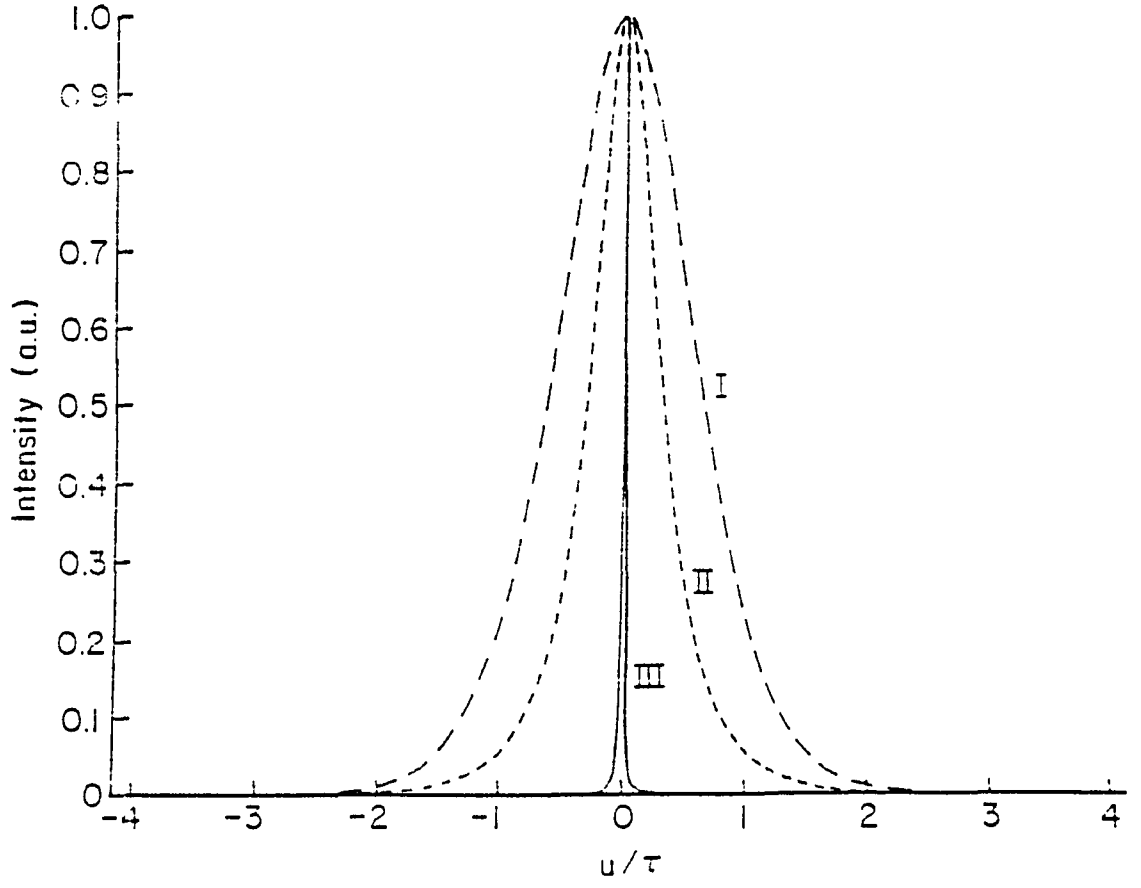

Fig. 5.3.4 The normalized intensity of the pulse as function of time.

p=0.99999.

(i) z/L_d =1; (ii) z/L_d=3; (iii) z/L_d=100.

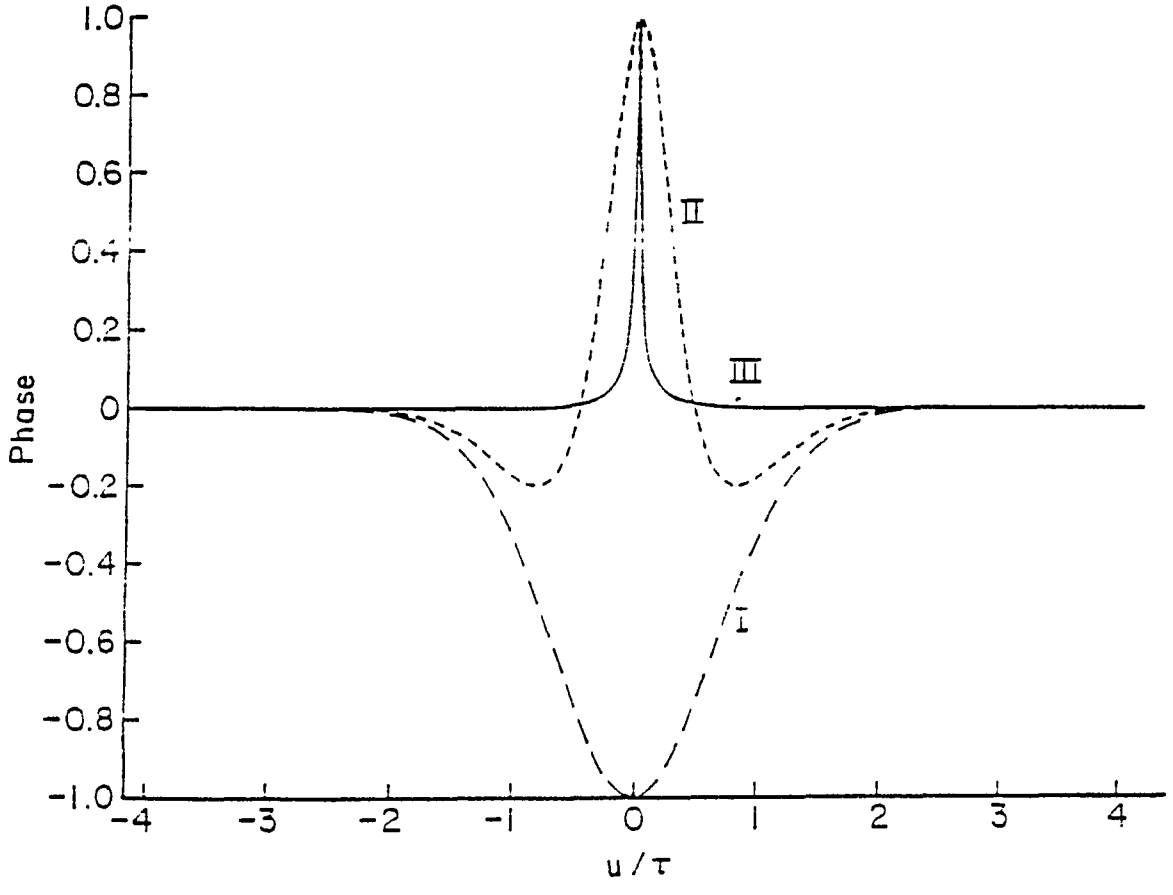

Fig. 5.3.5 The regularized longitudinal phase as function of time. p=0.99999.

(i) $z/L_d = 1$; (ii) $z/L_d=3$; (iii) $z/L_d=100$. [The values of the phase peaks are respectively -0.285 , 0.25, 46.87. The corresponding phases for SPM theory are respectively 0.5, -1.5, -50.].

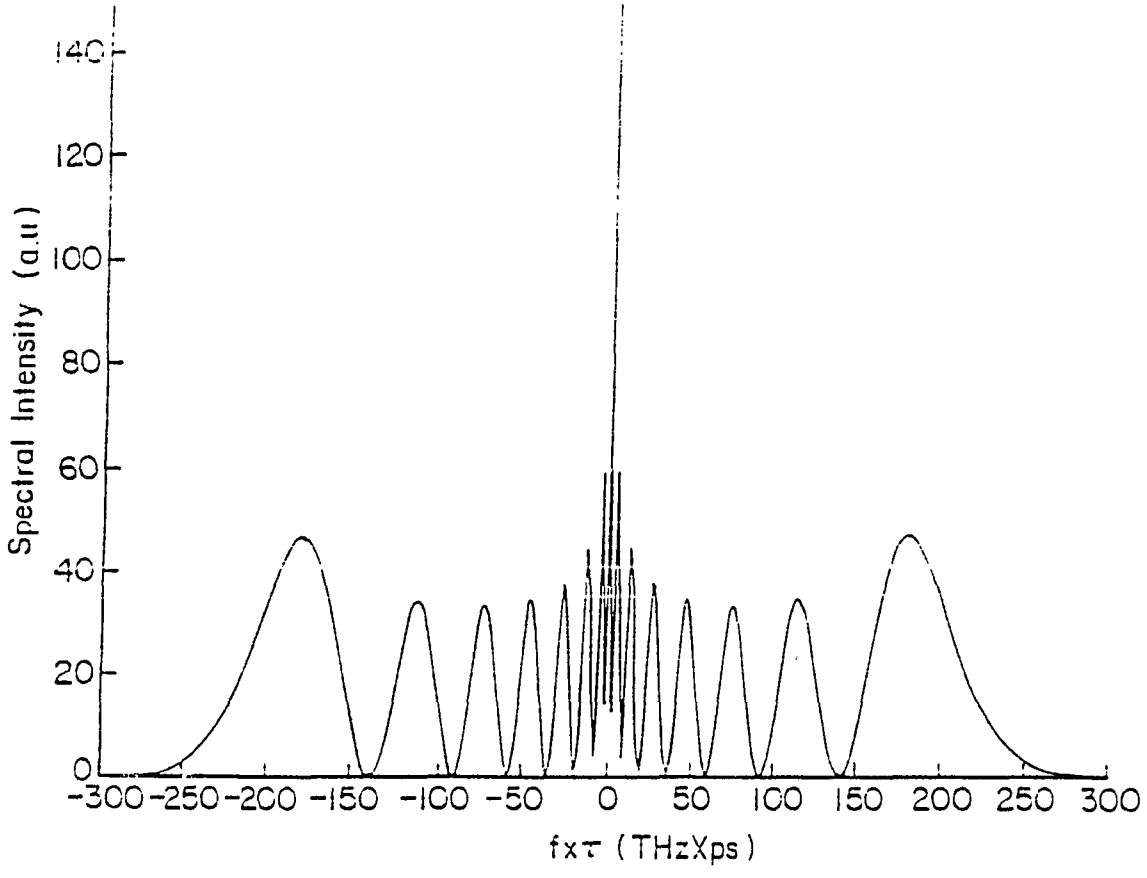

Fig. 5.3.6 The spectral distribution intensity as function of the normalized frequency difference . p=0.99999, z/L_d=100.

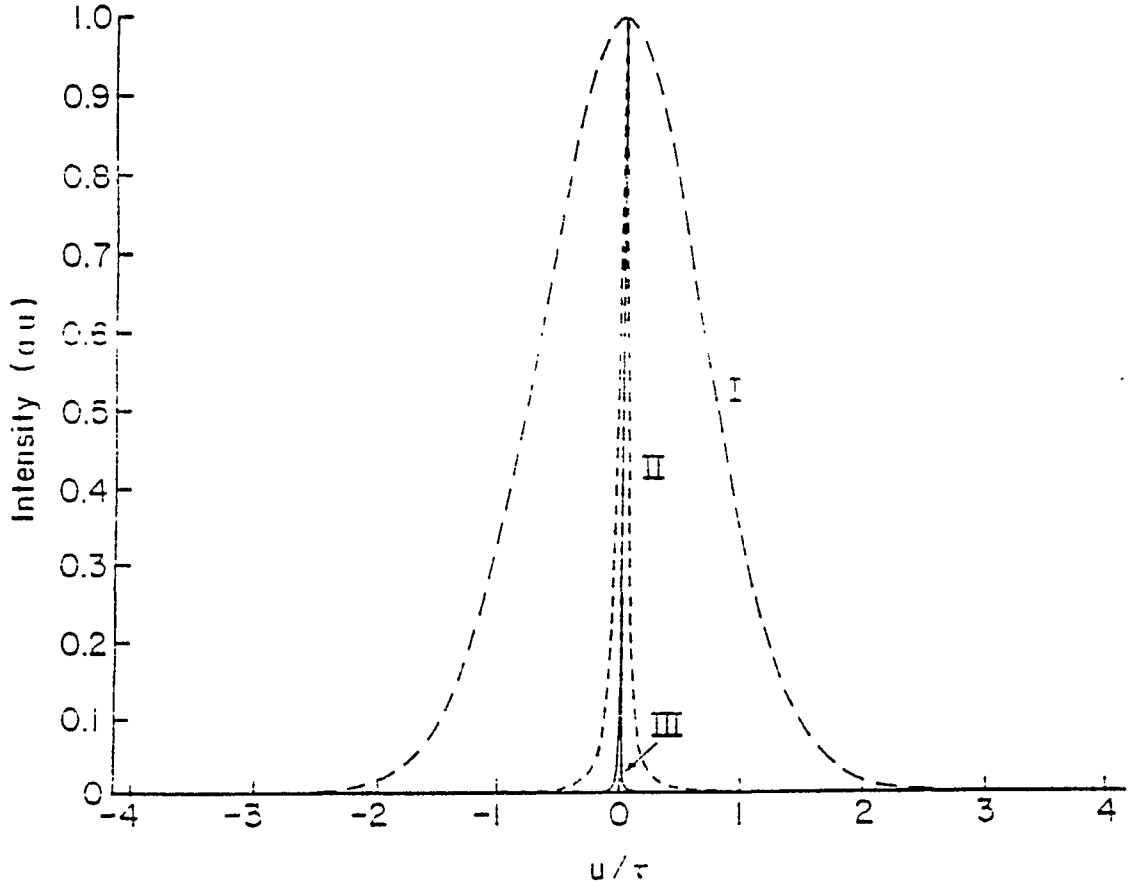

Fig. 5.3.7 The normalized intensity (e^2/ω^2) of the pulse as function of time. p=10.

(i) z/L_d=0.1; (ii) z/L_d=.333; (iii) z/L_d=0.3333.

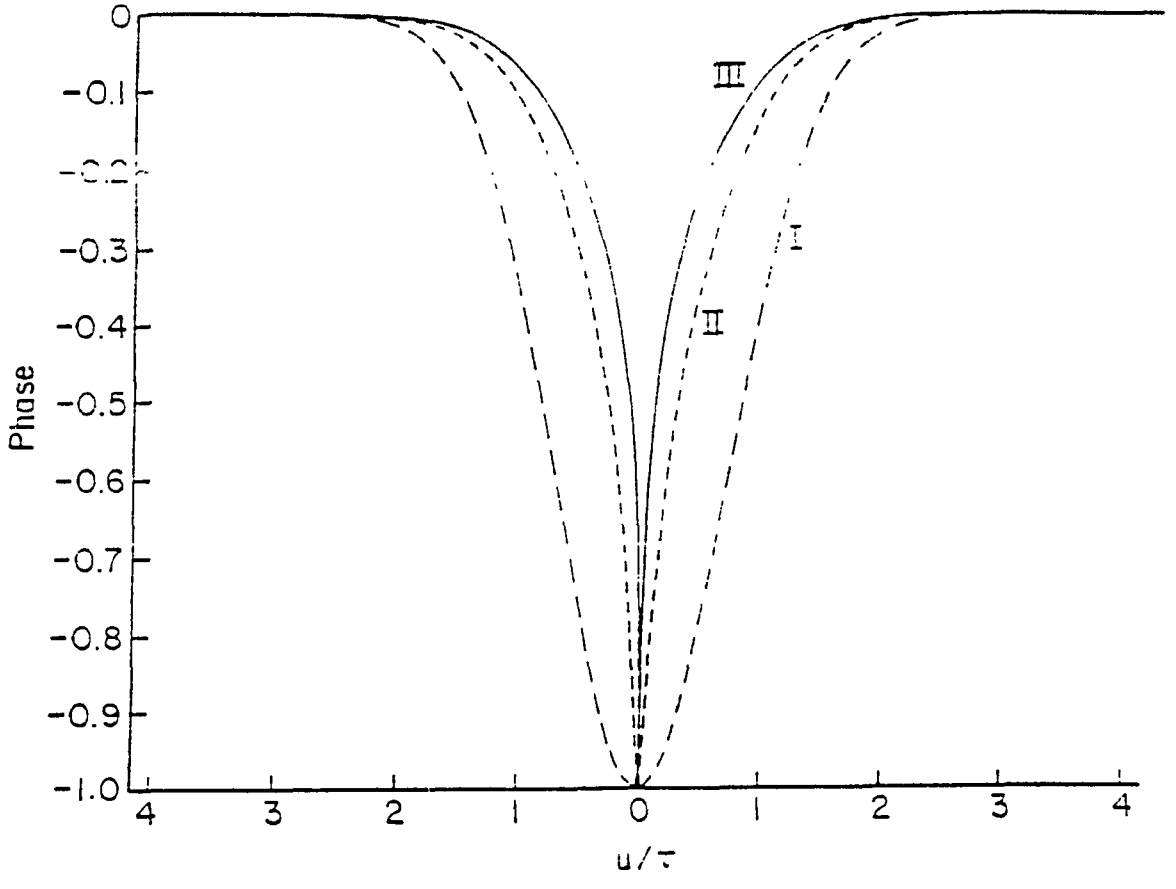

Fig. 5.3.8 The regularized longitudinal phase as function of time. p=10.

(i) z/L_d=0.1; (ii) z/L_d=.333; (iii) z/L_d=0.3333. [The values of the phase peaks are respectively -.51, -5.4, -8.4. The corresponding phases for the plane wave theory of SPM are respectively: -0.5, -1.67, -1.67]

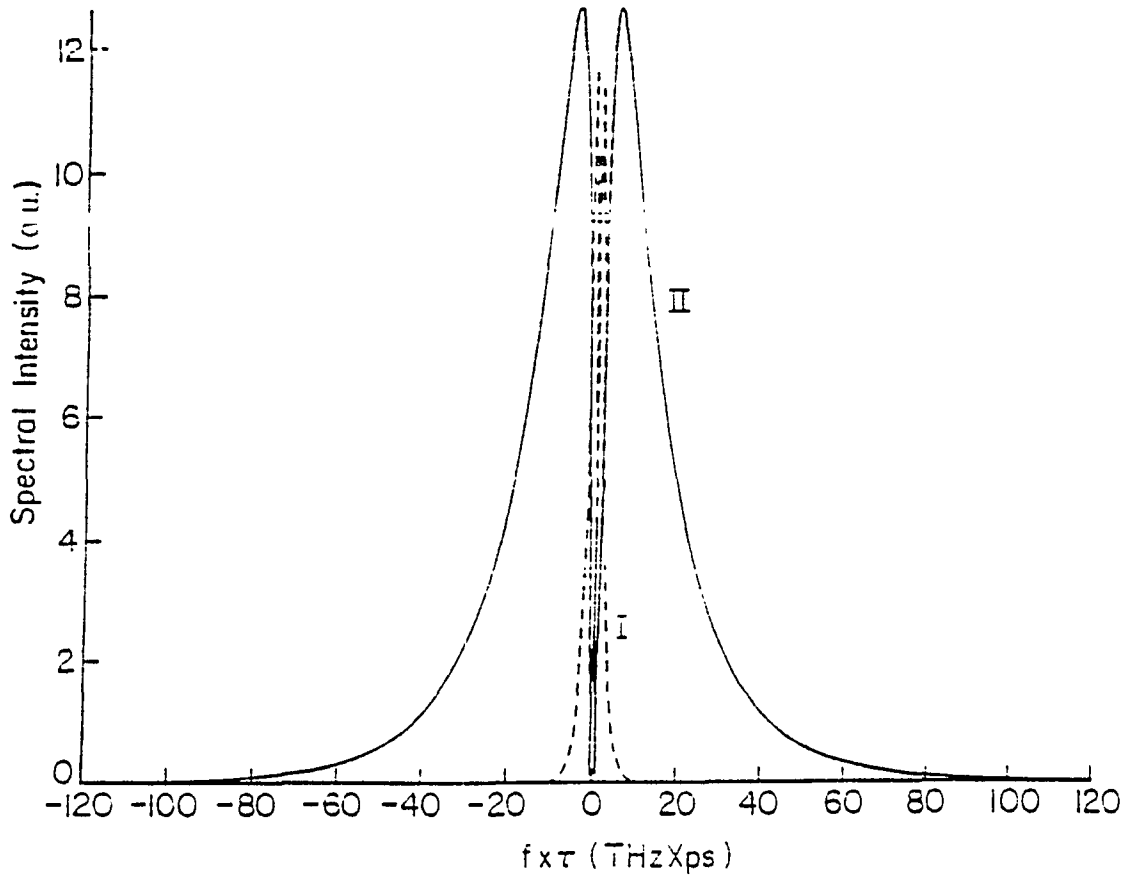

Fig. 5.3.9 The spectral distribution intensity as function of the normalized frequency difference. p=10. (ii) z/L_d=0.333; (iii) z/L_d=0.33333; [z=1/3 is the self-focusing length for p=10].

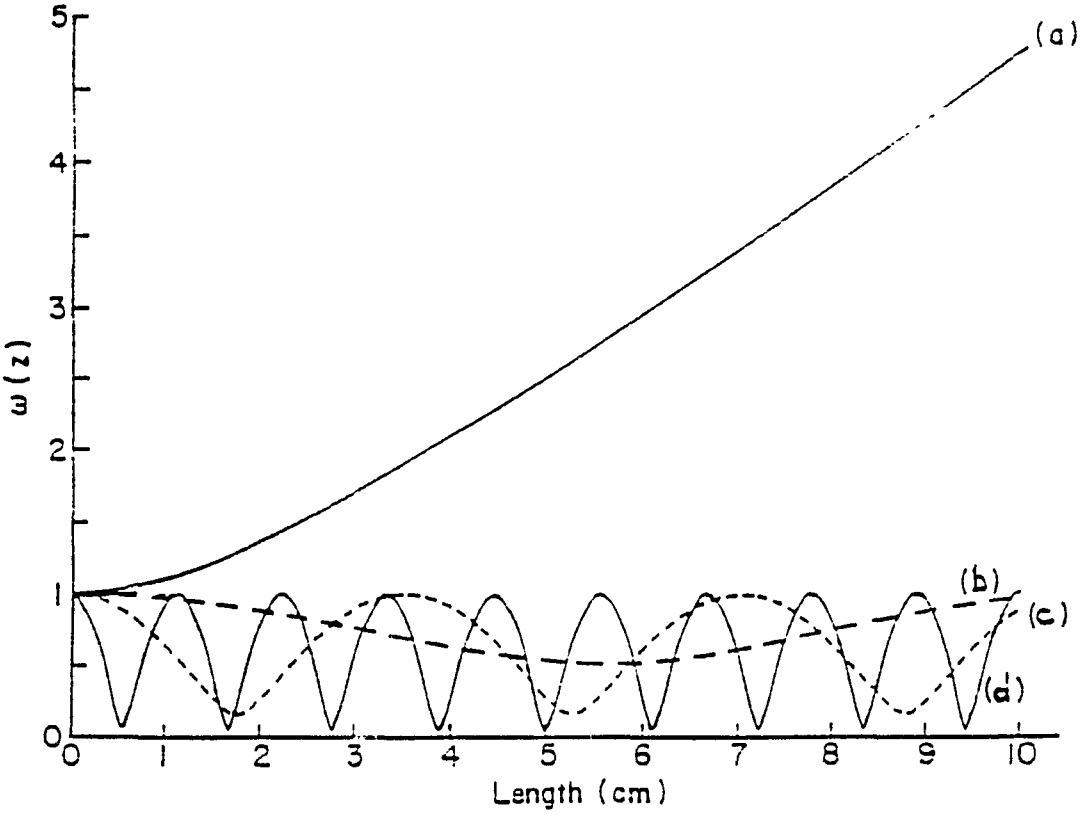

Fig. 5.4.1 The normalized probe beam diameter as a function of the material thickness. (a) p=0, $|\delta'|=0$; (b) p=0.9, $|\delta'|=0$; (c) p=0.9, $|\delta'|=2.5\times10^{-3}$; (d) p=0.9, $|\delta'|=7.8\times10^{-3}$; (e) p=0.9, $|\delta'|=2.5\times10^{-2}$.

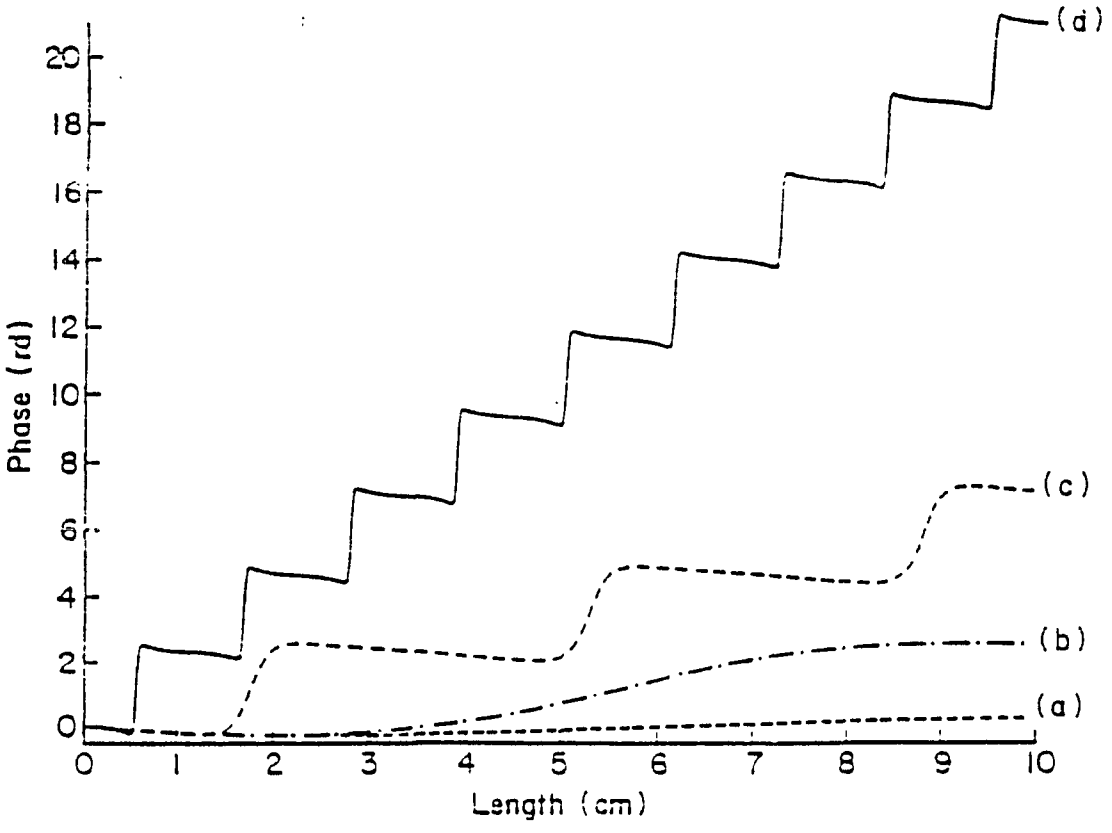

Fig. 5.4.2 The longitudinal probe phase, at u=0, as a function of the material thickness. p=0.9. (a) $|d'|=0$; (b) $|\delta'|=2.5 \times 10^{-3}$; (c) $|\delta'|=7.8 \times 10^{-3}$; (d) $|\delta'|=2.5 \times 10^{-2}$.

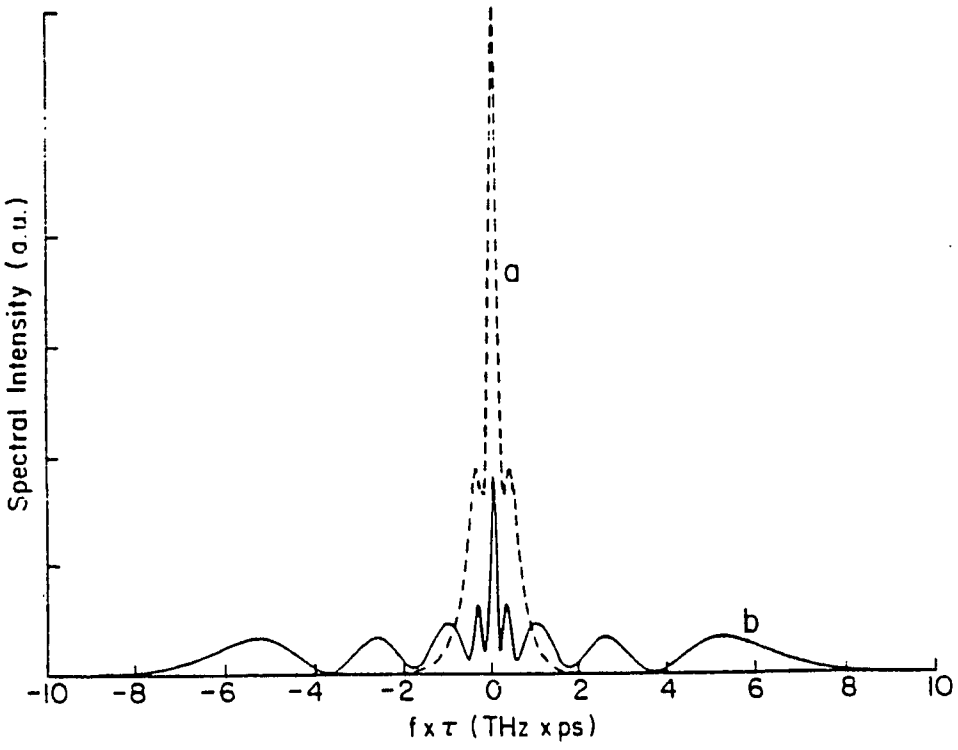

Fig. 5.4.3 The probe spectral distribution for r=0, z=10 cm, and p=0.9.

(a) $|\delta'|=2.5\times10^{-3}$; (b) $|\delta'|=2.5\times10^{-2}$.

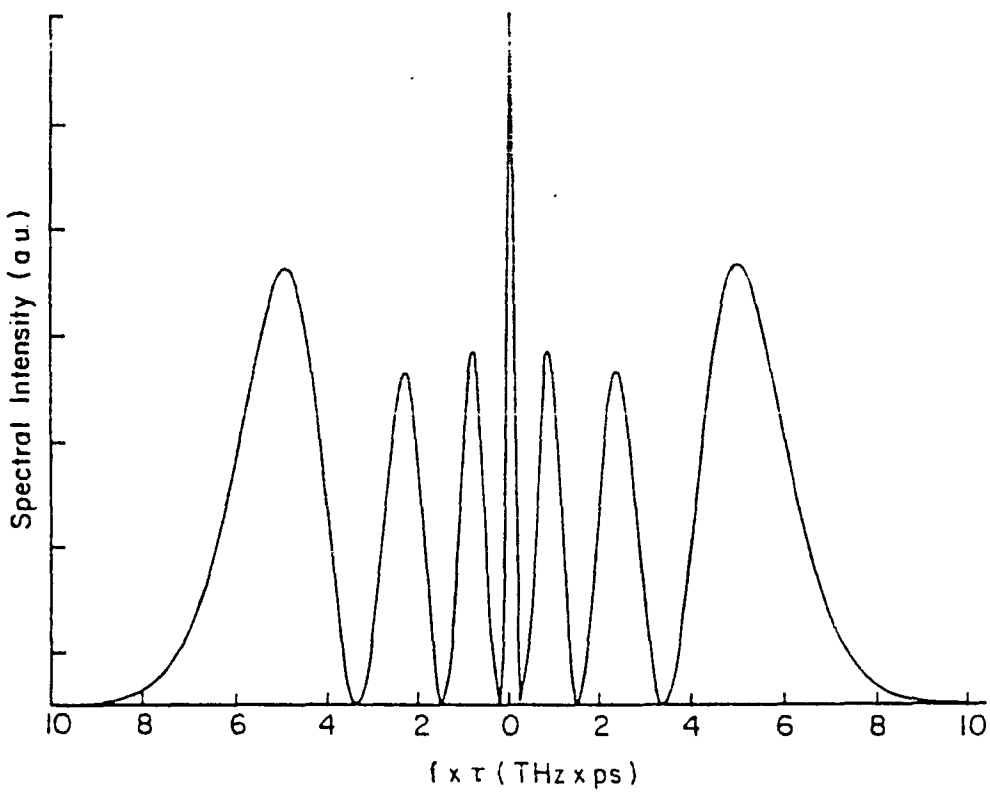

Fig. 5.4.4 The probe spectral distribution for r=0, z=9.44 cm, p=0.9 and $|\delta'| = 2.5 \times 10^{-2}$.

5.6 References

1. Overviews and references on self-focusing in condensed media are given by D.H. Auston, in *Ultrafast Light Pulses*, S.L. Shapiro, ed. (Springer-Verlag, Berlin, Heilderberg, 1977); Y.R. Shen, *The Principles of Nonlinear Optics*, (Wiley, New York, 1984); and in *The Supercontinuum Laser Source*, R.R. Alfano, ed. (Springer-Verlag, Berlin, Heilderberg, 1989).

2. P.L. Kelley, Phys. Rev. Lett. **15**, 1085 (1965).

3. E. Garmire, R.Y. Chiao, and C.H. Townes. Phys. Rev. Lett. **16**, 347 (1966).

4. R.R. Alfano and S.L. Shapiro. Phys. Rev. Lett. **24**, 592 (1970).

5. P.L. Baldeck, F. Raccah, and R.R. Alfano. Opt. Lett. **12**, 588-589 (1987).

6. G. Keiser, in *Optical Fiber Communications* (McGraw-Hill, New York, 1983).

7. A.B. Grudinin, E.M. Dianov, D.V. Korbkin, A.M. Prokhorov, and D.V. Khaidarov. [Pis'ma Zh. Eksp. Teor. Fiz. **47**, 297-300 (1988)]. JEPT Lett. **47**, 356-359 (1988).

8. Z.V. Nesterova et al. [Pis'ma Zh. Eksp. Teor. Fiz. **34**, 391 (1981)]. JEPT Lett. **34**, 371 (1981).

9. Jamal T. Manassah, P.L. Baldeck, R.R. Alfano. Opt. Lett. **13**, 589 (1988).

10. For example, J. Gowar, *Optical Communications Systems*, [Prentice Hall, New York, 1983].

11. A. Yariv. *Quantum Electronics*, [Wiley, New York, 1975].

12. J.H. Marburger. Prog. Quantum Electron, **4**, 35 (1975).

13. H. Kogelnik. Appl. Opt. **4**, 1562 (1965).

14. P.K. Tien, J.P. Gordon, and J.R. Whinnery. Proc. IEEE **53**, 129 (1965).

15. R.H. Stolen, and C. Lin, Phys. Rev. **A 17**, 1448 (1978).

16. Jamal T. Manassah, P.L. Baldeck, R.R. Alfano. Opt. Lett. **13**, 1090 (1988).

17. J.P. Gordon, R.C.C. Leite, R.S. Moore, S.P.S. Porto and J.R. Whinnery. J. Applied Phys. **36**, 3, 1965.

18. R.R. Alfano and S.L. Shapiro. Phys. Rev. **A2**, 2376 (1970).

19. G.B. Morey, "Properties of Glass," in *International Critical Tables*, Vol. 2 (McGraw-Hill, New York, 1933).

20. F.W. Dabby and J.R. Whinnery. **13**, Appl. Phys. Lett., 284 (1968).

21. B.O. Seraphin and H.E. Bennet, in *Semiconductors and Semimetals*, edited by R.K. Willadrson and A.C. Beer, **3**, 499 (Academic, New York, 1967).

22. Jamal T. Manassah, P.L. Baldeck, R.R. Alfano. Appl. Opt. **27**, 3586-3587 (1988).

CHAPTER 6

FUTURE APPLICATIONS

6.1 Future Applications of Cross-Phase Modulation for the Ultrashort Pulse Technology

Over the last 20 years, picosecond and femtosecond laser sources and detection systems have been developed. Researchers are now pursuing new applications to use these unique properties of ultrashort pulses and nonlinear materials. The main efforts are towards the design of communication and information networks and optical computers with data streams, eventually, into the terahertz regime. For these high repetition rates, electronic components are too slow and all-optical schemes will be needed. Our discovery of cross-phase modulation effects on ultrashort pulses appears as a major breakthrough towards the real-time all-optical coding/decoding of such short pulses.

This section describes some examples of XPM-based signal processors. To name a few: a frequency shifter, a pulse-compression switch and a spatial light deflector. These all-optical devices are based on spectral, temporal and spatial effects of cross-phase modulation on ultrashort pulses. As they are based on effects which have a very fast response time (<100 fs for n_2 in glass)

these devices can be used for the processing of ultrashort pulses with terahertz repetition rates.

The first XPM-based technique to control ultrashort pulses was developed in the early 70's. It is the well-known optical Kerr gate which is shown in Fig. 6.1. A probe pulse can be transmitted through a pair of cross-polarizers only when a pump pulse induces the (cross-) phase (modulation) needed for the change of polarization of the probe pulse. The principle of the optical Kerr gate was demonstrated using nonlinear liquids,[1-2] and optical fibers.[3-5] In optical fibers, induced-phase effects can be generated with milliwatt peak powers because of their long interaction lengths and small cross-sections.[6] Recently, XPM effects in optical fibers have been shown to alter the transmission of frequency multiplexed signals,[7-8] but also to allow quantum nondemolition measurements.[9-10] In addition, phase effects arising from XPM have been used to make all-fiber logic gates,[11] ultrafast optical multi/demultiplexers,[12] and nonlinear interferometers.[13]

The novelty of our most recent work and my thesis was to show that XPM not only leads to phase effects, but to more important spectral, temporal and spatial effects on the propagation of ultrashort pulses. New schemes of XPM-based optical signal processors are proposed in Fig. 6.2. The design of an ultrafast frequency shifter is shown in Fig. 6.2-a. It is based on spectral changes which occur when pulses copropagate in a nonlinear dispersive medium. In absence of pump pulse, the weak signal pulse passes undistorted through the nonlinear medium. When the signal pulse copropagates in the nonlinear medium with a pump pulse, its carrier-wavelength can be changed by an

amount $\Delta\lambda$ which is linearly proportional which the peak power of the pump pulse. Thus, in Fig. 6.2, the signal pulses S1, S2, have their frequencies shifted by $\Delta\lambda_1$, and $\Delta\lambda_2$ by the pump pulses P1 and P2, while S3 is not affected by the stream of pump pulses.

The proposed design of a pulse-compression switch is shown in Fig. 6.2-b. It is a modified version the usual optical fiber/grating-pair pulse-compression scheme. First, the probe pulse is spectrally broadened by a copropagating pump pulse in the nonlinear medium. Then, or simultaneously, it is compressed in time by a dispersive element. Thus, in presence of the pump pulse, the signal pulse is compressed ("on" state) , while in its absence, the signal pulse is widely broadened ("off" state) by the device.

An model of an all-optical spatial light deflector based on spatial effects of XPM is shown in Fig. 6.2-c. In this scheme, the pump pulse profile leads to an induced-focusing of the signal pulse through the induced nonlinear refractive index. The key point in Fig. 6.2-c is that half of the pump pulse profile is cut by a mask which leads to an asymmetrical induced-focusing effect, and a spatial deflection of the signal pulse. This effect is very similar to the self-deflection of asymmetrical optical beams[14] which has been observed using the nonlinearity of liquid crystals. In the proposed device, pump pulses originate either from path P1 or path P2, which have, respectively, their left-side or right side blocked. Thus, if a signal pulse copropagates with a pump pulse from P1 or P2, it is deflected on, respectively, the right or left side of the non deflected signal pulse.

The prime property of future XPM-based optical devices for information, signal and computation processors will be on their switching speed. They will be controlled by ultrashort pulses which will turn "on" or "off" the induced nonlinearity responsible for XPM effects. With short pulses, the nonlinearity will originate from the fast electronic response of the interacting material. As an example, the time response of electronic nonlinearity in optical fibers is about 3 fs.[15-17] With such a response time, one can envisionne the optical processing of femtosecond pulses with repetition rates up to 100 THz.

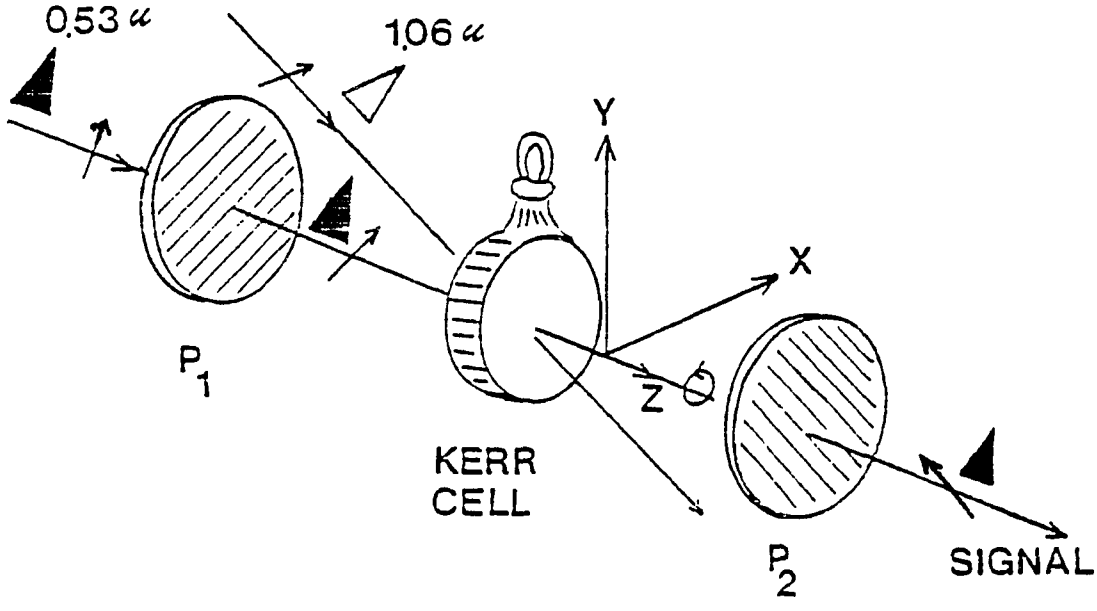

Fig. 6.1 Schematic diagram of an optical Kerr gate.

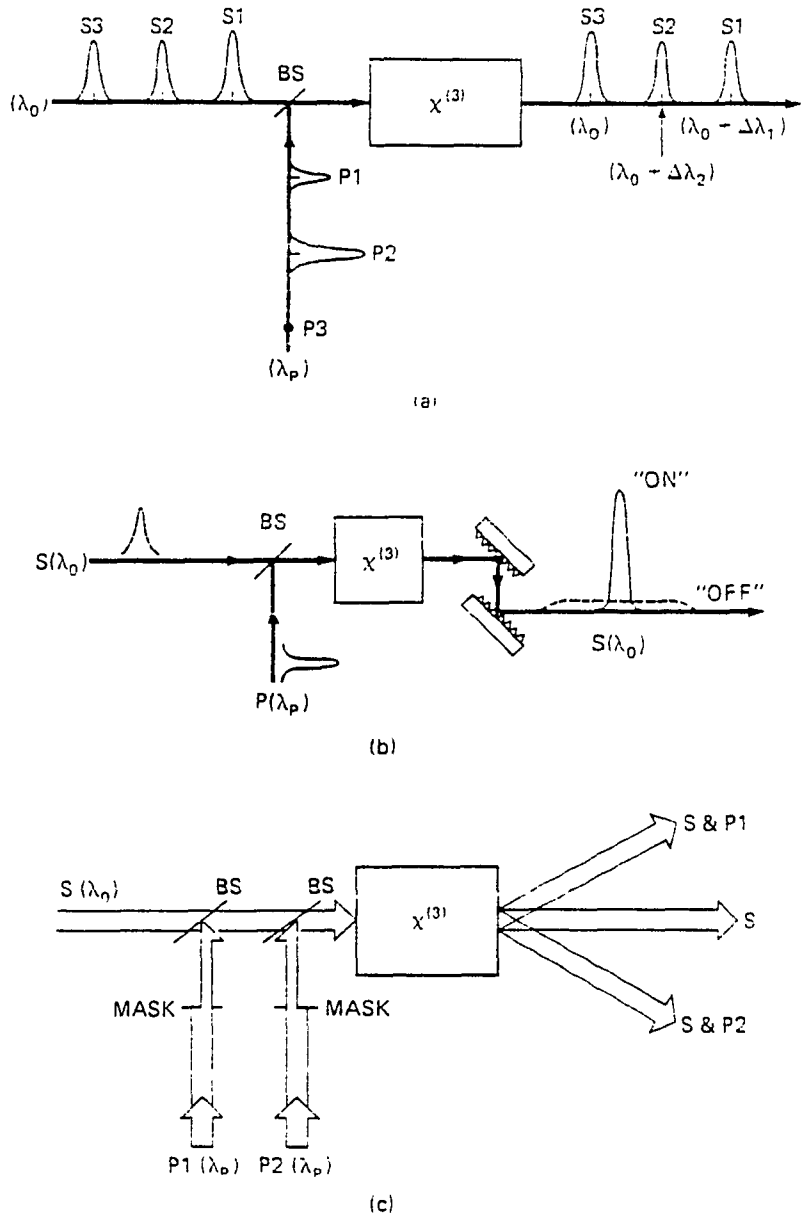

Fig. 6.2 Schematic diagrams of ultrafast optical processeurs based on cross-phase modulation effects. (a) Ultrafast frequency shifter; (b) all-optical pulse compression switch; (c) all-optical spatial light deflector.

6.3 References

1. Shimizu, F. and B. P. Stoicheff . IEEE J. Quantum Electron. **QE-5**, 544 (1969) .

2. Duguay, M. A. and J. W. Hansen. Appl. Phys. Lett. **15**, 192-194 (1969).

3. Stolen, R. H. and A. Ashkin. Appl. Phys. Lett. **22**, 294-296 (1972).

4. Dziedzic, J. M., R. H. Stolen, and A. Ashkin. Appl. Opt. **20**, 1403-1406 (1981).

5. Ayral, J. L., J. P. Pochelle, J. Raffy, and M. Papuchon. Opt. Commun. **49**, 405-408 (1984).

6. White, I. H., R. V. Penty, and R. E. Epworth. Electron. Lett. **24** (1988).

7. Chraplyvy, A. R. and J. Stones. Electron. Lett. **20**, 996-997 (1984) .

8. Chraplyvy, A. R., D. Marcuse and P. S. Henry. J. Lightwave Technol. **LT-2**, 6-10 (1984) .

9. Levenson, M. D., R. M. Shelby, M. Reid, and D. F. Walls. Phys. Rev. Lett. **57**, 2473-2476 (1986).

10. Imoto, N., S. Watkins, and Y. Sasaki. Optics Commun. **61**, 159-163 (1987).

11. Kitayama, K. I. , Y. Kimura, and S. Seikai. Appl. Phys. Lett. 46, 317-319 (1985a).

12. Morioka, T., M. Saruwatari, and A. Takada. Electron. Lett. **23**, 453-454 (1987).

13. Monerie, M. and Y. Durteste. Electron. Lett. **23**, 961-962 (1987).

14. Swartzlander, G. A., Jr and A. E. Kaplan. J. Opt. Soc. Am. **B 5**, 765-768 (1988).

15. R.R. Alfano, Editor, *The Supercontinuum Laser Source*, (Springer-Verlag, Berlin, Heilderberg, 1989).

16. R.R. Alfano and S.L. Shapiro. Phys. Rev. Lett. **24**, 584-587, 592-594, and 1219-1222 (1970).

17. Grudinin, A. B., E. M. Dianov, D. V. Korobkin, A. M. Prokhorov, V. N. Serkinand , and D. V. Khaidarov. Pis'ma Zh. Eksp. Teor. Fiz. **46**, 175-177 (1987). [Sov. Phys. JETP Lett. **46**, 221, 225.]

CHAPTER 7

FUTURE PROBLEMS

In this thesis I have experimentally and theoretically studied new effects arising from self-phase modulation and cross-phase modulation on the propagation of ultrashort pulses in optical fibers. Five areas were investigated in the thesis: 1) the self-phase modulation (SPM) generation of supercontinuum femtosecond pulses using optical fibers, 2) cross-phase modulation (XPM) effects on copropagating pulses in optical fibers, 3) the terahertz pulse generation arising from modulation instability, 4) spatial effects on the nonlinear propagation of pulses in large-core optical fibers, and 5) future applications.

In this chapter, I briefly discuss some key problems unanswered and produced by my investigation.

7.1 Nonlinear Propagation of Femtosecond Pulses in Optical Fibers

In Chapter 2, the thesis studied the generation and pulse compression of femtosecond supercontinuum pulses. The main goal of such experiments is to generate broadband tunable pulses in the 10 to 20 fsec regime. One of the most fundamental problem lies on one understanding of the nonlinear propagation of intense ultrashort pulses in optical fibers. Our work and

previous experimental and theoretical works using 50 fsec pulses have lead to a good qualitative understanding of spectral broadening and compression using optical fibers, gratings and prisms.

There is not a complete understanding of the nonlinear propagation of ultrashort pulses in optical fibers. Bourkoff and al. and Boyer and al. (Ref. 11-14 in chapter 2) present the most recent theoretical and experimental comparisons of spectral broadening in 7-mm long optical fibers using 50-fsec pulses. There is not clear cut evidences to distinguish the relative importance of effects such as 3rd order GVD, self-steepening, and stimulated Raman scattering. As a consequence, it is not possible to determine the parameters (for example: the values of $\beta^{(3)}$ and the input pulse asymmetry) to use in theoretical simulations. This is why there is not theoretical work which uses the nonlinear wave equation with second order terms to predict the minimum pulse width and tunability of pulses obtainable with gratings and prisms. For each experimental condition (input pulse width, peak power, symmetry and chirp) it is necessary to determine experimentally the optimum fiber length and compressor characteristics. In addition, one do not know what are the optimum conditions to generate the shortest pulses. Is it preferable to use 100-fsec pulses and cm-long optical fibers, or 30-fsec pulses and mm-long fibers ? Moreover, the spectral broadening generated in optical fibers, up to 150-nm, allows the generation of <3-fsec pulses. Adequate theoretical calculations based on parameters obtained from new temporal and spectral measurements should tell us whether it possible to generate such short pulse using fibers.

Most of the previous theoretical work involved the nonlinear propagation of >50 fsec pulses. What does happen in the <20 fsec regime when the time relaxation of the nonlinearity becomes important ? Agrawal predicts that a modulation instability regime exists even in the normal dispersion regime when the nonlinearity time relaxation is not negligible. Is it possible to generate pulse trains of a few femtoseconds by modulation instability of <20 fsec pulses ? What is happening when pulses get as short as 6 to 10 fsec ?

Most of femtosecond studies have considered the propagation of pulses in the visible region of the spectrum which corresponds to the normal dispersion regime of silica fibers. There is an important interest for studying the nonlinear propagation of femtosecond pulses in other regions of the spectrum. For example, pulses with wavelengths larger than 1.3 μm can propagate as solitons. What are the shortest femtosecond solitons which can be propagated over long distances for terahertz telecommunications or optical processing schemes ? In addition, the propagation of <30 fsec solitons pulses in long fibers should allow us to enhance and study the effect of stimulated Raman scattering ? An underlying problem is the measure of the nonlinearity time relaxation: what are the time responses and relative importance of the vibrational and electronic nonlinear responses in the femtosecond regime of propagation in optical fibers ?

It is possible to make single-mode optical fibers in the blue-green region of the spectrum. It could be of interest to study the generation and compression of supercontinuum pulses in this region of the spectrum.

Applications could included the generation of tunable (UV, blue, yellow, and green) pulses for spectroscopic applications, and the generation of <6 fsec pulses.

7.2 Cross-Phase Modulation of Femtosecond Pulses in Optical Fibers

In chapter 3, the thesis presents the theory and some experimental measurements of cross-phase modulation in optical fibers. Future works are needed for the characterization of XPM effects on femtosecond pulses and for a better understanding of some "unexplained" XPM features.

We have theoretically predicted that XPM could be used to alter the time duration of optical pulses. In particular, we have calculated that the nonlinear interaction with a intense pulse could be used to compress a weaker pulse even in the normal dispersion regime of optical fibers. In addition, the induced pulse reshaping could lead to optical wave breaking. Future works could investigate these temporal effects on the propagation of femtosecond pulses in optical fibers. As calculated such temporal effects would be more efficiently observed by studying the nonlinear interaction of <100-fsec pulses. The tunable weaker pulse could be obtained by selecting part of a supercontinuum generated by an amplified 60-fsec pulse.

In addition, XPM measurements with femtosecond pulses are needed to demonstrate the possibility of using cross-phase modulation to process data streams with repetition rates in the terahertz regime. Future works could

investigate the possibility to control the frequency and the time duration of <100 fsec ultrashort pulses, i.e. potentially a repetition rate of 10 terahertz.

More XPM measurements are also needed to fully understand phenomena such as the optical gain which has been shown to be induced by the cross-phase modulation interaction. A this stage of our research we believe that the optical gain is the result of a modulation instability gain induced by the finite time response of the nonlinearity. Theoretically the XPM-induced optical gain could be explained by including the relaxation term of the induced-nonlinearity in the coupled nonlinear wave equations. Such a modulation instability gain could also explain the very wide spectral broadening generated by XPM in the case of long interaction lengths (Sec. 3.3.2).

The generation of ultrashort stimulated Raman scattering pulses via impulse scatterings is a complicated process which involves the transfer of energy via phonon coupling, the group-velocity mismatch, self-phase modulation and cross-phase modulation effects. Up-to-date theories cannot explain the spectral features that we obtained by propagating picosecond pulses in meter-long optical fibers. In particular, we observed spectral broadenings one order of magnitude larger than expected by the SPM and XPM theories. Future works on impulse stimulated Raman scattering in optical fibers should investigate the effect of the finite bandwidth of the Raman gain (i.e. time relaxation of the Raman process) on the generation of psec and fsec pulses. In addition, there should be more studies on the combined effects of SPM, XPM, and GVD in relation to modulation

instability. Preliminary calculations shows that the SPM-XPM chirp is very complicated, and that the mixing of frequencies in time has very important effects (instabilities) on the temporal shape and spectrum of the Raman pulse via impulse scattering.

7.3 Modulation Instability in the Normal Dispersion Regime of Optical Fibers

As discussed in chapter 4, modulation instability is a technique to generate trains of femtosecond pulses with repetition rates in the terahertz regime. One of the most intriguing result of the thesis is the generation of modulation instability sidebands in the spectrum of intense nanosecond pulses at 532 nm propagating in short lengths of optical fibers (10 to 100 cm). This result is surprising as it suggests the generation of modulation instability in the normal dispersion regime of optical fibers, which is not possible in the framework of the conventional theory of modulation instability. However, this result could be justified in the context of cross-phase modulation, or in conditions such as the sign of SPM is reversed (see next section). Future works should try to measure the temporal modulation expected to be within the nanosecond pulse shape to completely demonstrate this new and surprising phenomena.

7.4 Spatial Effects of Nonlinearities on the Sign of Self-Phase Modulation

Most theoretical analysis on the nonlinear propagation of optical pulses in single-mode optical fibers are based on the nonlinear wave equation derived in the plane wave approximation. There are numerous cases for which the plane wave approximation does not hold. For example, in graded-index fibers, and large core optical fibers. In addition, we believe that even in the case of single-mode step index fiber, the optical field intensity is not distributed uniformly in the fiber core, and the plane wave approximation might not hold at high intensities. In chapter 5 of thesis we have shown that the corrective phase associated with a non-uniform distribution of light in a fiber core can lead to a reverse of the self-phase modulation sign. Future experiments could verify this prediction and investigate its consequences.

The beam diameter of pulses propagating in a multimode graded-index fiber varies periodically between maxima and minima. Our theory in section 5.2 shows that this kind of beam propagation can lead to a reverse of the SPM sign of the on-axis light. A future experiment could study the generation of supercontinuum in such kind of fibers and pulse compression. In particular one could measure the sign of the frequency chirp and the time duration of outgoing pulses to see pulse compression. If our predictions are correct one expects to measure a negative chirp (blue-shifted frequencies at the pulse front) and to observe the propagation of solitons in the normal dispersion regime of silica optical fibers.

In section 5.1 we report the self-focusing of picosecond pulses in large core optical fibers. In this experiment self-focusing occurred during the generation of multi-order stimulated Raman scattering. Future experiments

could investigate these effects in the femtosecond regime. In the femtosecond regime supercontinuum effects would be stronger than Raman effects. In this case one would be measuring the spatial effects of the nonlinearity on the guiding properties in large core optical fibers. Such studies would give informations on the mechanism of nonlinear mode coupling in large core optical fibers. One could be very interested by such an experiment if it could allow to control the excitation of femtosecond pulse in the fundamental mode of large core optical fibers. Thus, one could build fiber-grating pulse compressors with better coupling efficiency and higher peak powers.

An other experiment could investigate intensity effects on the spatial distribution of light in single-mode optical. For example, one could measure whether the change of refractive index and the distribution of supercontinuum frequencies are uniform across the core diameter as the conventional theory predicts. If it is not the case, one should investigate the possibility to observe the propagation of solitons and modulation instability in the normal dispersion regime of optical fibers. As another example, one could investigate the spatial dependence of the stimulated Raman scattering process and check whether the multi-order stimulated Raman scattering lines are generated in decreasing diameters inside the fiber core.

Theoretical computations should try to include spatial effects in the supercontinuum generation, stimulated Raman scattering, impulse scatterings, and modulation instability processes. The first condition is to NOT use the plane wave approximation in the Maxwell equations. One

should also keep the boundary conditions as such, possibly by describing the 3-D propagation of light in a super-Gaussian graded-index medium.

LIST OF BALDECK'S PAPERS AND CONFERENCE ABSTRACTS

Publications:

1. P.L. Baldeck, F. Raccah, and R.R. Alfano. Observation of self-focusing in optical fibers with picosecond pulses. Opt. Lett. **12,** 588-589 (1987).

2. P.L. Baldeck, and R.R. Alfano. Intensity effects on the stimulated four photon spectra generated by picosecond pulses in optical fibers. J. Lightwave Technol. **L.T-5,** 1712-1715 (1987).

3. P.L. Baldeck, P.P. Ho, R.R. Alfano. Effects of self, induced, and cross phase modulations on the generation of picosecond and femtosecond white light supercontinua. Rev. Phys. Appl. **22,** 1677-1694 (1987).

4. P.L. Baldeck, R. Garuthara, F. Raccah, and R.R. Alfano. Spectral and temporal investigation of cross-phase modulation effects on picosecond pulses in singlemode optical fibers. In *Proceedings of the Third International Laser Science Conference* , Atlantic City, N.J. (1987).

5. P.L. Baldeck, R.R. Alfano, and Govind P. Agrawal. Induced-frequency shift of copropagating pulses. Appl. Phys. Lett. **52,** 1939 (1988).

6. R.R. Alfano, P.L. Baldeck, F. Raccah, and P.P. Ho. Cross-phase modulation measured in optical fibers. Appl. Opt. **26,** 3491-3492 (1987).

7. P.L. Baldeck, and R.R. Alfano. Induced-frequency shift, induced spectral broadening and optical amplification of picosecond pulses in a single-mode optical fiber. In *Proceedings of the Electrochemical Society Symposium on Nonlinear Optics and Ultrafast Phenomena* , Chicago, Illinois (1988).

8. Jamal T. Manassah, P.L. Baldeck, and R.R. Alfano. Self-focusing and self-phase modulation in a parabolic graded-index optical fiber. Opt. Lett. **13,** 589-591 (1988).

9. Jamal T. Manassah, P.L. Baldeck, and R.R. Alfano. Thermal focusing effects on the supercontinuum. Appl. Optics **27**, 3586-3587 (1988).

10. Jamal T. Manassah, P.L. Baldeck, and R.R. Alfano. Self-focusing, self-phase modulation and diffraction in bulk homogeneous material. Opt. Lett. **13**, 1090-1992 (1988).

11. P.L. Baldeck, R.R. Alfano, and Govind P. Agrawal. Generation of sub-100-fsec pulses at 532 nm from modulation instability induced by cross-phase modulation in optical fibers. In *Ultrafast Phenomena 6* , (Springer-Verlag, Berlin, Heilderberg 1988), p 53-55.

12. Govind P. Agrawal, P.L. Baldeck, and R.R. Alfano. Optical wave breaking and pulse compression due to cross-phase modulation in optical fibers. Opt. Lett. **14**, 137-139 (1989).

13. Govind P. Agrawal, P.L. Baldeck, and R.R. Alfano. Modulation instability induced by cross-phase modulation in optical fibers. Phys. Rev. **A 39**, 3406-3413 (1989).

14. R.R. Alfano, P.L. Baldeck, and P.P. Ho. Cross-phase modulation and induced-focusing of optical nonlinearities in optical fibers and bulk material. J. Opt. Soc. Am. **B 6**, 824-829 (1989).

15. P.P. Ho, P.L. Baldeck, K.S. Wong, K. Yoo, Don Lee, and R.R. Alfano. Time dynamics of photon migration in semi-opaque random media. Appl. Opt. **12**, 2304-2310 (1989).

16. P.L. Baldeck, P.P. Ho, and R.R. Alfano. Cross-phase modulation: a new technique for controlling the spectral, temporal, and spatial properties of ultrashort pulses. Chapter 4 in *The Supercontinuum Laser Source* , (Springer Verlag, Berlin 1989), p 117-183.

17. Ching-Yue Wang, P. L. Baldeck, Yury Budanski, and R. R. Alfano. 15 terahertz pulse generation arising from modulation instability oscillation in a colliding-pulse mode-locking dye laser. Opt. Lett. **14**, 497-499 (1989).

18. Govind P. Agrawal, P.L. Baldeck, and R.R. Alfano. Temporal and spectral effects of cross-phase modulation on copropagating ultrashort pulses in optical fibers. Phys. Rev. A, submitted for publication.

19. P.L. Baldeck, R.R. Alfano, and Govind P. Agrawal. Observation of modulation instability in the normal dispersion regime of single-mode optical fibers. Opt. Lett., submitted for publication.

20. P.L. Baldeck, S.Y. Yang, R.R. Alfano, R.H. Callender, C. Bennet, and W.H. Waddel. Laser-induced binding of precured rubber compounds. Opt. Eng., submitted for publication.

21. Yao Li, P.L. Baldeck, and R.R. Alfano. All-optical deflection based on an induced area modulation in nonlinear material. Appl. Opt., submitted for publication.

22. P.L. Baldeck, P.P. Ho, and R.R. Alfano. Cross-phase modulation: a new technique for controlling the spectral, temporal, and spatial properties of ultrashort pulses. In Proceedings of The International Congress of Optical Science and Engineering (SPIE conference), Paris, France (1989).

Conference Presentations:

1. P.L. Baldeck, and R.R. Alfano. Intensity effects on the stimulated four photon spectra generated by picosecond pulses in optical fibers. Conference Abstract # FQ 7, March Meeting of the American Physical Society (1987).

2. P.L. Baldeck, P.P. Ho, R.R. Alfano. Experimental evidences for cross-phase modulation, induced-phase modulation, and self-focusing on picosecond pulses in optical fibers. Conference abstract #TuV4, In the Digest of OSA 87 Annual meeting, Rochester N.Y. (1987).

3. P.L. Baldeck, R. Garuthara, F. Raccah, and R.R. Alfano. Spectral and temporal investigation of cross-phase modulation effects on picosecond pulses in singlemode optical fibers. Proceeding paper #TuC4, ILS-III, Atlantic City, N.J. (1987).

4. P.L. Baldeck, R.R. Alfano, and Govind P. Agrawal. Generation of sub-100-fsec pulses at 532 nm from modulation instability induced by cross-phase modulation in optical fibers. Proceeding paper # PD2, ICUP'88, Mont Hei, Japan (1987).

5. R.R. Alfano, P.L. Baldeck, and P.P. Ho. Cross-phase modulation and induced-focusing of optical nonlinearities in optical fibers and bulk materials. Optical Society of America. Topical meeting on nonlinear optical properties of materials, Troy N.Y (1988).

6. P.L. Baldeck, and R.R. Alfano. Induced-frequency shift, induced spectral broadening and optical amplification of picosecond pulses in a single-

mode optical fiber. Proceeding paper # 624. Electrochemical Society symposium on nonlinear optics and ultrafast phenomena, Chicago, Illinois (1988).

7. P.L. Baldeck, R.R. Alfano, and Govind P. Agrawal. Observation of modulation instability induced by cross-phase modulation. Conference abstract #MBB7, In the Digest of OSA 88 Annual meeting, Santa Clara, C.A. (1988).

8. Jamal T. Manassah, P.L. Baldeck, and R.R. Alfano. Self-focusing, self-phase modulation and diffraction in homogeneous media and graded-index optical fibers. Conference abstract #FS2, In the Digest of OSA 88 Annual meeting, Santa Clara, C.A. (1988).

9. Govind P. Agrawal, P.L. Baldeck, and R.R. Alfano. Optical wave breaking due to Cross-phase modulation in optical fibers. Conference abstract #MW3, In the Digest of OSA 88 Annual meeting, Santa Clara, C.A. (1988).

10. P.L. Baldeck, and R.R. Alfano. Cross-phase modulation: a new technique for controlling the spectral, temporal, and spatial properties of ultrashort pulses. The International Congress of Optical Science and Engineering (SPIE conference), Paris, France (1989).

11. P.L. Baldeck, C.W. Wang, Y. Budanski, and R. R. Alfano. Observation of modulation instability oscillation in a colliding-pulse mode-locking dye laser. CLEO 1989, Baltimore (1989).

BIBLIOGRAPHY

Agrawal, G. P. (1987) Modulation instability induced by cross-phase modulation. Phys. Rev. Lett. **59**, 880-883.

Agrawal, G. P. (1989)*Nonlinear Fiber Optics,* (Academic Press, London).

Agrawal, G. P. and M. J. Potasek (1986) Nonlinear pulse distortion in single-mode optical fibers at the zero-dispersion wavelength. Phys. Rev. **3**, 1765-1776.

Agrawal, G. P., P. L. Baldeck, and R. R. Alfano (1988) Optical wave breaking and pulse compression due to cross-phase modulation in optical fibers. Conference abstract #MW3, in *Digest of the 1988 OSA annual meeting,*. Optical Society of America, Washington, D. C.. Opt. Lett. **14**, 137-139.

Agrawal, G. P., P. L. Baldeck, and R. R. Alfano (1989a) Temporal and spectral effects of cross-phase modulation on copropagating ultrashort pulses in optical fibers. Submitted for publication.

Agrawal, G. P., P. L. Baldeck, and R. R. Alfano (1989b) Modulation instability induced by cross-phase modulation in optical fibers. Phys. Rev. **A 39**, 3406-3413.

Alfano R.R (1989), Editor, *The Supercontinuum Laser Source,* (Springer-Verlag, Berlin, Heilderberg).

Alfano, R. R. and P. P. Ho (1988) Self-, cross-, and induced-phase modulations of ultrashort laser pulse propagation. IEEE J. Quantum Electron. **24**, 351-364.

Alfano, R. R., and S. L. Shapiro (1970) Emission in the region 4000-7000 Å via four-photon coupling in glass. Phys. Rev. Lett. **24**, 584-587. Observation of self-phase modulation and small scale filaments in crystals and glasses. Phys. Rev. Lett. **24**, 592-594.

Alfano, R. R., Hope L., and S. L. Shapiro (1972) Electronic mechanism for production of self-phase modulation. Phys. Rev. **A6**, 443-438.

Alfano, R. R, Q. Li, T. Jimbo, J. T. Manassah, and P. P. Ho (1986) Induced spectral broadening of a weak picosecond pulse in glass produced by an intense ps pulse. Opt. Lett. **11**, 626-628.

Alfano, R. R., Q. Z. Wang , T. Jimbo, and P. P. Ho (1987a) Induced spectral broadening about a second harmonic generated by an intense primary ultrafast laser pulse in ZnSe crystals. Phys. Rev. **A35**, 459-462 .

Alfano, R. R., P. L. Baldeck, F. Raccah, and P. P. Ho (1987b) Cross-phase modulation measured in optical fibers. Appl. Opt. **26**, 3491-3492.

Alfano, R. R., P. L. Baldeck, and P. P. Ho (1988) Cross-phase modulation and induced-focusing of optical nonlinearities in optical fibers and bulk materials. Conference abstract #ThA3, In *Digest of the OSA topical meeting on nonlinear optical properties of materials,*. Optical Society of America, Washington, D. C

Auston, D. H. (1977) In *Ultrafast Light Pulses,* S.L. Shapiro, ed. (Springer-Verlag, Berlin, Heilderberg).

Ayral, J. L., J. P. Pochelle, J. Raffy, and M. Papuchon (1984) Optical Kerr coefficient measurement at 1.15 μm in single-mode optical fibers. Opt. Commun. **49**, 405-408.

Baldeck, P. L. and R. R. Alfano (1987) Intensity effects on the stimulated four-photon spectra generated by picosecond pulses in optical fibers. Conference Abstract # FQ 7, March meeting of the American Physical Society, New York, New York, 1987; J. Lightwave Technol. **L.T-5**, 1712-1715.

Baldeck, P. L., F. Raccah, and Alfano R.R. (1987a) Observation of self-focusing in optical fibers with picosecond pulses. Opt. Lett. **12**, 588-589.

Baldeck, P. L., P. P. Ho, and R. R. Alfano (1987b) Effects of self-, induced-, and cross-phase modulations on the generation of picosecond and femtosecond white light supercontinua. Rev. Phys. Appl. **22**, 1677-1694.

Baldeck, P. L., P. P. Ho, and R. R. Alfano (1987c) Experimental evidences for cross-phase modulation, induced-phase modulation and self-focusing on picosecond pulses in optical fibers. Conference abstract #TuV4, in *Digest of the 1987 OSA annual meeting,*. Optical Society of America, Washington, D. C.

Baldeck, P.L., F. Raccah, R. Garuthara, and R. R. Alfano (1987d) Spectral and temporal investigation of cross-phase modulation effects on picosecond pulses in singlemode optical fibers. Proceeding paper #TuC4, International Laser Science conference ILS-III, Atlantic City, New Jersey, 1987.

Baldeck, P. L., R. R. Alfano, and G. P. Agrawal (1988a) Induced-frequency shift of copropagating pulses. Appl. Phys. Lett. **52**, 1939-1941.

Baldeck, P. L., R. R. Alfano, and G. P. Agrawal (1988b) Observation of modulation instability in the normal dispersion regime of optical fibers. Conference abstract #MBB7, in *Digest of the 1988 OSA annual meeting,*. Optical Society of America, Washington, D. C.

Baldeck P. L., R. R. Alfano, and G. P. Agrawal (1988c) Induced-frequency shift, induced spectral broadening and optical amplification of picosecond pulses in a single-mode optical fiber. Proceeding paper #624, Electrochemical Society symposium on nonlinear optics and ultrafast phenomena, Chicago, Illinois, 1988.

Baldeck, P. L., R. R. Alfano, and G. P. Agrawal (1988d) Generation of sub-100-fsec pulses at 532 nm from modulation instability induced by cross-phase modulation in single-mode optical fibers. Proceeding paper #PD2, in*Ultrafast Phenomena 6* . (Springer Verlag, Berlin, Heilderberg).

Baldeck, P. L., R. R. Alfano (1989) Cross-phase modulation: a new technique for controlling the spectral, temporal and spatial properties of ultrashort pulses. 1989 SPIE Optical Science Engineering conference, Paris, France.

Chraplyvy, A. R. and J. Stone (1984) Measurement of cross-phase modulation in coherent wavelength-division multiplexing using injection lasers. Electron. Lett. **20**, 996-997.

Chraplyvy, A. R., D. Marcuse and P. S. Henry (1984) Carrier-induced phase noise in angle-modulated optical-fiber systems. J. Lightwave Technol. **LT-2**, 6-10.

Cornelius, P. and L. Harris (1981) Role of self-phase modulation in stimulated Raman scattering from more than one mode. Opt. Lett. **6**, 129-131.

Dianov, E. M., A. Y. Karasik, P. V. Mamyshev, G. I. Onishchukov, A. M. Prokhorov, M. F. Stel'Makh, and A. A. Formichev (1984) Picosecond structure of the pump pulse in stimulated Raman scattering in optical fibers. Opt. Quantum Electron. **17**, 187.

Dorsinville R., P. Delfyett P., and Alfano R.R. (1987). Appl. Opt. **26**.

Duguay, M. A. and J. W. Hansen (1969) An ultrafast light gate. Appl. Phys. Lett. **15**, 192-194.

Dziedzic, J. M., R. H. Stolen, and A. Ashkin (1981) Optical Kerr effect in long fibers. Appl. Opt. **20**, 1403-1406.

French, P. M. W., A. S. L. Gomes, A. S. Gouveia-Neto, and J. R. Taylor (1986) Picosecond stimulated Raman generation, pump pulse fragmentation, and fragment compression in single-mode optical fibers. IEEE J. Quantum Electron. **QE-22**, 2230.

Gersten J., R. R. Alfano, and M. Belic (1980) Combined stimulated Raman scattering and continuum self-phase modulation. Phys. Rev. **A #21**, 1222-1224 . Equation (22) has been corrected.

Gomes, A. S. L., W. Sibbet, and J. R. Taylor (1986) Spectral and temporal study of picosecond-pulse propagation in a single-mode optical fibers. Appl. Phys. **B #39**, 44-46.

Gomes, A. S. L., V. L. da Silva, and J. R. Taylor (1988) Direct measurement of nonlinear frequency chirp of Raman radiation in single-mode optical fibers using a spectral window method. J. Opt. Soc. Am. **B #5**, 373-380.

Gouveia-Neto, A. S., M. E. Faldon, A. S. B. Sombra, P. G. J. Wigley, and J. R. Taylor (1988a) Subpicosecond-pulse generation through cross-phase modulation-induced modulation instability in optical fibers. Opt. Lett. **12**, 901-906.

Gouveia-Neto, A. S., M. E. Faldon, and J. R. Taylor (1988b) Raman amplification of modulation instability and solitary-wave formation. Opt. Lett. **12**, 1029-1031.

Grudinin, A. B., E. M. Dianov, D. V. Korobkin, A. M. Prokhorov, V. N. Serkinand , and D. V. Khaidarov (1987) Decay of femtosecond pulses in single-mode optical fibers. Pis'ma Zh. Eksp. Teor. Fiz. **46**, 175-177. [Sov. Phys. JETP Lett. **46**, 221, 225.]

Hasegawa, A. (1975). *Plasma Instabilities and Nonlinear Effects.* Springer-Verlag, Heidelberg.

Ho, P. P., Q. Z. Wang, D. Ji, and R.R. Alfano (1988) Propagation of harmonic cross-phase-modulation pulses in ZnSe. Accepted for publication in Appl. Phys. Lett.

Hook, A., D. Anderson, and M. Lisak (1988) Soliton-like pulses in stimulated Raman scattering. Opt. Lett. **12**, (1988).

Imoto, N., S. Watkins, and Y. Sasaki (1987) A nonlinear optical-fiber interferometer for nondemolition measurement of photon number. Optics Commun. **61**, 159-163.

Islam, M. N., L. F. Mollenauer, R. H. Stolen (1986) Fiber Raman amplification soliton laser, in*Ultrafast Phenomena 5.* (Springer Verlag, Berlin, Heilderberg).

Islam, M. N., L. F. Mollenauer, R. H. Stolen, J. R. Simson, and H. T. Shang (1987a) Cross-phase modulation in optical fibers. Opt. Lett. **12**, 625-627.

Islam, M. N., L. F. Mollenauer, R. H. Stolen, J. R. Simson, and H. T. Shang (1987b) Amplifier/compressor fiber Raman lasers. Opt. Lett. **12**, 814-816.

Jaskorzynska, B. and D. Schadt (1988) All-fiber distributed compression of weak pulses in the regime of negative group-velocity dispersion. IEEE J. Quantum Electron. **QE-24**, 2117-2120.

Johnson, A. M., R. H. Stolen, and W. M. Simpson (1986) The observation of chirped stimulated Raman scattered light in fibers. In *Ultrafast Phenomena 5* . (Springer Verlag, Berlin, Heilderberg).

Keiser, G. (1983) In *Optical Fiber Communications* . (McGraw-Hill, New York).

Kelley, P.L. (1965) Self-focusing of optical beams. Phys. Rev. Lett. **15**, 1085.

Kimura, Y., K. I. Kitayama, N. Shibata, and S. Seikai (1986) All-fibre-optic logic "AND" gate. Electron. Lett. **22**, 277-278.

Kitayama, K. I. , Y. Kimura, and S. Seikai (1985a) Fiber-optic logic gate. Appl. Phys. Lett. **46**, 317-319.

Kitayama, K. I., Y. Kimura, K. Okamoto , and S. Seikai (1985) Optical sampling using an all-fiber optical Kerr shutter. Appl. Phys. Lett. **46**, 623-625.

Levenson, M. D., R. M. Shelby, M. Reid, and D. F. Walls (1986) Quantum nondemolition detection of optical quadrature amplitudes. Phys. Rev. Lett. **57**, 2473-2476.

Lin, C. and M. A. Bosh (1981) Large Stokes-shift stimulated four-photon mixing in optical fibers. Appl. Phys. Lett. **38**, 479-481.

Lu, Hian-Hua, Yu-Lin Li, and Jia-Lin Jiang (1985) On combined self-phase modulation and stimulated Raman scattering in fibers. Opt. Quantum Electron. **17**, 187.

Manassah, J. T. (1987a) Induced phase modulation of the Raman pulse in optical fibers. Appl. Opt. **26**, 3747-3749.

Manassah, J. T. (1987b) Time-domain characteristics of a Raman pulse in the presence of a pump. Appl. Opt. **26**, 3750-3751.

Manassah, J. T. (1987c) Amplitude and phase of a pulsed second-harmonic signal. J. Opt. Soc. Am. **B #4**, 1235-1240.

Manassah, J. T. (1988) Pulse compression of an induced-phase modulated weak signal. Opt. Lett. **13**, 752-755.

Manassah, J. T. and O. R. Cockings (1987) Induced phase modulation of a generated second-harmonic signal. Opt. Lett. **12**, 1005-1007.

Manassah, J. T., M. Mustafa, R. R. Alfano, and P. P. Ho (1985) Induced supercontinuum and steepening of an ultrafast laser pulse. Phys. Lett. **113A**, 242-247.

Monerie, M. and Y. Durteste (1987) Direct interferometric measurement of nonlinear refractive index of optical fibres by cross-phase modulation. Electron. Lett. **23**, 961-962.

Morioka, T., M. Saruwatari, and A. Takada (1987) Ultrafast optical multi/ demultiplexer using optical Kerr effect in polarization-maintaining single-mode optical fibers. Electron. Lett. **23**, 453-454.

Nakashima, T., M. Nakazawa, K. Nishi, and H. Kubuta (1987) Effect of stimulated Raman scattering on pulse-compression characteristics. Opt. Lett. **6**, 404-406.

Schadt, D., B. Jaskorzynska, and U. Osterberg (1986) Numerical study on combined stimulated Raman scattering and self-phase modulation in optical fibers influenced by walk-off between pump and Stokes pulses. J. Opt. Soc. Am. **B #3**, 1257-1260.

Schadt, D. and B. Jaskorzynska (1987a) Frequency chirp and spectra due to self-phase modulation and stimulated Raman scattering influenced by walk-off in optical fibers. J. Opt. Soc. Am. **B #4**, 856-862.

Schadt, D. and B. Jaskorzynska (1987b) Generation of short pulses from CW light by influence of cross-phase modulation in optical fibres. Electron. Lett. **23**, 1091-1092 .

Schadt, D. and B. Jaskorzynska (1988) Suppression of the Raman self-frequency shift by cross-phase modulation. J. Opt. Soc. Am. **B #5**, 2374-2378.

Shen, Y. R. (1984) In *The Principles of Nonlinear Optics* . (Wiley, New York).

Shimizu, F. and B. P. Stoicheff (1969) Study of the duration and birefringence of self-trapped filaments in CS_2. IEEE J. Quantum Electron. **QE-5**, 544.

Stolen, R.H. (1975) Phase-matched stimulated four-photon mixing. IEEE J. Quantum Electron. **QE-11**, 213-215.

Stolen, R. H. (1979) In *Nonlinear properties of optical fibers*, S.E. Miller and A.G. Chynoweth, eds. (Academic Press, New York), Chapter 5.

Stolen, R. H. and A. Ashkin (1972) Optical Kerr effect in glass waveguide. Appl. Phys. Lett. **22**, 294-296.

Stolen, R. H. , M. A. Bosh, and C. Lin (1981) Phase matching in birefringent fibers. Opt. Lett. **6**, 213-215.

Stolen, R. H. and A. M. Johnson (1986) The effect of pulse walk-off on stimulated Raman scattering in optical fibers. IEEE J. Quantum Electron. **QE-22**, 2230.

Swartzlander, G. A., Jr and A. E. Kaplan (1988) Self-deflection of laser beams in a thin nonlinear film. J. Opt. Soc. Am. **B 5**, 765-768.

Tai, K., A. Hasegawa, and A. Tomita (1986) Observation of modulation instability in optical fibers. Phys. Rev. Lett. **56**, 135-138.

Tomlinson, W. J., R. H. Stolen, and A. M. Johnson (1985) Optical wave breaking of pulses in nonlinear optical fibers. Opt. Lett. **10**, 457-459.

Trillo, S., S. Wabnitz, E. M. Wright, and G. I. Stegeman (1988) Optical solitary waves induced by cross-phase modulation. Opt. Lett. **13**, 871-873.

Washio, K. , K. Inoue, and T. Tanigawa (1980) Efficient generation near-IR stimulated light scattering in optical fibers pumped in low-dispersion region at 1.3 mm. Electron. Lett. **16**, 331-333.

Weiner, A. M., J. P. Heritage, and R. H. Stolen (1986) Effect of stimulated Raman scattering and pulse walk-off on self-phase modulation in optical fibers. In *Digest of the Conference on Lasers and Electro-Optics* . Optical Society of America, Washington, D.C., p. 246.

Weiner, A. M., J. P. Heritage, and R. H. Stolen (1988) Self-phase modulation and optical pulse compression influenced by stimulated Raman scattering in fibers. J. Opt. Soc. Am. **B5**, 364-372.

White, I. H., R. V. Penty, and R. E. Epworth (1988) Demonstration of the optical Kerr effect in an all-fibre Mach-Zehnder interferometer at laser diode powers. Electron. Lett. **24**.

Zysset B. and H. P. Weber (1986) Temporal and spectral investigation of Nd:YAG pulse compression in optical fibers and its application to pulse compression. In *Digest of the Conference on Lasers and Electro-Optics* . Optical Society of America, Washington, D.C., p. 182.